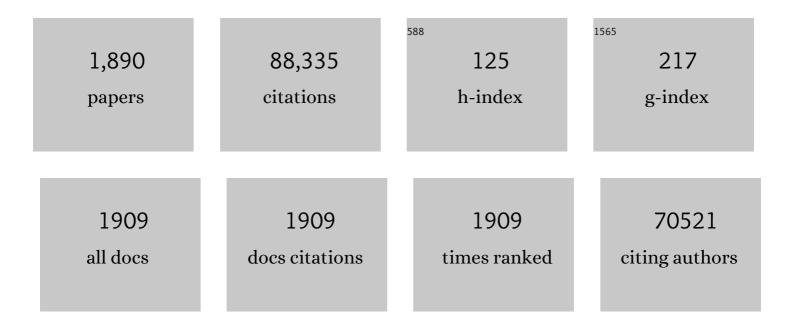
List of Publications by Year in descending order

Source: https://exaly.com/author-pdf/5067831/publications.pdf Version: 2024-02-01



Рли Сни

#	Article	IF	CITATIONS
1	Surface modification of titanium, titanium alloys, and related materials for biomedical applications. Materials Science and Engineering Reports, 2004, 47, 49-121.	14.8	2,804
2	Plasma-surface modification of biomaterials. Materials Science and Engineering Reports, 2002, 36, 143-206.	14.8	1,317
3	Characterization of amorphous and nanocrystalline carbon films. Materials Chemistry and Physics, 2006, 96, 253-277.	2.0	967
4	Ultrasmall Black Phosphorus Quantum Dots: Synthesis and Use as Photothermal Agents. Angewandte Chemie - International Edition, 2015, 54, 11526-11530.	7.2	906
5	From Black Phosphorus to Phosphorene: Basic Solvent Exfoliation, Evolution of Raman Scattering, and Applications to Ultrafast Photonics. Advanced Functional Materials, 2015, 25, 6996-7002.	7.8	862
6	Biodegradable black phosphorus-based nanospheres for in vivo photothermal cancer therapy. Nature Communications, 2016, 7, 12967.	5.8	835
7	Antibacterial coatings on titanium implants. Journal of Biomedical Materials Research - Part B Applied Biomaterials, 2009, 91B, 470-480.	1.6	732
8	Anionic Group Self-Doping as a Promising Strategy: Band-Gap Engineering and Multi-Functional Applications of High-Performance CO <sub>3</sub> <sup>2–</sup> -Doped Bi <sub>2</sub> O <sub>2</sub> CO <sub>3</sub> . ACS Catalysis, 2015, 5, 4094-4103.	5.5	690
9	Fabrication of Multiple Heterojunctions with Tunable Visible-Light-Active Photocatalytic Reactivity in BiOBr–BiOI Full-Range Composites Based on Microstructure Modulation and Band Structures. ACS Applied Materials & Interfaces, 2015, 7, 482-492.	4.0	671
10	Antibacterial nano-structured titania coating incorporated with silver nanoparticles. Biomaterials, 2011, 32, 5706-5716.	5.7	670
11	Flexible and ion-conducting membrane electrolytes for solid-state lithium batteries: Dispersion of garnet nanoparticles in insulating polyethylene oxide. Nano Energy, 2016, 28, 447-454.	8.2	651
12	Versatile Approach for Integrative and Functionalized Tubes by Strain Engineering of Nanomembranes on Polymers. Advanced Materials, 2008, 20, 4085-4090.	11.1	608
13	In vitro studies of biomedical magnesium alloys in a simulated physiological environment: A review. Acta Biomaterialia, 2011, 7, 1452-1459.	4.1	602
14	Photo-Inspired Antibacterial Activity and Wound Healing Acceleration by Hydrogel Embedded with Ag/Ag@AgCl/ZnO Nanostructures. ACS Nano, 2017, 11, 9010-9021.	7.3	591
15	A biodegradable polymer-based coating to control the performance of magnesium alloy orthopaedic implants. Biomaterials, 2010, 31, 2084-2096.	5.7	521
16	Scalable synthesis of ant-nest-like bulk porous silicon for high-performance lithium-ion battery anodes. Nature Communications, 2019, 10, 1447.	5.8	494
17	3D printing of hydrogels: Rational design strategies and emerging biomedical applications. Materials Science and Engineering Reports, 2020, 140, 100543.	14.8	494
18	Surface Coordination of Black Phosphorus for Robust Air and Water Stability. Angewandte Chemie - International Edition, 2016, 55, 5003-5007.	7.2	479

#	Article	IF	CITATIONS
19	Metalâ€lonâ€Modified Black Phosphorus with Enhanced Stability and Transistor Performance. Advanced Materials, 2017, 29, 1703811.	11.1	431
20	Cyclodextrin-Based Host–Guest Supramolecular Nanoparticles for Delivery: From Design to Applications. Accounts of Chemical Research, 2014, 47, 2017-2025.	7.6	418
21	The influence of hierarchical hybrid micro/nano-textured titanium surface with titania nanotubes on osteoblast functions. Biomaterials, 2010, 31, 5072-5082.	5.7	401
22	Facile Fabrication of Superhydrophobic Surface with Excellent Mechanical Abrasion and Corrosion Resistance on Copper Substrate by a Novel Method. ACS Applied Materials & Interfaces, 2014, 6, 8762-8770.	4.0	387
23	Synthesis, dispersion, and cytocompatibility of graphene oxide and reduced graphene oxide. Colloids and Surfaces B: Biointerfaces, 2012, 89, 79-85.	2.5	354
24	Influence of aggressive ions on the degradation behavior of biomedical magnesium alloy in physiological environment. Acta Biomaterialia, 2008, 4, 2008-2015.	4.1	341
25	Synergistic effects of dual Zn/Ag ion implantation in osteogenic activity and antibacterial ability of titanium. Biomaterials, 2014, 35, 7699-7713.	5.7	340
26	Plasma immersion ion implantation—a fledgling technique for semiconductor processing. Materials Science and Engineering Reports, 1996, 17, 207-280.	14.8	335
27	Antibacterial effects and biocompatibility of titanium surfaces with graded silver incorporation in titania nanotubes. Biomaterials, 2014, 35, 4255-4265.	5.7	319
28	Mechanism of apatite formation on wollastonite coatings in simulated body fluids. Biomaterials, 2004, 25, 1755-1761.	5.7	315
29	Low-dimensional SiC nanostructures: Fabrication, luminescence, and electrical properties. Progress in Materials Science, 2006, 51, 983-1031.	16.0	312
30	Surface design of biodegradable magnesium alloys — A review. Surface and Coatings Technology, 2013, 233, 2-12.	2.2	309
31	Biological actions of silver nanoparticles embedded in titanium controlled by micro-galvanic effects. Biomaterials, 2011, 32, 693-705.	5.7	307
32	Design of magnesium alloys with controllable degradation for biomedical implants: From bulk to surface. Acta Biomaterialia, 2016, 45, 2-30.	4.1	306
33	The effects of titania nanotubes with embedded silver oxide nanoparticles on bacteria and osteoblasts. Biomaterials, 2014, 35, 4223-4235.	5.7	305
34	Recent progress of transition metal nitrides for efficient electrocatalytic water splitting. Sustainable Energy and Fuels, 2019, 3, 366-381.	2.5	305
35	Cytocompatibility, osseointegration, and bioactivity of three-dimensional porous and nanostructured network on polyetheretherketone. Biomaterials, 2013, 34, 9264-9277.	5.7	302
36	Blackâ€Phosphorusâ€Incorporated Hydrogel as a Sprayable and Biodegradable Photothermal Platform for Postsurgical Treatment of Cancer. Advanced Science, 2018, 5, 1700848.	5.6	289

#	Article	IF	CITATIONS
37	Experimental Evidence for the Quantum Confinement Effect in 3C-SiC Nanocrystallites. Physical Review Letters, 2005, 94, 026102.	2.9	288
38	New Ultraviolet Photodetector Based on Individual Nb <sub>2</sub> O <sub>5</sub> Nanobelts. Advanced Functional Materials, 2011, 21, 3907-3915.	7.8	285
39	A General and Facile Approach to Heterostructured Core/Shell BiVO <sub>4</sub> /BiOI <i>p–n</i> Junction: Room-Temperature <i>in Situ</i> Assembly and Highly Boosted Visible-Light Photocatalysis. ACS Sustainable Chemistry and Engineering, 2015, 3, 3262-3273.	3.2	285
40	Rose-bengal-conjugated gold nanorods for inÂvivo photodynamic and photothermal oral cancer therapies. Biomaterials, 2014, 35, 1954-1966.	5.7	276
41	Effects of micropitted/nanotubular titania topographies on bone mesenchymal stem cell osteogenic differentiation. Biomaterials, 2012, 33, 2629-2641.	5.7	273
42	Osteogenic activity and antibacterial effects on titanium surfaces modified with Zn-incorporated nanotube arrays. Biomaterials, 2013, 34, 3467-3478.	5.7	269
43	Group IV Nanoparticles: Synthesis, Properties, and Biological Applications. Small, 2010, 6, 2080-2098.	5.2	264
44	Enhanced Ion Conductivity in Conducting Polymer Binder for Highâ€Performance Silicon Anodes in Advanced Lithiumâ€Ion Batteries. Advanced Energy Materials, 2018, 8, 1702314.	10.2	258
45	TiL <sub>4</sub> oordinated Black Phosphorus Quantum Dots as an Efficient Contrast Agent for In Vivo Photoacoustic Imaging of Cancer. Small, 2017, 13, 1602896.	5.2	251
46	Recent advance and prospectives of electrocatalysts based on transition metal selenides for efficient water splitting. Nano Energy, 2020, 78, 105234.	8.2	250
47	Small gold nanorods laden macrophages for enhanced tumor coverage in photothermal therapy. Biomaterials, 2016, 74, 144-154.	5.7	247
48	Rapid Sterilization and Accelerated Wound Healing Using Zn <sup>2+</sup> and Graphene Oxide Modified g <sub>3</sub> N <sub>4</sub> under Dual Light Irradiation. Advanced Functional Materials, 2018, 28, 1800299.	7.8	246
49	Hollow chitosan–silica nanospheres as pH-sensitive targeted delivery carriers in breast cancer therapy. Biomaterials, 2011, 32, 4976-4986.	5.7	245
50	Surface nano-functionalization of biomaterials. Materials Science and Engineering Reports, 2010, 70, 275-302.	14.8	244
51	A CRISPR–Cas9-triggered strand displacement amplification method for ultrasensitive DNA detection. Nature Communications, 2018, 9, 5012.	5.8	244
52	Stimulation of bone growth following zinc incorporation into biomaterials. Biomaterials, 2014, 35, 6882-6897.	5.7	241
53	Photothermal Contribution to Enhanced Photocatalytic Performance of Graphene-Based Nanocomposites. ACS Nano, 2014, 8, 9304-9310.	7.3	240
54	Raman scattering study of zinc blende and wurtzite ZnS. Journal of Applied Physics, 2009, 106, .	1.1	235

#	Article	IF	CITATIONS
55	Surface energy, wettability, and blood compatibility phosphorus doped diamond-like carbon films. Diamond and Related Materials, 2005, 14, 78-85.	1.8	230
56	Balancing Bacteria–Osteoblast Competition through Selective Physical Puncture and Biofunctionalization of ZnO/Polydopamine/Arginine-Glycine-Aspartic Acid-Cysteine Nanorods. ACS Nano, 2017, 11, 11250-11263.	7.3	230
57	Synthesis and low-temperature photoluminescence properties of SnO2nanowires and nanobelts. Nanotechnology, 2006, 17, 1695-1699.	1.3	228
58	Tuning the Bandgap of Photo-Sensitive Polydopamine/Ag <sub>3</sub> PO <sub>4</sub> /Graphene Oxide Coating for Rapid, Noninvasive Disinfection of Implants. ACS Central Science, 2018, 4, 724-738.	5.3	227
59	High-Performance Two-Ply Yarn Supercapacitors Based on Carbon Nanotube Yarns Dotted with Co <sub>3</sub> O <sub>4</sub> and NiO Nanoparticles. Small, 2015, 11, 854-861.	5.2	226
60	Synergistic Bacteria Killing through Photodynamic and Physical Actions of Graphene Oxide/Ag/Collagen Coating. ACS Applied Materials & Interfaces, 2017, 9, 26417-26428.	4.0	223
61	Antibacterial effects of titanium embedded with silver nanoparticles based on electron-transfer-induced reactive oxygen species. Biomaterials, 2017, 124, 25-34.	5.7	219
62	Engineering Nanoparticle-Coated Bacteria as Oral DNA Vaccines for Cancer Immunotherapy. Nano Letters, 2015, 15, 2732-2739.	4.5	213
63	Symmetrical dual D-shape photonic crystal fibers for surface plasmon resonance sensing. Optics Express, 2018, 26, 9039.	1.7	213
64	The osteogenic activity of strontium loaded titania nanotube arrays on titanium substrates. Biomaterials, 2013, 34, 19-29.	5.7	212
65	Inâ€Plane Black Phosphorus/Dicobalt Phosphide Heterostructure for Efficient Electrocatalysis. Angewandte Chemie - International Edition, 2018, 57, 2600-2604.	7.2	209
66	Functionalized TiO <sub>2</sub> Based Nanomaterials for Biomedical Applications. Advanced Functional Materials, 2014, 24, 5464-5481.	7.8	208
67	Enhanced osteointegration on tantalum-implanted polyetheretherketone surface with bone-like elastic modulus. Biomaterials, 2015, 51, 173-183.	5.7	206
68	InÂvitro and inÂvivo anti-biofilm effects of silver nanoparticles immobilized on titanium. Biomaterials, 2014, 35, 9114-9125.	5.7	205
69	Metabolizable Ultrathin Bi <sub>2</sub> Se <sub>3</sub> Nanosheets in Imagingâ€Guided Photothermal Therapy. Small, 2016, 12, 4136-4145.	5.2	203
70	Bioactive SrTiO <sub>3</sub> Nanotube Arrays: Strontium Delivery Platform on Ti-Based Osteoporotic Bone Implants. ACS Nano, 2009, 3, 3228-3234.	7.3	198
71	Enhanced antimicrobial properties, cytocompatibility, and corrosion resistance of plasma-modified biodegradable magnesium alloys. Acta Biomaterialia, 2014, 10, 544-556.	4.1	194
72	Gold-nanorods-siRNA nanoplex for improved photothermal therapy by gene silencing. Biomaterials, 2016, 78, 27-39.	5.7	192

#	Article	IF	CITATIONS
73	Corrosion behavior of biomedical AZ91 magnesium alloy in simulated body fluids. Journal of Materials Research, 2007, 22, 2004-2011.	1.2	189
74	Intrinsic Dipole-Field-Driven Mesoscale Crystallization of Coreâ^'Shell ZnO Mesocrystal Microspheres. Journal of the American Chemical Society, 2009, 131, 9405-9412.	6.6	189
75	Influence of sulfur content on bone formation and antibacterial ability of sulfonated PEEK. Biomaterials, 2016, 83, 115-126.	5.7	189
76	Zincâ€Modified Sulfonated Polyetheretherketone Surface with Immunomodulatory Function for Guiding Cell Fate and Bone Regeneration. Advanced Science, 2018, 5, 1800749.	5.6	184
77	Direct Growth of Graphene Film on Germanium Substrate. Scientific Reports, 2013, 3, 2465.	1.6	181
78	Recent progress in nanostructured transition metal nitrides for advanced electrochemical energy storage. Journal of Materials Chemistry A, 2019, 7, 14-37.	5.2	181
79	Near-infrared light control of bone regeneration with biodegradable photothermal osteoimplant. Biomaterials, 2019, 193, 1-11.	5.7	181
80	Quantum confinement effects across two-dimensional planes in MoS2 quantum dots. Applied Physics Letters, 2015, 106, .	1.5	180
81	Simultaneous nanostructure and heterojunction engineering of graphitic carbon nitride via in situ Ag doping for enhanced photoelectrochemical activity. Applied Catalysis B: Environmental, 2015, 163, 611-622.	10.8	180
82	Controlled-temperature photothermal and oxidative bacteria killing and acceleration of wound healing by polydopamine-assisted Au-hydroxyapatite nanorods. Acta Biomaterialia, 2018, 77, 352-364.	4.1	180
83	VO <sub>2</sub> /TiN Plasmonic Thermochromic Smart Coatings for Roomâ€Temperature Applications. Advanced Materials, 2018, 30, 1705421.	11.1	179
84	Few-Layer Antimonene: Anisotropic Expansion and Reversible Crystalline-Phase Evolution Enable Large-Capacity and Long-Life Na-Ion Batteries. ACS Nano, 2018, 12, 1887-1893.	7.3	175
85	Identification of oxygen vacancy types from Raman spectra of SnO <sub>2</sub> nanocrystals. Journal of Raman Spectroscopy, 2012, 43, 1423-1426.	1.2	172
86	Electrochemical surface engineering of titanium-based alloys for biomedical application. Electrochimica Acta, 2018, 271, 699-718.	2.6	168
87	Noninvasive rapid bacteria-killing and acceleration of wound healing through photothermal/photodynamic/copper ion synergistic action of a hybrid hydrogel. Biomaterials Science, 2018, 6, 2110-2121.	2.6	168
88	3C–SiC Nanocrystals as Fluorescent Biological Labels. Small, 2008, 4, 1058-1062.	5.2	165
89	Electrochemical corrosion behavior of biodegradable Mg–Y–RE and Mg–Zn–Zr alloys in Ringer's solution and simulated body fluid. Corrosion Science, 2015, 91, 160-184.	3.0	162
90	Improvement of corrosion resistance and biocompatibility of rare-earth WE43 magnesium alloy by neodymium self-ion implantation. Corrosion Science, 2015, 94, 142-155.	3.0	161

#	Article	IF	CITATIONS
91	Influence of heat treatment on degradation behavior of bio-degradable die-cast AZ63 magnesium alloy in simulated body fluid. Materials Science & Engineering A: Structural Materials: Properties, Microstructure and Processing, 2007, 456, 350-357.	2.6	160
92	Mechanism of Photoluminescence from Chemically Derived Graphene Oxide: Role of Chemical Reduction. Advanced Optical Materials, 2013, 1, 926-932.	3.6	160
93	Evaporative Selfâ€Assembly of Gold Nanorods into Macroscopic 3D Plasmonic Superlattice Arrays. Advanced Materials, 2016, 28, 2511-2517.	11.1	160
94	Freestanding carbon encapsulated mesoporous vanadium nitride nanowires enable highly stable sulfur cathodes for lithium-sulfur batteries. Nano Energy, 2017, 40, 655-662.	8.2	159
95	Stable and Multifunctional Dye-Modified Black Phosphorus Nanosheets for Near-Infrared Imaging-Guided Photothermal Therapy. Chemistry of Materials, 2017, 29, 7131-7139.	3.2	158
96	Surface plasmon resonance (SPR) infrared sensor based on D-shape photonic crystal fibers with ITO coatings. Optics Communications, 2020, 464, 125496.	1.0	157
97	In vitro corrosion degradation behaviour of Mg–Ca alloy in the presence of albumin. Corrosion Science, 2010, 52, 3341-3347.	3.0	154
98	An antibacterial platform based on capacitive carbon-doped TiO2 nanotubes after direct or alternating currentÂcharging. Nature Communications, 2018, 9, 2055.	5.8	153
99	Sn-C bonding riveted SnSe nanoplates vertically grown on nitrogen-doped carbon nanobelts for high-performance sodium-ion battery anodes. Nano Energy, 2018, 54, 322-330.	8.2	152
100	Antithrombogenic investigation of surface energy and optical bandgap and hemocompatibility mechanism of Ti(Ta+5)O2 thin films. Biomaterials, 2002, 23, 2545-2552.	5.7	150
101	Designing Core–Shell Gold and Selenium Nanocomposites for Cancer Radiochemotherapy. ACS Nano, 2017, 11, 4848-4858.	7.3	150
102	Biomass-derived robust three-dimensional porous carbon for high volumetric performance supercapacitors. Journal of Power Sources, 2019, 412, 1-9.	4.0	150
103	Hydrogenated V <sub>2</sub> O <sub>5</sub> Nanosheets for Superior Lithium Storage Properties. Advanced Functional Materials, 2016, 26, 784-791.	7.8	149
104	Activation of platelets adhered on amorphous hydrogenated carbon (a-C:H) films synthesized by plasma immersion ion implantation-deposition (PIII-D). Biomaterials, 2003, 24, 2821-2829.	5.7	148
105	Light-emitting diodes enhanced by localized surface plasmon resonance. Nanoscale Research Letters, 2011, 6, 199.	3.1	147
106	Graphitic carbon nitride-based materials for photocatalytic antibacterial application. Materials Science and Engineering Reports, 2021, 145, 100610.	14.8	145
107	Biodegradable Mg-Cu alloys with enhanced osteogenesis, angiogenesis, and long-lasting antibacterial effects. Scientific Reports, 2016, 6, 27374.	1.6	144
108	Mechanical and biological characteristics of diamond-like carbon coated poly aryl-ether-ether-ketone. Biomaterials, 2010, 31, 8181-8187.	5.7	143

#	Article	IF	CITATIONS
109	Mechanical and thermal properties of basalt fiber reinforced poly(butylene succinate) composites. Materials Chemistry and Physics, 2012, 133, 845-849.	2.0	142
110	Precisely controlled delivery of magnesium ions thru sponge-like monodisperse PLGA/nano-MgO-alginate core-shell microsphere device to enable in-situ bone regeneration. Biomaterials, 2018, 174, 1-16.	5.7	140
111	Inactivation of a 25.5µm Enterococcus faecalis biofilm by a room-temperature, battery-operated, handheld air plasma jet. Journal Physics D: Applied Physics, 2012, 45, 165205.	1.3	138
112	Engineering and functionalization of biomaterials via surface modification. Journal of Materials Chemistry B, 2015, 3, 2024-2042.	2.9	138
113	Biomedical Applications of Functionalized ZnO Nanomaterials: from Biosensors to Bioimaging. Advanced Materials Interfaces, 2016, 3, 1500494.	1.9	138
114	Analysis of a Surface Plasmon Resonance Probe Based on Photonic Crystal Fibers for Low Refractive Index Detection. Plasmonics, 2018, 13, 779-784.	1.8	137
115	Magnetite-loaded fluorine-containing polymeric micelles for magnetic resonance imaging and drug delivery. Biomaterials, 2012, 33, 3013-3024.	5.7	136
116	Principles and characteristics of a new generation plasma immersion ion implanter. Review of Scientific Instruments, 1997, 68, 1866-1874.	0.6	135
117	Ni/Co-based nanosheet arrays for efficient oxygen evolution reaction. Nano Energy, 2018, 52, 360-368.	8.2	135
118	In situ crystallization for fabrication of a core–satellite structured BiOBr–CdS heterostructure with excellent visible-light-responsive photoreactivity. Nanoscale, 2015, 7, 11702-11711.	2.8	134
119	Degradation behaviour of pure magnesium in simulated body fluids with different concentrations of. Corrosion Science, 2011, 53, 1522-1528.	3.0	133
120	Interaction of electromagnetic waves with a magnetized nonuniform plasma slab. IEEE Transactions on Plasma Science, 2003, 31, 405-410.	0.6	131
121	Green light stimulates terahertz emission from mesocrystal microspheres. Nature Nanotechnology, 2011, 6, 103-106.	15.6	131
122	Plasma surface modification of poly vinyl chloride for improvement of antibacterial properties. Biomaterials, 2006, 27, 44-51.	5.7	130
123	Degradation susceptibility of surgical magnesium alloy in artificial biological fluid containing albumin. Journal of Materials Research, 2007, 22, 1806-1814.	1.2	130
124	Two-dimensional black phosphorus: Synthesis, modification, properties, and applications. Materials Science and Engineering Reports, 2017, 120, 1-33.	14.8	130
125	Origin of low-temperature photoluminescence from SnO2 nanowires fabricated by thermal evaporation and annealed in different ambients. Applied Physics Letters, 2006, 88, 183112.	1.5	128
126	Is There Real Upconversion Photoluminescence from Graphene Quantum Dots?. Advanced Optical Materials, 2013, 1, 554-558.	3.6	128

#	Article	IF	CITATIONS
127	MoS <sub>2</sub> â€Quantumâ€Dotâ€Interspersed Li <sub>4</sub> Ti <sub>5</sub> O <sub>12</sub> Nanoshee with Enhanced Performance for Li―and Naâ€Ion Batteries. Advanced Functional Materials, 2016, 26, 3349-3358.	ts 7.8	128
128	Nano Ag/ZnO-Incorporated Hydroxyapatite Composite Coatings: Highly Effective Infection Prevention and Excellent Osteointegration. ACS Applied Materials & amp; Interfaces, 2018, 10, 1266-1277.	4.0	127
129	Evading strength-corrosion tradeoff in Mg alloys via dense ultrafine twins. Nature Communications, 2021, 12, 4616.	5.8	126
130	Carbon plasma immersion ion implantation of nickel–titanium shape memory alloys. Biomaterials, 2005, 26, 2265-2272.	5.7	125
131	Synthesis, Growth Mechanism, and Electrochemical Properties of Hollow Mesoporous Carbon Spheres with Controlled Diameter. Journal of Physical Chemistry C, 2011, 115, 17717-17724.	1.5	125
132	Radiation tolerance of Cu/W multilayered nanocomposites. Journal of Nuclear Materials, 2011, 413, 11-15.	1.3	125
133	A Biomimetic Hierarchical Scaffold: Natural Growth of Nanotitanates on Three-Dimensional Microporous Ti-Based Metals. Nano Letters, 2008, 8, 3803-3808.	4.5	124
134	Fabrication, modification, and biomedical applications of anodized TiO <sub>2</sub> nanotube arrays. RSC Advances, 2014, 4, 17300-17324.	1.7	124
135	Au Nanoparticles Decorated TiO <sub>2</sub> Nanotube Arrays as a Recyclable Sensor for Photoenhanced Electrochemical Detection of Bisphenol A. Environmental Science & Technology, 2016, 50, 4430-4438.	4.6	124
136	Mo2C/VC heterojunction embedded in graphitic carbon network: An advanced electrocatalyst for hydrogen evolution. Nano Energy, 2019, 60, 520-526.	8.2	124
137	A bifunctional hydrogel incorporated with CuS@MoS2 microspheres for disinfection and improved wound healing. Chemical Engineering Journal, 2020, 382, 122849.	6.6	124
138	Microstructure of Ti/Al ohmic contacts for n-AlGaN. Applied Physics Letters, 1998, 73, 2582-2584.	1.5	122
139	Highly Conductive, Mechanically Robust, and Electrochemically Inactive TiC/C Nanofiber Scaffold for High-Performance Silicon Anode Batteries. ACS Nano, 2011, 5, 8346-8351.	7.3	122
140	A surface-engineered polyetheretherketone biomaterial implant with direct and immunoregulatory antibacterial activity against methicillin-resistant Staphylococcus aureus. Biomaterials, 2019, 208, 8-20.	5.7	122
141	Blood compatibility and sp3/sp2 contents of diamond-like carbon (DLC) synthesized by plasma immersion ion implantation-deposition. Surface and Coatings Technology, 2002, 156, 289-294.	2.2	121
142	Synergistic WO <sub>3</sub> ·2H <sub>2</sub> O Nanoplates/WS <sub>2</sub> Hybrid Catalysts for High-Efficiency Hydrogen Evolution. ACS Applied Materials & Interfaces, 2016, 8, 13966-13972.	4.0	120
143	Surface functionalization of biomaterials by radical polymerization. Progress in Materials Science, 2016, 83, 191-235.	16.0	120
144	Vanadium carbide nanoparticles encapsulated in graphitic carbon network nanosheets: A high-efficiency electrocatalyst for hydrogen evolution reaction. Nano Energy, 2016, 26, 603-609.	8.2	120

#	Article	IF	CITATIONS
145	Effects and Mechanism of Atmospheric-Pressure Dielectric Barrier Discharge Cold Plasmaon Lactate Dehydrogenase (LDH) Enzyme. Scientific Reports, 2015, 5, 10031.	1.6	119
146	In situ segregation of cobalt nanoparticles on VN nanosheets via nitriding of Co 2 V 2 O 7 nanosheets as efficient oxygen evolution reaction electrocatalysts. Nano Energy, 2017, 34, 1-7.	8.2	119
147	Electron storage mediated dark antibacterial action of bound silver nanoparticles: Smaller is not always better. Acta Biomaterialia, 2013, 9, 5100-5110.	4.1	116
148	Black Phosphorus Based Photocathodes in Wideband Bifacial Dye‧ensitized Solar Cells. Advanced Materials, 2016, 28, 8937-8944.	11.1	116
149	Surface Coordination of Black Phosphorus for Robust Air and Water Stability. Angewandte Chemie, 2016, 128, 5087-5091.	1.6	116
150	Near-infrared light-triggered drug delivery system based on black phosphorus for inÂvivo bone regeneration. Biomaterials, 2018, 179, 164-174.	5.7	115
151	Ni-doped amorphous iron phosphide nanoparticles on TiN nanowire arrays: An advanced alkaline hydrogen evolution electrocatalyst. Nano Energy, 2018, 53, 66-73.	8.2	115
152	2D black phosphorus dotted with silver nanoparticles: An excellent lubricant additive for tribological applications. Chemical Engineering Journal, 2020, 392, 123631.	6.6	115
153	Synergistic treatment of ovarian cancer by co-delivery of survivin shRNA and paclitaxel via supramolecular micellar assembly. Biomaterials, 2012, 33, 6580-6591.	5.7	114
154	Valence State Manipulation of Cerium Oxide Nanoparticles on a Titanium Surface for Modulating Cell Fate and Bone Formation. Advanced Science, 2018, 5, 1700678.	5.6	114
155	Highly Stretchable Conductive Glue for Highâ€Performance Silicon Anodes in Advanced Lithiumâ€Ion Batteries. Advanced Functional Materials, 2018, 28, 1704858.	7.8	113
156	Black Phosphorus: Bioactive Nanomaterials with Inherent and Selective Chemotherapeutic Effects. Angewandte Chemie - International Edition, 2019, 58, 769-774.	7.2	113
157	Corrosion behavior of ZrN/Zr coated biomedical AZ91 magnesium alloy. Surface and Coatings Technology, 2009, 203, 2554-2557.	2.2	112
158	The role of sterilization in the cytocompatibility of titania nanotubes. Biomaterials, 2010, 31, 2055-2063.	5.7	112
159	Low-modulus Mg/PCL hybrid bone substitute for osteoporotic fracture fixation. Biomaterials, 2013, 34, 7016-7032.	5.7	112
160	In situ formation of N-doped carbon-coated porous MoP nanowires: a highly efficient electrocatalyst for hydrogen evolution reaction in a wide pH range. Applied Catalysis B: Environmental, 2020, 263, 118358.	10.8	112
161	The effects of amorphous carbon films deposited on polyethylene terephthalate on bacterial adhesion. Biomaterials, 2004, 25, 3163-3170.	5.7	111
162	Corrosion behavior of AZ91 magnesium alloy treated by plasma immersion ion implantation and deposition in artificial physiological fluids. Thin Solid Films, 2007, 516, 422-427.	0.8	111

#	Article	IF	CITATIONS
163	Recent advances and challenges in electroplastic manufacturing processing of metals. Journal of Materials Research, 2010, 25, 1215-1224.	1.2	111
164	Synergistic antibacterial activity of physical-chemical multi-mechanism by TiO2 nanorod arrays for safe biofilm eradication on implant. Bioactive Materials, 2021, 6, 12-25.	8.6	111
165	Plasma-treated nanostructured TiO2 surface supporting biomimetic growth of apatite. Biomaterials, 2005, 26, 6143-6150.	5.7	110
166	Influence of Test Solutions on In Vitro Studies of Biomedical Magnesium Alloys. Journal of the Electrochemical Society, 2010, 157, C238.	1.3	110
167	Fabrication and enhanced dielectric properties of graphene–polyvinylidene fluoride functional hybrid films with a polyaniline interlayer. Journal of Materials Chemistry A, 2013, 1, 884-890.	5.2	110
168	Synthesis of nano-Cu/graphene oxide composites by supercritical CO2-assisted deposition as a novel material for reducing friction and wear. Chemical Engineering Journal, 2015, 281, 11-19.	6.6	110
169	Synthesis and Photocatalytic Activity of Highly Ordered TiO <sub>2</sub> and SrTiO <sub>3</sub> /TiO <sub>2</sub> Nanotube Arrays on Ti Substrates. Journal of the American Ceramic Society, 2010, 93, 2771-2778.	1.9	108
170	Mesoporous nitrogen-doped carbon hollow spheres as high-performance anodes for lithium-ion batteries. Journal of Power Sources, 2016, 324, 233-238.	4.0	108
171	Freestanding hollow double-shell Se@CNx nanobelts as large-capacity and high-rate cathodes for Li-Se batteries. Nano Energy, 2017, 32, 1-9.	8.2	108
172	High-Efficiency Electrochemical Hydrogen Evolution Based on Surface Autocatalytic Effect of Ultrathin 3C-SiC Nanocrystals. Nano Letters, 2012, 12, 1545-1548.	4.5	107
173	Recent developments and applications of plasma immersion ion implantation. Journal of Vacuum Science & Technology an Official Journal of the American Vacuum Society B, Microelectronics Processing and Phenomena, 2004, 22, 289.	1.6	106
174	Bioactivity and cytocompatibility of zirconia (ZrO2) films fabricated by cathodic arc deposition. Biomaterials, 2006, 27, 3904-3911.	5.7	106
175	Effects of zirconium and oxygen plasma ion implantation on the corrosion behavior of ZK60 Mg alloy in simulated body fluids. Corrosion Science, 2014, 82, 7-26.	3.0	106
176	Corrosion resistance and cytocompatibility of tantalum-surface-functionalized biomedical ZK60 Mg alloy. Corrosion Science, 2017, 114, 45-56.	3.0	106
177	Electrostatic Self-Assembly of Ti <sub>3</sub> C <sub>2</sub> T <sub><i>x</i></sub> MXene and Gold Nanorods as an Efficient Surface-Enhanced Raman Scattering Platform for Reliable and High-Sensitivity Determination of Organic Pollutants. ACS Sensors, 2019, 4, 2303-2310.	4.0	106
178	Conductive amorphous carbon-coated 316L stainless steel as bipolar plates in polymer electrolyte membrane fuel cells. International Journal of Hydrogen Energy, 2009, 34, 6771-6777.	3.8	105
179	Identification of Surface Structures on 3C-SiC Nanocrystals with Hydrogen and Hydroxyl Bonding by Photoluminescence. Nano Letters, 2009, 9, 4053-4060.	4.5	105
180	Charged Diphenylalanine Nanotubes and Controlled Hierarchical Self-Assembly. ACS Nano, 2011, 5, 4448-4454.	7.3	105

#	Article	IF	CITATIONS
181	Nanostructured TiO2 for energy conversion and storage. RSC Advances, 2013, 3, 24758.	1.7	105
182	Bamboo leaf derived ultrafine Si nanoparticles and Si/C nanocomposites for high-performance Li-ion battery anodes. Nanoscale, 2015, 7, 13840-13847.	2.8	105
183	Black Phosphorus/Platinum Heterostructure: A Highly Efficient Photocatalyst for Solarâ€Driven Chemical Reactions. Advanced Materials, 2018, 30, e1803641.	11.1	105
184	NiFe-Layered Double Hydroxide Synchronously Activated by Heterojunctions and Vacancies for the Oxygen Evolution Reaction. ACS Applied Materials & amp; Interfaces, 2020, 12, 42850-42858.	4.0	105
185	Biocompatibility and bioactivity of plasma-treated biodegradable poly(butylene succinate). Acta Biomaterialia, 2009, 5, 279-287.	4.1	104
186	Nitrogenâ€Doped Carbon Encapsulated Mesoporous Vanadium Nitride Nanowires as Selfâ€Supported Electrodes for Flexible Allâ€Solidâ€State Supercapacitors. Advanced Materials Interfaces, 2015, 2, 1500211.	1.9	104
187	Relationship between osseointegration and superelastic biomechanics in porous NiTi scaffolds. Biomaterials, 2011, 32, 330-338.	5.7	103
188	Biomimetic osteogenic peptide with mussel adhesion and osteoimmunomodulatory functions to ameliorate interfacial osseointegration under chronic inflammation. Biomaterials, 2020, 255, 120197.	5.7	103
189	Improvement of surface bioactivity on titanium by water and hydrogen plasma immersion ion implantation. Biomaterials, 2005, 26, 6129-6135.	5.7	102
190	Supercritical Fluid Synthesis and Tribological Applications of Silver Nanoparticle-decorated Graphene in Engine Oil Nanofluid. Scientific Reports, 2016, 6, 31246.	1.6	102
191	Antibacterial Activity of Silver Doped Titanate Nanowires on Ti Implants. ACS Applied Materials & Interfaces, 2016, 8, 16584-16594.	4.0	102
192	Preferential production of reactive species and bactericidal efficacy of gas-liquid plasma discharge. Chemical Engineering Journal, 2019, 362, 402-412.	6.6	102
193	High-efficiency hydrogen evolution from seawater using hetero-structured T/Td phase ReS2 nanosheets with cationic vacancies. Nano Energy, 2019, 55, 42-48.	8.2	102
194	Third-generation plasma immersion ion implanter for biomedical materials and research. Review of Scientific Instruments, 2001, 72, 1660.	0.6	100
195	Hemocompatibility and anti-bacterial properties of silver doped diamond-like carbon prepared by pulsed filtered cathodic vacuum arc deposition. Diamond and Related Materials, 2007, 16, 1353-1360.	1.8	100
196	Sequentially Triggered Delivery System of Black Phosphorus Quantum Dots with Surface Charge-Switching Ability for Precise Tumor Radiosensitization. ACS Nano, 2018, 12, 12401-12415.	7.3	100
197	Tuning the surface immunomodulatory functions of polyetheretherketone for enhanced osseointegration. Biomaterials, 2020, 230, 119642.	5.7	100
198	Synthesis and characterization of super hard, self-lubricating Ti–Si–C–N nanocomposite coatings. Acta Materialia, 2007, 55, 6350-6355.	3.8	99

#	Article	IF	CITATIONS
199	InÂvivo stimulation of bone formation by aluminum and oxygen plasma surface-modified magnesium implants. Biomaterials, 2013, 34, 9863-9876.	5.7	99
200	The role of integrin-linked kinase/β-catenin pathway in the enhanced MG63 differentiation by micro/nano-textured topography. Biomaterials, 2013, 34, 631-640.	5.7	99
201	Highly-crystalline ultrathin Li4Ti5O12 nanosheets decorated with silver nanocrystals as a high-performance anode material for lithium ion batteries. Journal of Power Sources, 2015, 276, 247-254.	4.0	99
202	Ultra-sensitive detection of cysteine by gold nanorod assembly. Biosensors and Bioelectronics, 2010, 25, 2078-2083.	5.3	97
203	Producing cobalt–graphene composite coating by pulse electrodeposition with excellent wear and corrosion resistance. Applied Surface Science, 2015, 351, 889-896.	3.1	97
204	Fabrication and dielectric properties of oriented polyvinylidene fluoride nanocomposites incorporated with graphene nanosheets. Materials Chemistry and Physics, 2012, 134, 867-874.	2.0	96
205	Biofunctionalization of carbon nanotubes/chitosan hybrids on Ti implants by atom layer deposited ZnO nanostructures. Applied Surface Science, 2017, 400, 14-23.	3.1	96
206	Effects of copper nanoparticles in porous TiO2 coatings on bacterial resistance and cytocompatibility of osteoblasts and endothelial cells. Materials Science and Engineering C, 2018, 82, 110-120.	3.8	96
207	Antibacterial Surface Design of Titanium-Based Biomaterials for Enhanced Bacteria-Killing and Cell-Assisting Functions Against Periprosthetic Joint Infection. ACS Applied Materials & Interfaces, 2016, 8, 11162-11178.	4.0	95
208	Flexible Nb2O5 nanowires/graphene film electrode for high-performance hybrid Li-ion supercapacitors. Journal of Power Sources, 2016, 328, 599-606.	4.0	95
209	Phaseâ€Changing Microcapsules Incorporated with Black Phosphorus for Efficient Solar Energy Storage. Advanced Science, 2020, 7, 2000602.	5.6	95
210	Nanoparticles for improving cancer diagnosis. Materials Science and Engineering Reports, 2013, 74, 35-69.	14.8	94
211	Biodegradable near-infrared-photoresponsive shape memory implants based on black phosphorus nanofillers. Biomaterials, 2018, 164, 11-21.	5.7	94
212	Stable black phosphorus/Bi2O3 heterostructures for synergistic cancer radiotherapy. Biomaterials, 2018, 171, 12-22.	5.7	94
213	Effects of Ti/TiN multilayer on corrosion resistance of nickel–titanium orthodontic brackets in artificial saliva. Corrosion Science, 2007, 49, 3783-3796.	3.0	93
214	Determination of surface oxygen vacancy position in SnO2 nanocrystals by Raman spectroscopy. Solid State Communications, 2011, 151, 811-814.	0.9	93
215	Gettering of gold and copper with implanted carbon in silicon. Applied Physics Letters, 1988, 52, 889-891.	1.5	92
216	Controlled Assembly of Highly Ramanâ€Enhancing Silver Nanocap Arrays Templated by Porous Anodic Alumina Membranes. Small, 2009, 5, 2333-2337.	5.2	92

#	Article	IF	CITATIONS
217	Coaxial PANI/TiN/PANI nanotube arrays for high-performance supercapacitor electrodes. Chemical Communications, 2013, 49, 10172.	2.2	92
218	How Graphene Islands Are Unidirectionally Aligned on the Ge(110) Surface. Nano Letters, 2016, 16, 3160-3165.	4.5	92
219	Antimicrobial properties of copper plasma-modified polyethylene. Polymer, 2006, 47, 7441-7445.	1.8	91
220	Effects of Hydrogen Plasma Treatment on the Electrical and Optical Properties of ZnO Films: Identification of Hydrogen Donors in ZnO. ACS Applied Materials & Interfaces, 2010, 2, 1780-1784.	4.0	91
221	The role of the Wnt/l²-catenin pathway in the effect of implant topography on MG63 differentiation. Biomaterials, 2012, 33, 7993-8002.	5.7	91
222	Optical microcavities with tubular geometry: properties and applications. Laser and Photonics Reviews, 2014, 8, 521-547.	4.4	91
223	Numerical analysis of a photonic crystal fiber based on a surface plasmon resonance sensor with an annular analyte channel. Optics Communications, 2017, 382, 162-166.	1.0	91
224	Development and application of fuel cells in the automobile industry. Journal of Energy Storage, 2021, 42, 103124.	3.9	91
225	Near-infrared light II - assisted rapid biofilm elimination platform for bone implants at mild temperature. Biomaterials, 2021, 269, 120634.	5.7	90
226	Tin Oxide Nanoribbons with Vacancy Structures in Luminescence-Sensitive Oxygen Sensing. Nano Letters, 2009, 9, 1926-1931.	4.5	89
227	Strain effect on lattice vibration, heat capacity, and thermal conductivity of graphene. Applied Physics Letters, 2012, 101, 111904.	1.5	89
228	Novel Method for the Fabrication of Flexible Film with Oriented Arrays of Graphene in Poly(vinylidene) Tj ETQq0 10567-10573.	0 0 rgBT / 1.5	Overlock 10 T 89
229	Asymmetric carbon nanotube–MnO <sub>2</sub> two-ply yarn supercapacitors for wearable electronics. Nanotechnology, 2014, 25, 135401.	1.3	89
230	Zn/Ag micro-galvanic couples formed on titanium and osseointegration effects in the presence of S.Âaureus. Biomaterials, 2015, 65, 22-31.	5.7	89
231	Mesoporous TiO <sub>2</sub> Nanocrystals/Graphene as an Efficient Sulfur Host Material for High-Performance Lithium–Sulfur Batteries. ACS Applied Materials & Interfaces, 2016, 8, 23784-23792.	4.0	89
232	A Novel Hybrid‣ayered Organic Phototransistor Enables Efficient Intermolecular Charge Transfer and Carrier Transport for Ultrasensitive Photodetection. Advanced Materials, 2019, 31, e1900763.	11.1	89
233	UV-irradiation-induced bioactivity on TiO2 coatings with nanostructural surface. Acta Biomaterialia, 2008, 4, 544-552.	4.1	88
234	Microstructure, bioactivity and osteoblast behavior of monoclinic zirconia coating with nanostructured surface. Acta Biomaterialia, 2010, 6, 990-1000.	4.1	88

#	Article	IF	CITATIONS
235	Reduced graphene oxide encapsulated selenium nanoparticles for high-power lithium–selenium battery cathode. Journal of Power Sources, 2015, 288, 214-220.	4.0	88
236	Preparation of ultra-low dielectric constant silica/polyimide nanofiber membranes by electrospinning. Composites Part A: Applied Science and Manufacturing, 2016, 84, 292-298.	3.8	88
237	Luminescent small-diameter 3C-SiC nanocrystals fabricated via a simple chemical etching method. Nanotechnology, 2007, 18, 365603.	1.3	87
238	Recent advances in multifunctional magnetic nanoparticles and applications to biomedical diagnosis and treatment. RSC Advances, 2013, 3, 10598.	1.7	87
239	A Novel Nanomaterial of Graphene Oxide Dotted with Ni Nanoparticles Produced by Supercritical CO <sub>2</sub> -Assisted Deposition for Reducing Friction and Wear. ACS Applied Materials & Interfaces, 2015, 7, 11604-11612.	4.0	87
240	Spatially confined synthesis of vanadium nitride nanodots intercalated carbon nanosheets with ultrahigh volumetric capacitance and long life for flexible supercapacitors. Nano Energy, 2018, 51, 128-136.	8.2	87
241	Pore formation mechanism and characterization of porous NiTi shape memory alloys synthesized by capsule-free hot isostatic pressing. Acta Materialia, 2007, 55, 3437-3451.	3.8	86
242	Biodegradable poly-lactic acid based-composite reinforced unidirectionally with high-strength magnesium alloy wires. Biomaterials, 2015, 49, 135-144.	5.7	86
243	Peapod-like V2O3 nanorods encapsulated into carbon as binder-free and flexible electrodes in lithium-ion batteries. Journal of Power Sources, 2016, 331, 58-66.	4.0	86
244	Corrosion resistance of dicalcium phosphate dihydrate/poly(lactic-co-glycolic acid) hybrid coating on AZ31 magnesium alloy. Corrosion Science, 2016, 102, 209-221.	3.0	86
245	Self-selective electroless plating: An approach for fabrication of functional 1D nanomaterials. Materials Science and Engineering Reports, 2008, 61, 59-77.	14.8	85
246	Magnetic, fluorescent, and thermo-responsive Fe3O4/rare earth incorporated poly(St-NIPAM) core–shell colloidal nanoparticles in multimodal optical/magnetic resonance imaging probes. Biomaterials, 2013, 34, 2296-2306.	5.7	85
247	High-energy lithium-ion hybrid supercapacitors composed of hierarchical urchin-like WO <sub>3</sub> /C anodes and MOF-derived polyhedral hollow carbon cathodes. Nanoscale, 2016, 8, 16761-16768.	2.8	85
248	Au/Graphene Oxide Nanocomposite Synthesized in Supercritical CO <sub>2</sub> Fluid as Energy Efficient Lubricant Additive. ACS Applied Materials & Interfaces, 2017, 9, 39549-39559.	4.0	85
249	In Situ Synthesis of MoP Nanoflakes Intercalated Nâ€Doped Graphene Nanobelts from MoO <sub>3</sub> –Amine Hybrid for Highâ€Efficient Hydrogen Evolution Reaction. Small, 2018, 14, e1800667.	5.2	85
250	ZnL <sub>2</sub> -BPs Integrated Bone Scaffold under Sequential Photothermal Mediation: A Win–Win Strategy Delivering Antibacterial Therapy and Fostering Osteogenesis Thereafter. ACS Nano, 2021, 15, 17854-17869.	7.3	85
251	Functional replication of the tendon tissue microenvironment by a bioimprinted substrate and the support of tenocytic differentiation of mesenchymal stem cells. Biomaterials, 2012, 33, 7686-7698.	5.7	84
252	Bone integration capability of a series of strontiumâ€containing hydroxyapatite coatings formed by microâ€arc oxidation. Journal of Biomedical Materials Research - Part A, 2013, 101A, 2465-2480.	2.1	84

#	Article	IF	CITATIONS
253	Polymeric Nanoarchitectures on Ti-Based Implants for Antibacterial Applications. ACS Applied Materials & Interfaces, 2014, 6, 17323-17345.	4.0	84
254	Efficient Enrichment and Self-Assembly of Hybrid Nanoparticles into Removable and Magnetic SERS Substrates for Sensitive Detection of Environmental Pollutants. ACS Applied Materials & Interfaces, 2017, 9, 7472-7480.	4.0	84
255	A functionalized TiO2/Mg2TiO4 nano-layer on biodegradable magnesium implant enables superior bone-implant integration and bacterial disinfection. Biomaterials, 2019, 219, 119372.	5.7	84
256	Dispersion of linear waves in quantum plasmas. Physics of Plasmas, 2007, 14, 062102.	0.7	83
257	Thermal oxidation of titanium: Evaluation of corrosion resistance as a function of cooling rate. Materials Chemistry and Physics, 2013, 138, 565-572.	2.0	83
258	Mn <sup>2+</sup> -Bonded Reduced Graphene Oxide with Strong Radiative Recombination in Broad Visible Range Caused by Resonant Energy Transfer. Nano Letters, 2011, 11, 3951-3956.	4.5	82
259	Equivalent Circuit Derivation and Performance Analysis of a Single-Sided Linear Induction Motor Based on the Winding Function Theory. IEEE Transactions on Vehicular Technology, 2012, 61, 1515-1525.	3.9	82
260	Nanosized Carbon Black Combined with Ni <sub>2</sub> O <sub>3</sub> as "Universal―Catalysts for Synergistically Catalyzing Carbonization of Polyolefin Wastes to Synthesize Carbon Nanotubes and Application for Supercapacitors. Environmental Science & Technology, 2014, 48, 4048-4055.	4.6	82
261	Fundamentals and applications of surface-enhanced Raman spectroscopy–based biosensors. Current Opinion in Biomedical Engineering, 2020, 13, 51-59.	1.8	82
262	Freestanding, Hierarchical, and Porous Bilayered Na <sub><i>x</i></sub> V <sub>2</sub> O <sub>5</sub> · <i>n</i> H <sub>2</sub> O/rGO/CNT Composites as High-Performance Cathode Materials for Nonaqueous K-Ion Batteries and Aqueous Zinc-Ion Batteries. ACS Applied Materials & amp; Interfaces, 2020, 12, 706-716.	4.0	82
263	Effects of Carbon and Nitrogen Plasma Immersion Ion Implantation on In vitro and In vivo Biocompatibility of Titanium Alloy. ACS Applied Materials & Interfaces, 2013, 5, 1510-1516.	4.0	81
264	Facile fabrication of a robust and corrosion resistant superhydrophobic aluminum alloy surface by a novel method. RSC Advances, 2014, 4, 55556-55564.	1.7	81
265	Multilevel surface engineering of nanostructured TiO2 on carbon-fiber-reinforced polyetheretherketone. Biomaterials, 2014, 35, 5731-5740.	5.7	81
266	In situ synthesis of Ni(OH)2/TiO2 composite film on NiTi alloy for non-enzymatic glucose sensing. Sensors and Actuators B: Chemical, 2016, 232, 150-157.	4.0	80
267	Linker-free covalent immobilization of heparin, SDF-1α, and CD47 on PTFE surface for antithrombogenicity, endothelialization and anti-inflammation. Biomaterials, 2017, 140, 201-211.	5.7	80
268	Antibacterial copper-containing titanium nitride films produced by dual magnetron sputtering. Surface and Coatings Technology, 2007, 201, 8606-8609.	2.2	79
269	Ag and Ag/N2 plasma modification of polyethylene for the enhancement of antibacterial properties and cell growth/proliferation. Acta Biomaterialia, 2008, 4, 2028-2036.	4.1	79
270	Corrosion behavior of SS316L in simulated and accelerated PEMFC environments. International Journal of Hydrogen Energy, 2011, 36, 13032-13042.	3.8	79

#	Article	IF	CITATIONS
271	Systematic Study of Inherent Antibacterial Properties of Magnesium-based Biomaterials. ACS Applied Materials & Interfaces, 2016, 8, 9662-9673.	4.0	79
272	A Low ost Metalâ€Free Photocatalyst Based on Black Phosphorus. Advanced Science, 2019, 6, 1801321.	5.6	79
273	Structure and mechanical properties of magnesium alloy treated by micro-arc discharge oxidation using direct current and high-frequency bipolar pulsing modes. Materials Science & amp; Engineering A: Structural Materials: Properties, Microstructure and Processing, 2006, 435-436, 123-126.	2.6	78
274	Mechanical and tribological properties of TiC/amorphous hydrogenated carbon composite coatings fabricated by DC magnetron sputtering with and without sample bias. Diamond and Related Materials, 2007, 16, 181-186.	1.8	78
275	Magnetic and upconverted luminescent properties of multifunctional lanthanide doped cubic KGdF4 nanocrystals. Nanoscale, 2010, 2, 2805.	2.8	78
276	MXene-encapsulated hollow Fe <sub>3</sub> O <sub>4</sub> nanochains embedded in N-doped carbon nanofibers with dual electronic pathways as flexible anodes for high-performance Li-ion batteries. Nanoscale, 2021, 13, 4624-4633.	2.8	78
277	Improved electroluminescence from n-ZnO/AlN/p-GaN heterojunction light-emitting diodes. Applied Physics Letters, 2010, 96, 201102.	1.5	77
278	Folate-bovine serum albumin functionalized polymeric micelles loaded with superparamagnetic iron oxide nanoparticles for tumor targeting and magnetic resonance imaging. Acta Biomaterialia, 2015, 15, 117-126.	4.1	77
279	Oxygen Vacancy Enhanced Gas-Sensing Performance of CeO <sub>2</sub> /Graphene Heterostructure at Room Temperature. Analytical Chemistry, 2018, 90, 9821-9829.	3.2	77
280	Luminescence from colloidal 3C-SiC nanocrystals in different solvents. Applied Physics Letters, 2006, 88, 041909.	1.5	76
281	Current transport studies of ZnOâ^•p-Si heterostructures grown by plasma immersion ion implantation and deposition. Applied Physics Letters, 2006, 88, 132104.	1.5	76
282	Amorphous nickel/cobalt tungsten sulfide electrocatalysts for high-efficiency hydrogen evolution reaction. Applied Surface Science, 2015, 341, 149-156.	3.1	76
283	Tannic Acid/Fe <sup>3+</sup> /Ag Nanofilm Exhibiting Superior Photodynamic and Physical Antibacterial Activity. ACS Applied Materials & Interfaces, 2017, 9, 39657-39671.	4.0	76
284	Hierarchical CoMoO <sub>4</sub> @Co <sub>3</sub> O <sub>4</sub> nanocomposites on an ordered macro-porous electrode plate as a multi-dimensional electrode in high-performance supercapacitors. Journal of Materials Chemistry A, 2017, 5, 17312-17324.	5.2	76
285	Utilization of coal fly ash in China: a mini-review on challenges and future directions. Environmental Science and Pollution Research, 2021, 28, 18727-18740.	2.7	76
286	Fabrication of Ti–O/Ti–N duplex coatings on biomedical titanium alloys by metal plasma immersion ion implantation and reactive plasma nitriding/oxidation. Surface and Coatings Technology, 2001, 138, 296-300.	2.2	75
287	Corrosion resistance improvement of magnesium alloy using nitrogen plasma ion implantation. Surface and Coatings Technology, 2005, 198, 454-458.	2.2	75
288	Ion implantation of organisms. Materials Science and Engineering Reports, 2006, 54, 49-120.	14.8	75

#	Article	IF	CITATIONS
289	Antibacterial properties of plasma-modified and triclosan or bronopol coated polyethylene. Polymer, 2006, 47, 931-936.	1.8	75
290	Plasmonic nano-lasers. Nano Energy, 2012, 1, 25-41.	8.2	75
291	Multilayered paper-like electrodes composed of alternating stacked mesoporous Mo <sub>2</sub> N nanobelts and reduced graphene oxide for flexible all-solid-state supercapacitors. Journal of Materials Chemistry A, 2015, 3, 14617-14624.	5.2	75
292	Bimodal optical diagnostics of oral cancer based on Rose Bengal conjugated gold nanorod platform. Biomaterials, 2013, 34, 4274-4283.	5.7	74
293	Electrochemically-deposited nanostructured Co(OH) <sub>2</sub> flakes on three-dimensional ordered nickel/silicon microchannel plates for miniature supercapacitors. Journal of Materials Chemistry A, 2013, 1, 532-540.	5.2	74
294	Non-covalent doping of graphitic carbon nitride with ultrathin graphene oxide and molybdenum disulfide nanosheets: An effective binary heterojunction photocatalyst under visible light irradiation. Journal of Colloid and Interface Science, 2014, 431, 42-49.	5.0	74
295	Theoretical assessment of a highly sensitive photonic crystal fibre based on surface plasmon resonance sensor operating in the near-infrared wavelength. Journal of Modern Optics, 2019, 66, 1-6.	0.6	74
296	Electroluminescence behavior of ZnO/Si heterojunctions: Energy band alignment and interfacial microstructure. Journal of Applied Physics, 2010, 107, .	1.1	73
297	Plasma modified Mg–Nd–Zn–Zr alloy with enhanced surface corrosion resistance. Corrosion Science, 2014, 78, 121-129.	3.0	73
298	Self-assembly of mesoporous ZnCo <sub>2</sub> O <sub>4</sub> nanomaterials: density functional theory calculation and flexible all-solid-state energy storage. Journal of Materials Chemistry A, 2016, 4, 568-577.	5.2	73
299	Hydrogen induced silicon surface layer cleavage. Applied Physics Letters, 1997, 71, 1804-1806.	1.5	72
300	Plasma-Treated Biomaterials. IEEE Transactions on Plasma Science, 2007, 35, 181-187.	0.6	72
301	Texture evolution in cold-rolled AZ31 magnesium alloy during electropulsing treatment. Journal of Alloys and Compounds, 2009, 487, 309-313.	2.8	72
302	Surface structure and properties of biomedical NiTi shape memory alloy after Fenton's oxidation. Acta Biomaterialia, 2007, 3, 795-806.	4.1	71
303	Poly(ethylene glycol)/carbon quantum dot composite solid films exhibiting intense and tunable blue–red emission. Applied Surface Science, 2014, 311, 490-497.	3.1	71
304	Highly-crystalline ultrathin gadolinium doped and carbon-coated Li4Ti5O12 nanosheets for enhanced lithium storage. Journal of Power Sources, 2015, 295, 305-313.	4.0	71
305	Seamless lateral graphene p–n junctions formed by selective in situ doping for high-performance photodetectors. Nature Communications, 2018, 9, 5168.	5.8	71
306	Ultrafine Co nanodots embedded in N-doped carbon nanotubes grafted on hexagonal VN for highly efficient overall water splitting. Nano Energy, 2020, 73, 104788.	8.2	71

#	Article	IF	CITATIONS
307	Direct and Large-Area Growth of One-Dimensional ZnO Nanostructures from and on a Brass Substrate. Journal of Physical Chemistry C, 2007, 111, 5876-5881.	1.5	70
308	Porous magnetic manganese oxide nanostructures: Synthesis and their application in water treatment. Journal of Colloid and Interface Science, 2011, 359, 68-74.	5.0	70
309	Regulating Water Adhesion on Superhydrophobic TiO <sub>2</sub> Nanotube Arrays. Advanced Functional Materials, 2014, 24, 6381-6388.	7.8	70
310	Balancing the Osteogenic and Antibacterial Properties of Titanium by Codoping of Mg and Ag: An in Vitro and in Vivo Study. ACS Applied Materials & Interfaces, 2015, 7, 17826-17836.	4.0	70
311	A Highly Sensitive Dual-Core Photonic Crystal Fiber Based on a Surface Plasmon Resonance Biosensor with Silver-Graphene Layer. Plasmonics, 2017, 12, 1847-1853.	1.8	70
312	Decorated ultrathin bismuth selenide nanosheets as targeted theranostic agents for in vivo imaging guided cancer radiation therapy. NPG Asia Materials, 2017, 9, e439-e439.	3.8	70
313	Tailored Plum Puddingâ€Like Co <sub>2</sub> P/Sn Encapsulated with Carbon Nanobox Shell as Superior Anode Materials for Highâ€Performance Sodiumâ€Ion Capacitors. Advanced Energy Materials, 2019, 9, 1900091.	10.2	70
314	Surface plasmon resonance sensor based on photonic crystal fiber with indium tin oxide film. Optical Materials, 2020, 102, 109800.	1.7	70
315	Synthesis and magnetic properties of Zn1â~'xCoxO nanorods. Journal of Applied Physics, 2006, 99, 074303.	1.1	69
316	Thermal stability of titania films prepared on titanium by micro-arc oxidation. Materials Science & Engineering A: Structural Materials: Properties, Microstructure and Processing, 2008, 476, 78-82.	2.6	69
317	Recyclable and High-Sensitivity Electrochemical Biosensing Platform Composed of Carbon-Doped TiO <sub>2</sub> Nanotube Arrays. Analytical Chemistry, 2011, 83, 8138-8144.	3.2	69
318	Preparation and characterization of Cu2O–ZnO immobilized on diatomite for photocatalytic treatment of red water produced from manufacturing of TNT. Chemical Engineering Journal, 2011, 171, 61-68.	6.6	69
319	Restoration of chemosensitivity by multifunctional micelles mediated by P-gp siRNA to reverse MDR. Biomaterials, 2014, 35, 8621-8634.	5.7	69
320	Bactericidal Effects of Plasma Induced Reactive Species in Dielectric Barrier Gas–Liquid Discharge. Plasma Chemistry and Plasma Processing, 2017, 37, 415-431.	1.1	69
321	Twoâ€Dimensional Transition Metal Chalcogenides for Alkali Metal Ions Storage. ChemSusChem, 2020, 13, 1114-1154.	3.6	69
322	Photoelectrochemical Synthesis of Ammonia with Black Phosphorus. Advanced Functional Materials, 2020, 30, 2002731.	7.8	69
323	Regulation of extracellular bioactive cations in bone tissue microenvironment induces favorable osteoimmune conditions to accelerate in situ bone regeneration. Bioactive Materials, 2021, 6, 2315-2330.	8.6	69
324	Corrosion resistance of titanium ion implanted AZ91 magnesium alloy. Journal of Vacuum Science and Technology A: Vacuum, Surfaces and Films, 2007, 25, 334-339.	0.9	68

#	Article	IF	CITATIONS
325	Osteoblast behavior on polytetrafluoroethylene modified by long pulse, high frequency oxygen plasma immersion ion implantation. Biomaterials, 2010, 31, 413-419.	5.7	68
326	Characteristics of DC Gas-Liquid Phase Atmospheric-Pressure Plasma and Bacteria Inactivation Mechanism. Plasma Processes and Polymers, 2015, 12, 252-259.	1.6	68
327	Optical and Optoelectronic Properties of Black Phosphorus and Recent Photonic and Optoelectronic Applications. Small Methods, 2019, 3, 1900165.	4.6	68
328	Surface plasmon resonance chemical sensor composed of a microstructured optical fiber for the detection of an ultra-wide refractive index range and gas-liquid pollutants. Optics Express, 2021, 29, 40734.	1.7	68
329	Enhancement of surface properties of biomaterials using plasma-based technologies. Surface and Coatings Technology, 2007, 201, 8076-8082.	2.2	67
330	Intracellular pathways and nuclear localization signal peptide-mediated gene transfection by cationic polymeric nanovectors. Biomaterials, 2012, 33, 1135-1145.	5.7	67
331	Characteristics of atmospheric-pressure non-thermal N <sub>2</sub> and N <sub>2</sub> /O <sub>2</sub> gas mixture plasma jet. Journal of Applied Physics, 2014, 115, 033303.	1.1	67
332	Self-assembled magnetic fluorescent polymeric micelles for magnetic resonance and optical imaging. Biomaterials, 2014, 35, 344-355.	5.7	67
333	Hierarchical TiN nanoparticles-assembled nanopillars for flexible supercapacitors with high volumetric capacitance. Nanoscale, 2018, 10, 8728-8734.	2.8	67
334	Self-assembled anodization of NiTi alloys for biomedical applications. Applied Surface Science, 2020, 517, 146118.	3.1	67
335	From Si nanotubes to nanowires: Synthesis, characterization, and self-assembly. Journal of Crystal Growth, 2005, 277, 143-148.	0.7	66
336	Improvement of surface porosity and properties of alumina films by incorporation of Fe micrograins in micro-arc oxidation. Applied Surface Science, 2006, 253, 863-868.	3.1	66
337	Self-organized formation of silver nanowires, nanocubes and bipyramids via a solvothermal method. Acta Materialia, 2008, 56, 2508-2513.	3.8	66
338	Colorimetric and ultra-sensitive fluorescence resonance energy transfer determination of H2O2 and glucose by multi-functional Au nanoclusters. Analyst, The, 2014, 139, 1498.	1.7	66
339	Bioactivity of titanium following sodium plasma immersion ion implantation and deposition. Biomaterials, 2005, 26, 5465-5473.	5.7	65
340	Electrochemical Behavior Al[sub 2]O[sub 3]â^•Al Coated Surgical AZ91 Magnesium Alloy in Simulated Body Fluids. Journal of the Electrochemical Society, 2008, 155, C178.	1.3	65
341	Optical identification of oxygen vacancy types in SnO2 nanocrystals. Applied Physics Letters, 2013, 102, .	1.5	65
342	Effects of silicon plasma ion implantation on electrochemical corrosion behavior of biodegradable Mg–Y–RE Alloy. Corrosion Science, 2013, 69, 158-163.	3.0	65

#	Article	IF	CITATIONS
343	Surface nano-architectures and their effects on the mechanical properties and corrosion behavior of Ti-based orthopedic implants. Surface and Coatings Technology, 2013, 233, 13-26.	2.2	65
344	Eelectrochemical properties and corrosion resistance of carbon-ion-implanted magnesium. Corrosion Science, 2014, 82, 173-179.	3.0	65
345	Highly porous honeycomb manganese oxide@carbon fibers core–shell nanocables for flexible supercapacitors. Nano Energy, 2015, 13, 47-57.	8.2	65
346	Ag/AgBr-loaded mesoporous silica for rapid sterilization and promotion of wound healing. Biomaterials Science, 2018, 6, 1735-1744.	2.6	65
347	Lanthanideâ€Coordinated Black Phosphorus. Small, 2018, 14, e1801405.	5.2	65
348	Synthesis of tetragonal prismatic $\hat{I}^3$ -In2Se3 nanostructures with predominantly {110} facets and photocatalytic degradation of tetracycline. Applied Catalysis B: Environmental, 2020, 260, 118218.	10.8	65
349	Ultrathin hybrid nanobelts of single-crystalline VO2 and Poly(3,4-ethylenedioxythiophene) as cathode materials for aqueous zinc ion batteries with large capacity and high-rate capability. Journal of Power Sources, 2020, 463, 228223.	4.0	65
350	Graphene-encapsulated blackberry-like porous silicon nanospheres prepared by modest magnesiothermic reduction for high-performance lithium-ion battery anode. Rare Metals, 2021, 40, 383-392.	3.6	65
351	Overview of refractive index sensors comprising photonic crystal fibers based on the surface plasmon resonance effect [Invited]. Chinese Optics Letters, 2021, 19, 102202.	1.3	65
352	Plasma Surface Functionalized Polyetheretherketone for Enhanced Osseo-Integration at Bone-Implant Interface. ACS Applied Materials & Interfaces, 2016, 8, 3901-3911.	4.0	64
353	Dimensional-dependent antibacterial behavior on bioactive micro/nano polyetheretherketone (PEEK) arrays. Chemical Engineering Journal, 2020, 392, 123736.	6.6	64
354	Cationic fluorine-containing amphiphilic graft copolymers as DNA carriers. Biomaterials, 2010, 31, 2673-2685.	5.7	63
355	Improved corrosion resistance and cytocompatibility of magnesium alloy by two-stage cooling in thermal treatment. Corrosion Science, 2012, 59, 360-365.	3.0	63
356	Silicon Carbide Nanostructures. Engineering Materials and Processes, 2014, , .	0.2	63
357	Inactivation Effects of Nonâ€Thermal Atmosphericâ€Pressure Helium Plasma Jet on <i>Staphylococcus aureus</i> Biofilms. Plasma Processes and Polymers, 2015, 12, 827-835.	1.6	63
358	Cell-borne 2D nanomaterials for efficient cancer targeting and photothermal therapy. Biomaterials, 2017, 133, 37-48.	5.7	63
359	Black phosphorus: a two-dimensional reductant for in situ nanofabrication. Npj 2D Materials and Applications, 2017, 1, .	3.9	63
360	In vitro antimicrobial effects and mechanisms of direct current air-liquid discharge plasma on planktonic Staphylococcus aureus and Escherichia coli in liquids. Bioelectrochemistry, 2018, 121, 125-134.	2.4	63

#	Article	IF	CITATIONS
361	Conductive Mesoporous Niobium Nitride Microspheres/Nitrogen-Doped Graphene Hybrid with Efficient Polysulfide Anchoring and Catalytic Conversion for High-Performance Lithium–Sulfur Batteries. ACS Applied Materials & Interfaces, 2019, 11, 2961-2969.	4.0	63
362	Opportunities and challenges for aqueous metal-proton batteries. Matter, 2021, 4, 1252-1273.	5.0	63
363	Preparation and characterization of fluorinated acrylate copolymer latexes by miniemulsion polymerization under microwave irradiation. Journal of Fluorine Chemistry, 2010, 131, 417-425.	0.9	62
364	Ni–Cr Co-implanted 316L stainless steel as bipolar plate in polymer electrolyte membrane fuel cells. International Journal of Hydrogen Energy, 2010, 35, 690-700.	3.8	62
365	Paper-based plasmonic platform for sensitive, noninvasive, and rapid cancer screening. Biosensors and Bioelectronics, 2014, 54, 128-134.	5.3	62
366	Extracellular Electron Transfer from Aerobic Bacteria to Au-Loaded TiO <sub>2</sub> Semiconductor without Light: A New Bacteria-Killing Mechanism Other than Localized Surface Plasmon Resonance or Microbial Fuel Cells. ACS Applied Materials & Interfaces, 2016, 8, 24509-24516.	4.0	62
367	Large-Scale Synthesis and Mechanism of β-SiC Nanoparticles from Rice Husks by Low-Temperature Magnesiothermic Reduction. ACS Sustainable Chemistry and Engineering, 2016, 4, 6600-6607.	3.2	62
368	Enhancement of toughness and wear resistance by CrN/CrCN multilayered coatings for wood processing. Surface and Coatings Technology, 2018, 344, 204-213.	2.2	62
369	Experimental and theoretical investigation of reconstruction and active phases on honeycombed Ni3N-Co3N/C in water splitting. Applied Catalysis B: Environmental, 2021, 297, 120461.	10.8	62
370	Surface oxidation of NiTi shape memory alloy in a boiling aqueous solution containing hydrogen peroxide. Materials Science & Engineering A: Structural Materials: Properties, Microstructure and Processing, 2006, 417, 104-109.	2.6	61
371	Plasma surface treatment of artificial orthopedic and cardiovascular biomaterials. Surface and Coatings Technology, 2007, 201, 5601-5606.	2.2	61
372	Optical properties of rocksalt and zinc blende AlN phases: First-principles calculations. Journal of Applied Physics, 2008, 103, .	1.1	61
373	Plasma-Modified Biomaterials for Self-Antimicrobial Applications. ACS Applied Materials & Interfaces, 2011, 3, 2851-2860.	4.0	61
374	Gamma-Irradiated Carbon Nanotube Yarn As Substrate for High-Performance Fiber Supercapacitors. ACS Applied Materials & Interfaces, 2014, 6, 2553-2560.	4.0	61
375	Hierarchical 3-dimensional CoMoO <sub>4</sub> nanoflakes on a macroporous electrically conductive network with superior electrochemical performance. Journal of Materials Chemistry A, 2015, 3, 13776-13785.	5.2	61
376	Gas sensing properties of NiO/SnO2 heterojunction thin film. Sensors and Actuators B: Chemical, 2017, 252, 1163-1168.	4.0	61
377	Free-standing electrodes composed of carbon-coated Li 4 Ti 5 O 12 nanosheets and reduced graphene oxide for advanced sodium ion batteries. Journal of Power Sources, 2017, 337, 180-188.	4.0	61
378	Graphene-assisted metal transfer printing for wafer-scale integration of metal electrodes and two-dimensional materials. Nature Electronics, 2022, 5, 275-280.	13.1	61

#	Article	IF	CITATIONS
379	Formation of buried oxide in silicon using separation by plasma implantation of oxygen. Applied Physics Letters, 1995, 67, 2361-2363.	1.5	60
380	Intergrowth mechanism of silicon nanowires and silver dendrites. Journal of Electronic Materials, 2006, 35, 1879-1884.	1.0	60
381	One-step growth and field emission properties of quasialigned TiO2 nanowire/carbon nanocone core-shell nanostructure arrays on Ti substrates. Applied Physics Letters, 2008, 93, .	1.5	60
382	Removal of organic materials from TNT red water by Bamboo Charcoal adsorption. Chemical Engineering Journal, 2012, 193-194, 39-49.	6.6	60
383	Facile design of ultra-thin anodic aluminum oxide membranes for the fabrication of plasmonic nanoarrays. Nanotechnology, 2017, 28, 105301.	1.3	60
384	Neuromorphic Computing with Memristor Crossbar. Physica Status Solidi (A) Applications and Materials Science, 2018, 215, 1700875.	0.8	60
385	Achieving an acid resistant surface on magnesium alloy via bio-inspired design. Applied Surface Science, 2019, 478, 150-161.	3.1	60
386	Surface plasmon resonance sensor based on coupling effects of dual photonic crystal fibers for low refractive indexes detection. Results in Physics, 2020, 18, 103240.	2.0	60
387	Anode current effects in plasma electrolytic oxidation. Surface and Coatings Technology, 2007, 201, 5021-5024.	2.2	59
388	Synthesis and Field Emission Properties of Rutile TiO <sub>2</sub> Nanowires Arrays Grown Directly on a Ti Metal Self-Source Substrate. Journal of Nanoscience and Nanotechnology, 2009, 9, 3341-3346.	0.9	59
389	Corrosion behavior of NiTi alloy in fetal bovine serum. Electrochimica Acta, 2010, 55, 5551-5560.	2.6	59
390	Retardation of surface corrosion of biodegradable magnesium-based materials by aluminum ion implantation. Applied Surface Science, 2012, 258, 7651-7657.	3.1	59
391	Heterostructured TiO <sub>2</sub> Nanoparticles/Nanotube Arrays: Inâ€Situ Formation from Amorphous TiO <sub>2</sub> Nanotube Arrays in Water and Enhanced Photocatalytic Activity. ChemPlusChem, 2012, 77, 323-329.	1.3	59
392	Microstructure evolution and mechanical properties of vacuum-brazed C/C composite with AgCuTi foil. Materials Science & Engineering A: Structural Materials: Properties, Microstructure and Processing, 2013, 564, 192-198.	2.6	59
393	Aluminum plasmonic photocatalysis. Scientific Reports, 2015, 5, 15288.	1.6	59
394	Mitigation of Corrosion on Magnesium Alloy by Predesigned Surface Corrosion. Scientific Reports, 2015, 5, 17399.	1.6	59
395	A highly temperature-sensitive photonic crystal fiber based on surface plasmon resonance. Optics Communications, 2016, 359, 378-382.	1.0	59
396	Graphene for Energy Storage and Conversion: Synthesis and Interdisciplinary Applications. Electrochemical Energy Reviews, 2020, 3, 395-430.	13.1	59

#	Article	IF	CITATIONS
397	Evidence thatN2Ois a Stronger Oxidizing Agent than O2for the Post-Deposition Annealing of Ta2O5on Si Capacitors. Japanese Journal of Applied Physics, 1997, 36, 661-666.	0.8	58
398	Surface-enhanced Raman characteristics of Ag cap aggregates on silicon nanowire arrays. Nanotechnology, 2006, 17, 5769-5772.	1.3	58
399	Corrosion resistance and cytocompatibility of biodegradable surgical magnesium alloy coated with hydrogenated amorphous silicon. Journal of Biomedical Materials Research - Part A, 2009, 89A, 717-726.	2.1	58
400	Glycerol-Bonded 3C-SiC Nanocrystal Solid Films Exhibiting Broad and Stable Violet to Blue-Green Emission. Nano Letters, 2010, 10, 1466-1471.	4.5	58
401	Improved surface corrosion resistance of WE43 magnesium alloy by dual titanium and oxygen ion implantation. Thin Solid Films, 2013, 529, 407-411.	0.8	58
402	Engineered polycaprolactone–magnesium hybrid biodegradable porous scaffold for bone tissue engineering. Progress in Natural Science: Materials International, 2014, 24, 561-567.	1.8	58
403	Facet Cutting and Hydrogenation of In <sub>2</sub> O <sub>3</sub> Nanowires for Enhanced Photoelectrochemical Water Splitting. ACS Applied Materials & Interfaces, 2014, 6, 4081-4088.	4.0	58
404	Synthesis of mesoporous niobium nitride nanobelt arrays and their capacitive properties. Applied Surface Science, 2016, 383, 57-63.	3.1	58
405	Different-sized black phosphorus nanosheets with good cytocompatibility and high photothermal performance. RSC Advances, 2017, 7, 14618-14624.	1.7	58
406	High-performance asymmetrical supercapacitor composed of rGO-enveloped nickel phosphite hollow spheres and N/S co-doped rGO aerogel. Nano Research, 2018, 11, 1651-1663.	5.8	58
407	Highly Fluorescent and Stable Black Phosphorus Quantum Dots in Water. Small, 2018, 14, e1803132.	5.2	58
408	Crystalline Red Phosphorus Nanoribbons: Largeâ€6cale Synthesis and Electrochemical Nitrogen Fixation. Angewandte Chemie - International Edition, 2020, 59, 14383-14387.	7.2	58
409	Strategies to improve cobalt-based electrocatalysts for electrochemical water splitting. Journal of Catalysis, 2021, 398, 54-66.	3.1	58
410	Phase transformation behavior of porous NiTi alloys fabricated by capsule-free hot isostatic pressing. Journal of Alloys and Compounds, 2008, 449, 139-143.	2.8	57
411	Corrosion products on biomedical magnesium alloy soaked in simulated body fluids. Journal of Materials Research, 2009, 24, 2711-2719.	1.2	57
412	Osteogenesis Catalyzed by Titanium-Supported Silver Nanoparticles. ACS Applied Materials & Interfaces, 2017, 9, 5149-5157.	4.0	57
413	In vitro degradation kinetics of pure PLA and Mg/PLA composite: Effects of immersion temperature and compression stress. Acta Biomaterialia, 2017, 48, 468-478.	4.1	57
414	Degradable and Photocatalytic Antibacterial Au-TiO2/Sodium Alginate Nanocomposite Films for Active Food Packaging. Nanomaterials, 2018, 8, 930.	1.9	57

#	Article	IF	CITATIONS
415	Edge-Rich Black Phosphorus for Photocatalytic Nitrogen Fixation. Journal of Physical Chemistry Letters, 2020, 11, 1052-1058.	2.1	57
416	Corrosion resistance, surface mechanical properties, and cytocompatibility of plasma immersion ion implantation-treated nickel-titanium shape memory alloys. Journal of Biomedical Materials Research - Part A, 2005, 75A, 256-267.	2.1	56
417	Surface mechanical properties, corrosion resistance, and cytocompatibility of nitrogen plasma-implanted nickel–titanium alloys: A comparative study with commonly used medical grade materials. Journal of Biomedical Materials Research - Part A, 2007, 82A, 403-414.	2.1	56
418	Surface XPS characterization of NiTi shape memory alloy after advanced oxidation processes in UV/H2O2 photocatalytic system. Applied Surface Science, 2007, 253, 8507-8512.	3.1	56
419	Self-protection against corrosion of aged magnesium alloy in simulated physiological environment. Corrosion Science, 2013, 68, 279-285.	3.0	56
420	Nanostructured titanium–silver coatings with good antibacterial activity and cytocompatibility fabricated by one-step magnetron sputtering. Applied Surface Science, 2015, 355, 32-44.	3.1	56
421	Effects of annealing ambient on oxygen vacancies and phase transition temperature of VO <sub>2</sub> thin films. RSC Advances, 2016, 6, 79383-79388.	1.7	56
422	Direct anodic exfoliation of graphite onto high-density aligned graphene for large capacity supercapacitors. Nano Energy, 2017, 34, 515-523.	8.2	56
423	Low Work Function Surface Modifiers for Solutionâ€Processed Electronics: A Review. Advanced Materials Interfaces, 2018, 5, 1701404.	1.9	56
424	General synthesis of NiCo alloy nanochain arrays with thin oxide coating: a highly efficient bifunctional electrocatalyst for overall water splitting. Journal of Alloys and Compounds, 2019, 797, 1216-1223.	2.8	56
425	Direct Synthesis of Metalâ€Doped Phosphorene with Enhanced Electrocatalytic Hydrogen Evolution. Small Methods, 2019, 3, 1900083.	4.6	56
426	Biodegradable Bi <sub>2</sub> O <sub>2</sub> Se Quantum Dots for Photoacoustic Imagingâ€Guided Cancer Photothermal Therapy. Small, 2020, 16, e1905208.	5.2	56
427	Mediated Drug Release from Nanovehicles by Black Phosphorus Quantum Dots for Efficient Therapy of Chronic Obstructive Pulmonary Disease. Angewandte Chemie - International Edition, 2020, 59, 20568-20576.	7.2	56
428	Hierarchical Porous Carbon Materials Derived from Self-Template Bamboo Leaves for Lithium–Sulfur Batteries. Electrochimica Acta, 2017, 229, 352-360.	2.6	55
429	Inâ€Plane Black Phosphorus/Dicobalt Phosphide Heterostructure for Efficient Electrocatalysis. Angewandte Chemie, 2018, 130, 2630-2634.	1.6	55
430	Plasma surface modification of titanium for hard tissue replacements. Surface and Coatings Technology, 2004, 186, 227-233.	2.2	54
431	Glycine-assisted hydrothermal synthesis of peculiar porous α-Fe2O3 nanospheres with excellent gas-sensing properties. Analytica Chimica Acta, 2010, 659, 266-273.	2.6	54
432	Are all atmospheric pressure cold plasma jets electrically driven?. Applied Physics Letters, 2012, 100, .	1.5	54

#	Article	IF	CITATIONS
433	C/CrN multilayer coating for polymer electrolyte membrane fuel cell metallic bipolar plates. Journal of Power Sources, 2013, 222, 351-358.	4.0	54
434	Octahedral SnO <sub>2</sub> /Graphene Composites with Enhanced Gas-Sensing Performance at Room Temperature. ACS Applied Materials & Interfaces, 2019, 11, 12958-12967.	4.0	54
435	Recent advances of two-dimensional transition metal nitrides for energy storage and conversion applications. FlatChem, 2020, 19, 100149.	2.8	54
436	Antimicrobial polyethylene with controlled copper release. Journal of Biomedical Materials Research - Part A, 2007, 83A, 838-844.	2.1	53
437	Amperometric glucose sensor based on 3D ordered nickel–palladium nanomaterial supported by silicon MCP array. Sensors and Actuators B: Chemical, 2009, 141, 338-342.	4.0	53
438	Hot spots in highly Raman-enhancing silver nano-dendrites. Journal Physics D: Applied Physics, 2009, 42, 175403.	1.3	53
439	Effect of titanium incorporation on the structural, mechanical and biocompatible properties of DLC thin films prepared by reactive-biased target ion beam deposition method. Applied Surface Science, 2010, 257, 143-150.	3.1	53
440	Corrosion products and mechanism on NiTi shape memory alloy in physiological environment. Journal of Materials Research, 2010, 25, 350-358.	1.2	53
441	Cuprous oxide created on sepiolite: Preparation, characterization, and photocatalytic activity in treatment of red water from 2,4,6-trinitrotoluene manufacturing. Journal of Hazardous Materials, 2012, 217-218, 11-18.	6.5	53
442	Effects of zirconium and nitrogen plasma immersion ion implantation on the electrochemical corrosion behavior of Mg–Y–RE alloy in simulated body fluid and cell culture medium. Corrosion Science, 2014, 86, 239-251.	3.0	53
443	Emission from Trions in Carbon Quantum Dots. Journal of Physical Chemistry C, 2015, 119, 2956-2962.	1.5	53
444	CVD Growth of Graphene on NiTi Alloy for Enhanced Biological Activity. ACS Applied Materials & Interfaces, 2015, 7, 19876-19881.	4.0	53
445	Excellent corrosion resistance of P and Fe modified micro-arc oxidation coating on Al alloy. Journal of Alloys and Compounds, 2017, 710, 452-459.	2.8	53
446	Synthesis of lipid–black phosphorus quantum dot bilayer vesicles for near-infrared-controlled drug release. Chemical Communications, 2018, 54, 6060-6063.	2.2	53
447	Synthesis of high-quality black phosphorus sponges for all-solid-state supercapacitors. Materials Horizons, 2019, 6, 176-181.	6.4	53
448	Instrumental and process considerations for the fabrication of silicon-on-insulators (SOI) structures by plasma immersion ion implantation. IEEE Transactions on Plasma Science, 1998, 26, 79-84.	0.6	52
449	Effects of heat treatment on characteristics of porous Ni-rich NiTi SMA prepared by SHS technique. Transactions of Nonferrous Metals Society of China, 2006, 16, 49-53.	1.7	52
450	Biocompatibility of calcium and phosphorus doped diamond-like carbon thin films synthesized by plasma immersion ion implantation and deposition. Diamond and Related Materials, 2006, 15, 893-897.	1.8	52

#	Article	IF	CITATIONS
451	On the origin of light emission from porous anodic alumina formed in sulfuric acid. Solid State Communications, 2006, 137, 621-624.	0.9	52
452	Mechanism of cell repellence on quasi-aligned nanowire arrays on Ti alloy. Biomaterials, 2010, 31, 8341-8349.	5.7	52
453	Amplification of localized surface plasmon resonance signals by a gold nanorod assembly and ultra-sensitive detection of mercury. Chemical Communications, 2011, 47, 6897.	2.2	52
454	Corrosion behavior on orthopedic NiTi alloy with nanocrystalline/amorphous surface. Materials Chemistry and Physics, 2011, 126, 102-107.	2.0	52
455	High-current anodization: A novel strategy to functionalize titanium-based biomaterials. Electrochimica Acta, 2015, 173, 345-353.	2.6	52
456	Fabrication of Ni-Ti-O nanotube arrays by anodization of NiTi alloy and their potential applications. Scientific Reports, 2014, 4, 7547.	1.6	52
457	Investigation of dendritic growth and liquation cracking in laser melting deposited Inconel 718 at different laser input angles. Materials and Design, 2016, 105, 133-141.	3.3	52
458	One-Step Synthesis of Monodisperse and Hierarchically Mesostructured Silica Particles with a Thin Shell. Langmuir, 2010, 26, 13556-13563.	1.6	51
459	Immobilization of Ag nanoparticles/FGFâ€2 on a modified titanium implant surface and improved human gingival fibroblasts behavior. Journal of Biomedical Materials Research - Part A, 2011, 98A, 274-286.	2.1	51
460	Non-enzymatic hydrogen peroxide photoelectrochemical sensor based on WO3 decorated core–shell TiC/C nanofibers electrode. Electrochimica Acta, 2013, 108, 491-496.	2.6	51
461	Microstructure and mechanical properties of C/C composite/TC4 joint with inactive AgCu filler metal. Ceramics International, 2015, 41, 7021-7027.	2.3	51
462	Metabolizable Small Gold Nanorods: Size-dependent Cytotoxicity, Cell Uptake and <i>In Vivo</i> Biodistribution. ACS Biomaterials Science and Engineering, 2016, 2, 789-797.	2.6	51
463	Modulation of the mechanosensing of mesenchymal stem cells by laser-induced patterning for the acceleration of tissue reconstruction through the Wnt/l²-catenin signaling pathway activation. Acta Biomaterialia, 2020, 101, 152-167.	4.1	51
464	Photochemical Activity of Black Phosphorus for Nearâ€infrared Light Controlled In Situ Biomineralization. Advanced Science, 2020, 7, 2000439.	5.6	51
465	Formation of titanium nitride barrier layer in nickel–titanium shape memory alloys by nitrogen plasma immersion ion implantation for better corrosion resistance. Thin Solid Films, 2005, 488, 20-25.	0.8	50
466	Controlled Patterning of Plasmonic Dimers by Using an Ultrathin Nanoporous Alumina Membrane as a Shadow Mask. ACS Applied Materials & Interfaces, 2017, 9, 36199-36205.	4.0	50
467	Birefringent PCF-Based SPR Sensor for a Broad Range of Low Refractive Index Detection. IEEE Photonics Technology Letters, 2018, 30, 1471-1474.	1.3	50
468	Surface modification of polymeric materials by plasma immersion ion implantation. Nuclear Instruments & Methods in Physics Research B, 2005, 237, 417-421.	0.6	49

PAUL CHU

#	Article	IF	CITATIONS
469	Raman spectroscopy study of DLC films prepared by RF plasma and filtered cathodic arc. Surface and Coatings Technology, 2007, 201, 6734-6736.	2.2	49
470	Label-free optical biosensor based on localized surface plasmon resonance of immobilized gold nanorods. Colloids and Surfaces B: Biointerfaces, 2009, 71, 96-101.	2.5	49
471	Carbon coated stainless steel bipolar plates in polymer electrolyte membrane fuel cells. Diamond and Related Materials, 2010, 19, 1354-1361.	1.8	49
472	Controllable degradation of biomedical magnesium by chromium and oxygen dual ion implantation. Materials Letters, 2011, 65, 2171-2173.	1.3	49
473	Electrochemically deposited chitosan/Ag complex coatings on biomedical NiTi alloy for antibacterial application. Surface and Coatings Technology, 2013, 232, 370-375.	2.2	49
474	Enhanced Photocatalytic Oxygen Evolution by Crystal Cutting. Advanced Materials, 2013, 25, 2035-2039.	11.1	49
475	Thermosensitive poly(N-isopropylacrylamide-co-glycidyl methacrylate) microgels for controlled drug release. Colloids and Surfaces B: Biointerfaces, 2013, 101, 251-255.	2.5	49
476	Cubic In <sub>2</sub> O <sub>3</sub> Microparticles for Efficient Photoelectrochemical Oxygen Evolution. Journal of Physical Chemistry Letters, 2014, 5, 4298-4304.	2.1	49
477	Heterogeneous phosphorus-doped WO <sub>3â~'x</sub> /nitrogen-doped carbon nanowires with high rate and long life for advanced lithium-ion capacitors. Journal of Materials Chemistry A, 2018, 6, 6916-6921.	5.2	49
478	Recent advances in structural engineering of 2D hexagonal boron nitride electrocatalysts. Nano Energy, 2022, 91, 106661.	8.2	49
479	Ti <sub>3</sub> C <sub>2</sub> T <i><sub>X</sub></i> MXene Modified with ZnTCPP with Bacteria Capturing Capability and Enhanced Visible Light Photocatalytic Antibacterial Activity. Small, 2022, 18, .	5.2	49
480	In vivo study of Ti–O thin film fabricated by PIII. Surface and Coatings Technology, 2002, 156, 284-288.	2.2	48
481	Structure and properties of zirconia (ZrO2) films fabricated by plasma-assisted cathodic arc deposition. Journal Physics D: Applied Physics, 2007, 40, 2293-2299.	1.3	48
482	An eco-friendly and cleaner process for preparing architectural ceramics from coal fly ash: Pre-activation of coal fly ash by a mechanochemical method. Journal of Cleaner Production, 2019, 214, 419-428.	4.6	48
483	Hydrogels as Soft Ionic Conductors in Flexible and Wearable Triboelectric Nanogenerators. Advanced Science, 2022, 9, e2106008.	5.6	48
484	Anti-corrosion performance of oxidized and oxygen plasma-implanted NiTi alloys. Materials Science & Engineering A: Structural Materials: Properties, Microstructure and Processing, 2005, 390, 444-451.	2.6	47
485	Structure and microwave-absorbing properties of Fe-particle containing alumina prepared by micro-arc discharge oxidation. Surface and Coatings Technology, 2006, 201, 292-295.	2.2	47
486	Rapid degradation of biomedical magnesium induced by zinc ion implantation. Materials Letters, 2011, 65, 661-663.	1.3	47

#	Article	IF	CITATIONS
487	Tailoring of Mesenchymal Stem Cells Behavior on Plasmaâ€Modified Polytetrafluoroethylene. Advanced Materials, 2012, 24, 3315-3324.	11.1	47
488	Effects of surface alloying on electrochemical corrosion behavior of oxygen-plasma-modified biomedical magnesium alloy. Surface and Coatings Technology, 2012, 206, 3186-3195.	2.2	47
489	Size-dependent corrosion behavior and cytocompatibility of Ni–Ti–O nanotubes prepared by anodization of biomedical NiTi alloy. Corrosion Science, 2016, 103, 173-180.	3.0	47
490	Hierarchical porous carbon materials from nanosized metal-organic complex for high-performance symmetrical supercapacitor. Electrochimica Acta, 2018, 269, 580-589.	2.6	47
491	Orthopedic Implants. , 2019, , 425-439.		47
492	Three-dimensional carbon-coating silicon nanoparticles welded on carbon nanotubes composites for high-stability lithium-ion battery anodes. Applied Surface Science, 2019, 479, 896-902.	3.1	47
493	Molybdenum diselenide – black phosphorus heterostructures for electrocatalytic hydrogen evolution. Applied Surface Science, 2019, 467-468, 328-334.	3.1	47
494	Atomic-Scale Intercalation of Graphene Layers into MoSe <sub>2</sub> Nanoflower Sheets as a Highly Efficient Catalyst for Hydrogen Evolution Reaction. ACS Applied Materials & Interfaces, 2020, 12, 2460-2468.	4.0	47
495	Improvements of anti-corrosion and mechanical properties of NiTi orthopedic materials by acetylene, nitrogen and oxygen plasma immersion ion implantation. Nuclear Instruments & Methods in Physics Research B, 2005, 237, 411-416.	0.6	46
496	Thermal stability of metal-doped diamond-like carbon fabricated by dual plasma deposition. Diamond and Related Materials, 2005, 14, 1489-1493.	1.8	46
497	Characteristics and surface energy of silicon-doped diamond-like carbon films fabricated by plasma immersion ion implantation and deposition. Diamond and Related Materials, 2006, 15, 1276-1281.	1.8	46
498	Effects of coating process on the characteristics of Ag–SnO2 contact materials. Materials Chemistry and Physics, 2006, 98, 477-480.	2.0	46
499	Jeans instability in quantum magnetoplasma with resistive effects. Physics of Plasmas, 2009, 16, .	0.7	46
500	Preparation and characterization of novel nickel–palladium electrodes supported by silicon microchannel plates for direct methanol fuel cells. Journal of Power Sources, 2010, 195, 146-150.	4.0	46
501	Electron density measurements of atmospheric-pressure non-thermal N2 plasma jet by Stark broadening and irradiance intensity methods. Physics of Plasmas, 2014, 21, .	0.7	46
502	Controlling nitrogen migration through micro-nano networks. Scientific Reports, 2014, 4, 3665.	1.6	46
503	Functionalized Polymeric Membrane with Enhanced Mechanical and Biological Properties to Control the Degradation of Magnesium Alloy. Advanced Healthcare Materials, 2017, 6, 1601269.	3.9	46
504	Se-NiSe2 hybrid nanosheet arrays with self-regulated elemental Se for efficient alkaline water splitting. Journal of Materials Science and Technology, 2022, 118, 136-143.	5.6	46

#	Article	IF	CITATIONS
505	Radio-frequency plasma nitriding and nitrogen plasma immersion ion implantation of Ti-6A1-4V alloy. Surface and Coatings Technology, 1997, 93, 309-313.	2.2	45
506	Surface composition and surface energy of Teflon treated by metal plasma immersion ion implantation. Surface Science, 2004, 573, 426-432.	0.8	45
507	Hemocompatibility of nitrogen-doped, hydrogen-free diamond-like carbon prepared by nitrogen plasma immersion ion implantation-deposition. Journal of Biomedical Materials Research Part B, 2004, 70A, 107-114.	3.0	45
508	Surface structure and biomedical properties of chemically polished and electropolished NiTi shape memory alloys. Materials Science and Engineering C, 2008, 28, 1430-1434.	3.8	45
509	Rat calvaria osteoblast behavior and antibacterial properties of O2 and N2 plasma-implanted biodegradable poly(butylene succinate). Acta Biomaterialia, 2010, 6, 154-159.	4.1	45
510	Oxygen-vacancy and depth-dependent violet double-peak photoluminescence from ultrathin cuboid SnO2 nanocrystals. Applied Physics Letters, 2012, 100, 121903.	1.5	45
511	Hierarchical porous nanocomposite architectures from multi-wall carbon nanotube threaded mesoporous NaTi2(PO4)3 nanocrystals for high-performance sodium electrodes. Journal of Power Sources, 2016, 327, 580-590.	4.0	45
512	Relationship between Ni release and cytocompatibility of Ni-Ti-O nanotubes prepared on biomedical NiTi alloy. Corrosion Science, 2017, 123, 209-216.	3.0	45
513	The controlled drug release by pH-sensitive molecularly imprinted nanospheres for enhanced antibacterial activity. Materials Science and Engineering C, 2017, 77, 84-91.	3.8	45
514	Antibacterial, osteogenic, and angiogenic activities of SrTiO 3 nanotubes embedded with Ag 2 O nanoparticles. Materials Science and Engineering C, 2017, 75, 1049-1058.	3.8	45
515	Preparation of high entropy alloys and application to catalytical water electrolysis. APL Materials, 2022, 10, .	2.2	45
516	Quantum effects on Rayleighâ $\in$ "Taylor instability in magnetized plasma. Physics of Plasmas, 2008, 15, .	0.7	44
517	Crumpled N-doped carbon nanotubes encapsulated with peapod-like Ge nanoparticles for high-rate and long-life Li-ion battery anodes. Journal of Materials Chemistry A, 2016, 4, 7585-7590.	5.2	44
518	A high-sensitivity photonic crystal fiber (PCF) based on the surface plasmon resonance (SPR) biosensor for detection of density alteration in non-physiological cells (DANCE). Opto-electronics Review, 2018, 26, 50-56.	2.4	44
519	Molecular Dynamics Simulation of Nanocrack Propagation in Single-Layer MoS2Nanosheets. Journal of Physical Chemistry C, 2018, 122, 1351-1360.	1.5	44
520	Temperature-responsive tungsten doped vanadium dioxide thin film starves bacteria to death. Materials Today, 2019, 22, 35-49.	8.3	44
521	Dual light-induced <i>in situ</i> antibacterial activities of biocompatibleTiO <sub>2</sub> /MoS <sub>2</sub> /PDA/RGD nanorod arrays on titanium. Biomaterials Science, 2020, 8, 391-404.	2.6	44
522	Tuning surface topographies on biomaterials to control bacterial infection. Biomaterials Science, 2020, 8, 6840-6857.	2.6	44

#	Article	IF	CITATIONS
523	Optimization and cuttingâ€edge design of fuelâ€cell hybrid electric vehicles. International Journal of Energy Research, 2021, 45, 18392-18423.	2.2	44
524	Anti-corrosion characteristics of nitride-coated AISI 316L stainless steel coronary stents. Surface and Coatings Technology, 2006, 201, 2802-2806.	2.2	43
525	Optical and biological sensing capabilities of Au2S/AuAgS coated gold nanorods. Biomaterials, 2009, 30, 5622-5630.	5.7	43
526	XPS Study of the Bonding Properties of Lanthanum Oxide/Silicon Interface with a Trace Amount of Nitrogen Incorporation. Journal of the Electrochemical Society, 2010, 157, G49.	1.3	43
527	Effects of Water Molecules on Photoluminescence from Hierarchical Peptide Nanotubes and Water Probing Capability. Small, 2011, 7, 2801-2807.	5.2	43
528	Fabrication and degradation behavior of micro-arc oxidized biomedical magnesium alloy wires. Surface and Coatings Technology, 2012, 213, 307-312.	2.2	43
529	Synthesis of Layerâ€īunable Graphene: A Combined Kinetic Implantation and Thermal Ejection Approach. Advanced Functional Materials, 2015, 25, 3666-3675.	7.8	43
530	Large and porous carbon sheets derived from water hyacinth for high-performance supercapacitors. RSC Advances, 2016, 6, 29996-30003.	1.7	43
531	Targeting ETS1 with RNAi-based supramolecular nanoassemblies for multidrug-resistant breast cancer therapy. Journal of Controlled Release, 2017, 253, 110-121.	4.8	43
532	3D-printed nanocomposite scaffolds with tunable magnesium ionic microenvironment induce in situ bone tissue regeneration. Applied Materials Today, 2019, 16, 493-507.	2.3	43
533	Improving the plasma immersion ion implantation impact energy inside a cylindrical bore by using an auxiliary electrode. Applied Physics Letters, 1996, 69, 3815-3817.	1.5	42
534	lon-cut silicon-on-insulator fabrication with plasma immersion ion implantation. Applied Physics Letters, 1997, 71, 2767-2769.	1.5	42
535	Oxygen-induced nickel segregation in nitrogen plasma implanted AISI 304 stainless steel. Materials Science & Engineering A: Structural Materials: Properties, Microstructure and Processing, 2001, 316, 200-204.	2.6	42
536	Structure and properties of biomedical TiO2 films synthesized by dual plasma deposition. Surface and Coatings Technology, 2002, 156, 295-300.	2.2	42
537	Plasmaâ€Treated Polyethylene Surfaces for Improved Binding of Active Protein. Plasma Processes and Polymers, 2007, 4, 583-590.	1.6	42
538	Fluorescent Magnetic Fe <sub>3</sub> O <sub>4</sub> /Rare Earth Colloidal Nanoparticles for Dualâ€Modality Imaging. Small, 2013, 9, 2991-3000.	5.2	42
539	Band gap engineering design for construction of energy-levels well-matched semiconductor heterojunction with enhanced visible-light-driven photocatalytic activity. RSC Advances, 2014, 4, 41219-41227.	1.7	42
540	Ecofriendly and Biodegradable Soybean Protein Isolate Films Incorporated with ZnO Nanoparticles for Food Packaging. ACS Applied Bio Materials, 2019, 2, 2202-2207.	2.3	42

#	Article	IF	CITATIONS
541	Lubricating performances of graphene oxide and onion-like carbon as water-based lubricant additives for smooth and sand-blasted steel discs. Friction, 2020, 8, 47-57.	3.4	42
542	Calcium Phosphate Mineralized Black Phosphorous with Enhanced Functionality and Anticancer Bioactivity. Advanced Functional Materials, 2020, 30, 2003069.	7.8	42
543	Biofunctional Elements Incorporated Nano/Microstructured Coatings on Titanium Implants with Enhanced Osteogenic and Antibacterial Performance. Advanced Healthcare Materials, 2020, 9, e2000681.	3.9	42
544	Macroscale Superlubricity on Engineering Steel in the Presence of Black Phosphorus. Nano Letters, 2021, 21, 5308-5315.	4.5	42
545	Co-doped Ni3S2 porous nanocones as high-performance bifunctional electrocatalysts in water splitting. Chemical Engineering Journal, 2021, 425, 130455.	6.6	42
546	Numerical Study of Self-Heating Effects of MOSFETs Fabricated on SOAN Substrate. IEEE Transactions on Electron Devices, 2004, 51, 901-906.	1.6	41
547	Biomimetic growth of apatite on hydrogen-implanted silicon. Biomaterials, 2004, 25, 5575-5581.	5.7	41
548	Investigation of nickel suppression and cytocompatibility of surface-treated nickel-titanium shape memory alloys by using plasma immersion ion implantation. Journal of Biomedical Materials Research - Part A, 2005, 72A, 238-245.	2.1	41
549	Characteristics of nano Ti-doped SnO2 powders prepared by sol–gel method. Materials Science & Engineering A: Structural Materials: Properties, Microstructure and Processing, 2006, 426, 274-277.	2.6	41
550	Nickel release behavior, cytocompatibility, and superelasticity of oxidized porous single-phase NiTi. Journal of Biomedical Materials Research - Part A, 2007, 81A, 948-955.	2.1	41
551	Electrostatic drift modes in quantum dusty plasmas with Jeans terms. Physics of Plasmas, 2009, 16, .	0.7	41
552	Corrosion behavior and electrical conductivity of niobium implanted 316L stainless steel used as bipolar plates in polymer electrolyte membrane fuel cells. Surface and Coatings Technology, 2010, 205, 85-91.	2.2	41
553	Formation and electrochemical behavior of Al and O plasma-implanted biodegradable Mg-Y-RE alloy. Materials Chemistry and Physics, 2012, 132, 187-191.	2.0	41
554	Hybrid MnO <sub>2</sub> /C nano-composites on a macroporous electrically conductive network for supercapacitor electrodes. Journal of Materials Chemistry A, 2015, 3, 16695-16707.	5.2	41
555	Lithiation Kinetics in High-Performance Porous Vanadium Nitride Nanosheet Anode. Electrochimica Acta, 2016, 214, 201-207.	2.6	41
556	<i>In vitro</i> antimicrobial effects and mechanism of atmospheric-pressure He/O <sub>2</sub> plasma jet on <i>Staphylococcus aureus</i> biofilm. Journal Physics D: Applied Physics, 2017, 50, 105201.	1.3	41
557	Evolution of microstructures and properties of the GH4169 superalloy during short-term and high-temperature processing. Materials Science & Engineering A: Structural Materials: Properties, Microstructure and Processing, 2019, 744, 255-266.	2.6	41
558	Efficient electromagnetic wave absorption by SiC/Ni/NiO/C nanocomposites. Journal of Alloys and Compounds, 2020, 816, 152519.	2.8	41

#	Article	IF	CITATIONS
559	Near-infrared surface plasmon resonance sensor based on photonic crystal fiber with big open rings. Optik, 2020, 207, 164466.	1.4	41
560	Optoelectronic Artificial Synapses Based on Two-Dimensional Transitional-Metal Trichalcogenide. ACS Applied Materials & Interfaces, 2021, 13, 30797-30805.	4.0	41
561	Hofmeister Effect and Electrostatic Interaction Enhanced Ionic Conductive Organohydrogels for Electronic Applications. Advanced Functional Materials, 2022, 32, .	7.8	41
562	Structural analysis of arc deposited diamond-like carbon films by Raman and X-ray photoelectron spectroscopy. Materials Science and Engineering B: Solid-State Materials for Advanced Technology, 2002, 94, 95-101.	1.7	40
563	Plasma hydrogenation of strained Siâ^•SiGeâ^•Si heterostructure for layer transfer without ion implantation. Applied Physics Letters, 2005, 87, 091902.	1.5	40
564	Pd/Ni/Si-microchannel-plate-based amperometric sensor for ethanol detection. Electrochimica Acta, 2011, 56, 4197-4202.	2.6	40
565	Optical and electrical properties of ZnO:Al thin films synthesized by low-pressure pulsed laser deposition. Materials Science in Semiconductor Processing, 2011, 14, 48-51.	1.9	40
566	Interfacial reactions and zigzag groove strengthening of C/C composite and Rene N5 single crystal brazed joint. Ceramics International, 2015, 41, 11605-11610.	2.3	40
567	Fluorinated Graphene in Interface Engineering of Geâ€Based Nanoelectronics. Advanced Functional Materials, 2015, 25, 1805-1813.	7.8	40
568	Lithiated NiCo <sub>2</sub> O <sub>4</sub> Nanorods Anchored on 3D Nickel Foam Enable Homogeneous Li Plating/Stripping for High-Power Dendrite-Free Lithium Metal Anode. ACS Applied Materials & Interfaces, 2019, 11, 31824-31831.	4.0	40
569	Experimental and theoretical investigation of the control and balance of active sites on oxygen plasma-functionalized MoSe2 nanosheets for efficient hydrogen evolution reaction. Applied Catalysis B: Environmental, 2021, 288, 119983.	10.8	40
570	Silver nanocrystal superlattice coating for molecular sensing by surface-enhanced Raman spectroscopy. Applied Physics Letters, 2006, 89, 131914.	1.5	39
571	In vitro bioactivity of plasma-sprayed TiO2 coating after sodium hydroxide treatment. Surface and Coatings Technology, 2006, 200, 5487-5492.	2.2	39
572	Pump-power tunable white upconversion emission in lanthanide-doped hexagonal NaYF4 nanorods. Optical Materials, 2011, 33, 882-887.	1.7	39
573	The effect of interlayer on corrosion resistance of ceramic coating/Mg alloy substrate in simulated physiological environment. Surface and Coatings Technology, 2012, 206, 4892-4898.	2.2	39
574	Surface engineering and modification of biomaterials. Thin Solid Films, 2013, 528, 93-105.	0.8	39
575	Ni-coated Si microchannel plate electrodes in three-dimensional lithium-ion battery anodes. Electrochimica Acta, 2013, 87, 250-255.	2.6	39
576	Dual carbon layer hybridized mesoporous tin hollow spheres for fast-rechargeable and highly-stable lithium-ion battery anodes. Journal of Materials Chemistry A, 2017, 5, 14422-14429.	5.2	39

#	Article	IF	CITATIONS
577	Nonleaching Antibacterial Concept Demonstrated by In Situ Construction of 2D Nanoflakes on Magnesium. Advanced Science, 2020, 7, 1902089.	5.6	39
578	A programmed surface on polyetheretherketone for sequentially dictating osteoimmunomodulation and bone regeneration to achieve ameliorative osseointegration under osteoporotic conditions. Bioactive Materials, 2022, 14, 364-376.	8.6	39
579	Surface characteristics, mechanical properties, and cytocompatibility of oxygen plasma-implanted porous nickel titanium shape memory alloy. Journal of Biomedical Materials Research - Part A, 2006, 79A, 139-146.	2.1	38
580	Enhancement of antibacterial properties and biocompatibility of polyethylene by silver and copper plasma immersion ion implantation. Surface and Coatings Technology, 2008, 203, 909-912.	2.2	38
581	Formation mechanism and photoluminescence of AlN nanowhiskers. Journal Physics D: Applied Physics, 2008, 41, 025101.	1.3	38
582	Release of hydrogen during transformation from porous silicon to silicon oxide at normal temperature. International Journal of Hydrogen Energy, 2011, 36, 4513-4517.	3.8	38
583	New easy way preparation of core/shell structured SnO2@carbon spheres and application for lithium-ion batteries. Journal of Power Sources, 2012, 216, 475-481.	4.0	38
584	Optofluidic detection for cellular phenotyping. Lab on A Chip, 2012, 12, 3552.	3.1	38
585	Evaluation of corrosion resistance and cytocompatibility of graded metal carbon film on Ti and NiTi prepared by hybrid cathodic arc/glow discharge plasma-assisted chemical vapor deposition. Corrosion Science, 2015, 97, 126-138.	3.0	38
586	A surface-engineered multifunctional TiO2 based nano-layer simultaneously elevates the corrosion resistance, osteoconductivity and antimicrobial property of a magnesium alloy. Acta Biomaterialia, 2019, 99, 495-513.	4.1	38
587	Modulation of Phosphorene for Optimal Hydrogen Evolution Reaction. ACS Applied Materials & Interfaces, 2019, 11, 37787-37795.	4.0	38
588	Effects of Ion Energy and Density on the Plasma Etchingâ€Induced Surface Area, Edge Electrical Field, and Multivacancies in MoSe <sub>2</sub> Nanosheets for Enhancement of the Hydrogen Evolution Reaction. Small, 2020, 16, e2001470.	5.2	38
589	Additively manufactured high strength and ductility CrCoNi medium entropy alloy with hierarchical microstructure. Materials Science & Engineering A: Structural Materials: Properties, Microstructure and Processing, 2021, 820, 141545.	2.6	38
590	In vitro and in vivo characterization of novel plasma treated nickel titanium shape memory alloy for orthopedic implantation. Surface and Coatings Technology, 2007, 202, 1247-1251.	2.2	37
591	Quasi-Aligned Ag-Nb2O5 Nanobelt Arrays with Enhanced Photocatalytic and Antibacterial Activities. Journal of the American Ceramic Society, 2011, 94, 2330-2338.	1.9	37
592	Improved corrosion resistance of stainless steel 316L by Ti ion implantation. Materials Letters, 2012, 68, 450-452.	1.3	37
593	Improved corrosion resistance on biodegradable magnesium by zinc and aluminum ion implantation. Applied Surface Science, 2012, 263, 608-612.	3.1	37
594	Heterostructured Ni(OH)2–Co(OH)2 composites on 3D ordered Ni–Co nanoparticles fabricated on microchannel plates for advanced miniature supercapacitor. Journal of Alloys and Compounds, 2014, 589, 364-371.	2.8	37

#	Article	IF	CITATIONS
595	Lanthanide-integrated supramolecular polymeric nanoassembly with multiple regulation characteristics for multidrug-resistant cancer therapy. Biomaterials, 2017, 129, 83-97.	5.7	37
596	Interfacial electronic states and self-formed p–n junctions in hydrogenated MoS <sub>2</sub> /SiC heterostructure. Journal of Materials Chemistry C, 2018, 6, 4523-4530.	2.7	37
597	Structural stability and magnetic-exchange coupling in Mn-doped monolayer/bilayer MoS <sub>2</sub> . Physical Chemistry Chemical Physics, 2018, 20, 553-561.	1.3	37
598	Ultrafast hetero-assembly of monolithic interwoven V2O5 nanobelts/carbon nanotubes architectures for high-energy alkali-ion batteries. Journal of Power Sources, 2018, 395, 295-304.	4.0	37
599	Plasma-activated thermosensitive biogel as an exogenous ROS carrier for post-surgical treatment of cancer. Biomaterials, 2021, 276, 121057.	5.7	37
600	Inâ€Plane Mott–Schottky Effects Enabling Efficient Hydrogen Evolution from Mo <sub>5</sub> N <sub>6</sub> â€MoS <sub>2</sub> Heterojunction Nanosheets in Universalâ€pH Electrolytes. Small, 2022, 18, e2201137.	5.2	37
601	Special modulator for high frequency, low-voltage plasma immersion ion implantation. Review of Scientific Instruments, 1999, 70, 1824-1828.	0.6	36
602	Structure and properties of Ca-plasma-implanted titanium. Surface and Coatings Technology, 2005, 191, 43-48.	2.2	36
603	High-Sensitivity and Stable Cellular Fluorescence Imaging by Patterned Silver Nanocap Arrays. ACS Applied Materials & Interfaces, 2010, 2, 2465-2470.	4.0	36
604	Electrochemical stability of TiO2 nanotubes with different diameters in artificial saliva. Surface and Coatings Technology, 2011, 206, 63-67.	2.2	36
605	Effects of duty cycle on microstructure and corrosion behavior of TiC coatings prepared by DC pulsed plasma CVD. Applied Surface Science, 2012, 258, 3051-3057.	3.1	36
606	Hierarchical composites of conductivity controllable polyaniline layers on the exfoliated graphite for dielectric application. Composites Part A: Applied Science and Manufacturing, 2012, 43, 2039-2045.	3.8	36
607	Upregulation of BMSCs Osteogenesis by Positively-Charged Tertiary Amines on Polymeric Implants via Charge/iNOS Signaling Pathway. Scientific Reports, 2015, 5, 9369.	1.6	36
608	<i>In situ</i> growth of all-inorganic perovskite nanocrystals on black phosphorus nanosheets. Chemical Communications, 2018, 54, 2365-2368.	2.2	36
609	Tungstenâ€Doped CoP Nanoneedle Arrays Grown on Carbon Cloth as Efficient Bifunctional Electrocatalysts for Overall Water Splitting. ChemElectroChem, 2019, 6, 5229-5236.	1.7	36
610	Synergistic Antibacterial Activity of Black Phosphorus Nanosheets Modified with Titanium Aminobenzenesulfanato Complexes. ACS Applied Nano Materials, 2019, 2, 1202-1209.	2.4	36
611	Particle-in-cell and Monte Carlo simulation of the hydrogen plasma immersion ion implantation process. Journal of Applied Physics, 1999, 86, 1817-1821.	1.1	35
612	Intense blue-light emission from carbon-plasma-implanted porous silicon. Applied Physics Letters, 2001, 78, 37-39.	1.5	35

#	Article	IF	CITATIONS
613	Nitrogen plasma-implanted titanium as bipolar plates in polymer electrolyte membrane fuel cells. Journal of Power Sources, 2010, 195, 6798-6804.	4.0	35
614	The effect of the Hall term on Jeans instability in quantum magnetoplasma with resistive effects. Physics of Plasmas, 2010, 17, .	0.7	35
615	Miniature supercapacitors composed of nickel/cobalt hydroxide on nickel-coated silicon microchannel plates. Journal of Materials Chemistry, 2011, 21, 19093.	6.7	35
616	Preparation of Controllable Coreâ^'Shell Gold Nanoparticles and Its Application in Detection of Silver Ions. ACS Applied Materials & Interfaces, 2011, 3, 183-190.	4.0	35
617	Red mud/polypropylene composite with mechanical and thermal properties. Journal of Composite Materials, 2011, 45, 2811-2816.	1.2	35
618	First-principle study of energy band structure of armchair graphene nanoribbons. Solid State Communications, 2012, 152, 1089-1093.	0.9	35
619	Core–shell TiC/C nanofiber arrays decorated with copper nanoparticles for high performance non-enzymatic glucose sensing. Sensors and Actuators B: Chemical, 2014, 192, 474-479.	4.0	35
620	Enhanced ion conductivity and electrode–electrolyte interphase stability of porous Si anodes enabled by silicon nitride nanocoating for high-performance Li-ion batteries. Journal of Energy Chemistry, 2022, 69, 616-625.	7.1	35
621	Plasma immersion ion implantation of the interior surface of a large cylindrical bore using an auxiliary electrode. Journal of Applied Physics, 1998, 83, 44-49.	1.1	34
622	Kinetic model for plasma-based ion implantation of a short, cylindrical tube with auxiliary electrode. Applied Physics Letters, 1998, 72, 1826-1828.	1.5	34
623	Micro-structural and dielectric properties of porous TiO2 films synthesized on titanium alloys by micro-arc discharge oxidization. Materials Chemistry and Physics, 2006, 100, 31-33.	2.0	34
624	Surface characteristics, biocompatibility, and mechanical properties of nickel-titanium plasma-implanted with nitrogen at different implantation voltages. Journal of Biomedical Materials Research - Part A, 2007, 82A, 469-478.	2.1	34
625	A unique technology to transform inorganic nanorods into nano-networks. Nanotechnology, 2009, 20, 255302.	1.3	34
626	Core–shell TiC/C quasi-aligned nanofiber arrays on biomedical Ti6Al4V for sensitive electrochemical biosensing. Chemical Communications, 2010, 46, 6828.	2.2	34
627	Microstructural evolution in NiTi alloy subjected to surface mechanical attrition treatment and mechanism. Intermetallics, 2011, 19, 1136-1145.	1.8	34
628	Microelectrode arrays based on carbon nanomaterials: emerging electrochemical sensors for biological and environmental applications. RSC Advances, 2013, 3, 18698.	1.7	34
629	In Situ Thermal Imaging and Absolute Temperature Monitoring by Luminescent Diphenylalanine Nanotubes. Biomacromolecules, 2013, 14, 2112-2116.	2.6	34
630	Atmospheric pressure plasma jet utilizing Ar and Ar/H <sub>2</sub> O mixtures and its applications to bacteria inactivation. Chinese Physics B, 2014, 23, 075204.	0.7	34

#	Article	IF	CITATIONS
631	Recyclable Nonâ€Enzymatic Glucose Sensor Based on Ni/NiTiO <sub>3</sub> /TiO <sub>2</sub> Nanotube Arrays. ChemPlusChem, 2015, 80, 576-582.	1.3	34
632	Tunable photoluminescence from sheet-like black phosphorus crystal by electrochemical oxidation. Applied Physics Letters, 2015, 107, 021901.	1.5	34
633	General fabrication of mesoporous Nb <sub>2</sub> O <sub>5</sub> nanobelts for lithium ion battery anodes. RSC Advances, 2016, 6, 90489-90493.	1.7	34
634	Fully degradable PLA-based composite reinforced with 2D-braided Mg wires for orthopedic implants. Composites Science and Technology, 2017, 142, 180-188.	3.8	34
635	Three-dimensional tetsubo-like Co(OH)2 nanorods on a macroporous electrically conductive network as an efficient electroactive framework for the hydrogen evolution reaction. Journal of Materials Chemistry A, 2017, 5, 2629-2639.	5.2	34
636	Black Phosphorus: Bioactive Nanomaterials with Inherent and Selective Chemotherapeutic Effects. Angewandte Chemie, 2019, 131, 779-784.	1.6	34
637	A promising orthopedic implant material with enhanced osteogenic and antibacterial activity: Al2O3-coated aluminum alloy. Applied Surface Science, 2018, 457, 1025-1034.	3.1	34
638	Ex-centric core photonic crystal fiber sensor with gold nanowires based on surface plasmon resonance. Optik, 2019, 196, 163173.	1.4	34
639	A hybrid Co NPs@CNT nanocomposite as highly efficient electrocatalyst for oxygen evolution reaction. Applied Surface Science, 2020, 507, 145155.	3.1	34
640	Highly Durable and Efficient Ni-FeO <i><sub>x</sub></i> /FeNi <sub>3</sub> Electrocatalysts Synthesized by a Facile <i>In Situ</i> Combustion-Based Method for Overall Water Splitting with Large Current Densities. ACS Applied Materials & Interfaces, 2022, 14, 27842-27853.	4.0	34
641	Investigation of dose uniformity on the inner races of bearings treated by plasma immersion ion implantation. Journal of Applied Physics, 1999, 86, 120-123.	1.1	33
642	Fabrication and characterization of anodic ZnO nanoparticles. Applied Physics A: Materials Science and Processing, 2007, 86, 463-467.	1.1	33
643	Influence of Tris in simulated body fluid on degradation behavior of pure magnesium. Materials Chemistry and Physics, 2010, 124, 33-35.	2.0	33
644	Wear resistance of NiTi alloy after surface mechanical attrition treatment. Surface and Coatings Technology, 2010, 205, 506-510.	2.2	33
645	An atmospheric-pressure plasma brush driven by sub-microsecond voltage pulses. Plasma Sources Science and Technology, 2011, 20, 065009.	1.3	33
646	Structure, molecular simulation, and release of a spirin from intercalated Zn–Al-layered double hydroxides. Colloids and Surfaces B: Biointerfaces, 2015, 135, 339-345.	2.5	33
647	Design and theoretical analysis of a photonic crystal fiber based on surface plasmon resonance sensing. Journal of Nanophotonics, 2015, 9, 093050.	0.4	33
648	Strain-induced band structure and mobility modulation in graphitic blue phosphorus. Applied Surface Science, 2015, 356, 626-630.	3.1	33

#	Article	IF	CITATIONS
649	Mechanical and thermal properties of palygorskite poly(butylene succinate) nanocomposite. Applied Clay Science, 2016, 119, 96-102.	2.6	33
650	Germanium-Assisted Direct Growth of Graphene on Arbitrary Dielectric Substrates for Heating Devices. Small, 2017, 13, 1700929.	5.2	33
651	Nano mechanical and wear properties of multi-layer Ti/TiN coatings deposited on Al 7075 by high-vacuum magnetron sputtering. Thin Solid Films, 2017, 638, 96-104.	0.8	33
652	Vanadium Dioxide Nanocoating Induces Tumor Cell Death through Mitochondrial Electron Transport Chain Interruption. Global Challenges, 2019, 3, 1800058.	1.8	33
653	Design and synthesis of dendritic Co3O4@Co2(CO3)(OH)2 nanoarrays on carbon cloth for high-performance supercapacitors. Journal of Materials Science, 2020, 55, 12091-12102.	1.7	33
654	Interface Engineering-Assisted 3D-Graphene/Germanium Heterojunction for High-Performance Photodetectors. ACS Applied Materials & Interfaces, 2020, 12, 15606-15614.	4.0	33
655	Ferroelectric Enhanced Performance of a GeSn/Ge Dual-Nanowire Photodetector. Nano Letters, 2020, 20, 3872-3879.	4.5	33
656	Medium-temperature plasma immersion-ion implantation of austenitic stainless steel. Thin Solid Films, 2000, 366, 150-154.	0.8	32
657	Effect of annealing on structure and biomedical properties of amorphous hydrogenated carbon films. Surface and Coatings Technology, 2004, 186, 125-130.	2.2	32
658	Light-induced bioactive TiO2 surface. Applied Physics Letters, 2006, 88, 013905.	1.5	32
659	Control and improvement of p-type conductivity in indium and nitrogen codoped ZnO thin films. Applied Physics Letters, 2006, 89, 252113.	1.5	32
660	Temperature dependent photoluminescence from ZnO nanowires and nanosheets on brass substrate. Applied Physics Letters, 2008, 93, .	1.5	32
661	Microstructure, nickel suppression and mechanical characteristics of electropolished and photoelectrocatalytically oxidized biomedical nickel titanium shape memory alloy. Acta Biomaterialia, 2009, 5, 2238-2245.	4.1	32
662	Structural Regulation and Optical Properties of One-Dimensional ZnO Nanomaterials in Situ Grown from and on Brass Substrates. Journal of Physical Chemistry C, 2009, 113, 170-173.	1.5	32
663	Surface Characterization of Biomaterials. , 2013, , 105-174.		32
664	Evaluation of calcium chloride for synergistic demulsification of super heavy oil wastewater. Colloids and Surfaces A: Physicochemical and Engineering Aspects, 2013, 419, 46-52.	2.3	32
665	Facet-controlled synthesis and facet-dependent photocatalytic properties of SnO2 micropolyhedrons. Applied Surface Science, 2015, 349, 798-804.	3.1	32
666	MnO2–TiO2/C nanocomposite arrays for high-performance supercapacitor electrodes. Thin Solid Films, 2015, 584, 61-65.	0.8	32

#	Article	IF	CITATIONS
667	2D Material-Based Nanofibrous Membrane for Photothermal Cancer Therapy. ACS Applied Materials & Interfaces, 2018, 10, 1155-1163.	4.0	32
668	Black Phosphorus Based Multicolor Light-Modulated Transparent Memristor with Enhanced Resistive Switching Performance. ACS Applied Materials & Interfaces, 2020, 12, 25108-25114.	4.0	32
669	Sensitive and selective ctDNA detection based on functionalized black phosphorus nanosheets. Biosensors and Bioelectronics, 2020, 165, 112384.	5.3	32
670	Rice Husk-Derived Activated Carbon for Li Ion Battery Anode. Nanoscience and Nanotechnology Letters, 2014, 6, 68-71.	0.4	32
671	The effect of high-dose nitrogen plasma immersion ion implantation on silicone surfaces. Journal Physics D: Applied Physics, 2000, 33, 2869-2874.	1.3	31
672	Evolution of hydrogen and helium co-implanted single-crystal silicon during annealing. Journal of Applied Physics, 2001, 90, 3780-3786.	1.1	31
673	Germanium movement mechanism in SiGe-on-insulator fabricated by modified Ge condensation. Journal of Applied Physics, 2005, 97, 064504.	1.1	31
674	Stability of luminescent 3C-SiC nanocrystallites in aqueous solution. Physics Letters, Section A: General, Atomic and Solid State Physics, 2006, 360, 336-338.	0.9	31
675	Self-assembled growth of MgO nanosheet arrays via a micro-arc oxidation technique. Applied Surface Science, 2007, 253, 3987-3990.	3.1	31
676	Hydrothermal self-assembling of ZnO nanorods into sphere-like superstructures and their optical characteristics. Applied Surface Science, 2008, 255, 1982-1987.	3.1	31
677	Bandgap Modulation in ZnO by Size, Pressure, and Temperature. Journal of Physical Chemistry C, 2010, 114, 13370-13374.	1.5	31
678	Silver implanted 316L stainless steel as bipolar plates in polymer electrolyte membrane fuel cells. Materials Chemistry and Physics, 2011, 126, 6-11.	2.0	31
679	F and Fe co-doped TiO2 with enhanced visible light photocatalytic activity. Journal of Sol-Gel Science and Technology, 2011, 59, 387-391.	1.1	31
680	Hydrogen release from titanium hydride in foaming of orthopedic NiTi scaffolds. Acta Biomaterialia, 2011, 7, 1387-1397.	4.1	31
681	Stress-induced annihilation of Stone–Wales defects in graphene nanoribbons. Journal Physics D: Applied Physics, 2012, 45, 305303.	1.3	31
682	Biodegradable Poly(Butylene Succinate) Modified by Gas Plasmas and Their In vitro Functions as Bone Implants. ACS Applied Materials & Interfaces, 2012, 4, 4380-4386.	4.0	31
683	Preparation and characterization of a novel nickel–palladium electrode supported by silicon nanowires for direct glucose fuel cell. Electrochimica Acta, 2012, 65, 149-152.	2.6	31
684	Structure and corrosion resistance of Ti/TiC coatings fabricated by plasma immersion ion implantation and deposition on nickel–titanium. Surface and Coatings Technology, 2013, 229, 151-155.	2.2	31

#	Article	IF	CITATIONS
685	Enhanced corrosion resistance and hemocompatibility of biomedical NiTi alloy by atmospheric-pressure plasma polymerized fluorine-rich coating. Applied Surface Science, 2014, 297, 109-115.	3.1	31
686	Highly ordered Ni–Ti–O nanotubes for non-enzymatic glucose detection. Materials Science and Engineering C, 2015, 51, 37-42.	3.8	31
687	In situ random co-polycondensation for preparation of reduced graphene oxide/polyimide nanocomposites with amino-modified and chemically reduced graphene oxide. Journal of Materials Science, 2015, 50, 3860-3874.	1.7	31
688	Controlled chondrogenesis from adipose-derived stem cells by recombinant transforming growth factor-β3 fusion protein in peptide scaffolds. Acta Biomaterialia, 2015, 11, 191-203.	4.1	31
689	Anomalous but massive removal of two organic dye pollutants simultaneously. Journal of Hazardous Materials, 2016, 318, 54-60.	6.5	31
690	Effects of one-step hydrothermal treatment on the surface morphology and corrosion resistance of ZK60 magnesium alloy. Surface and Coatings Technology, 2017, 309, 490-496.	2.2	31
691	Nickel plasma modification of graphene for high-performance non-enzymatic glucose sensing. Sensors and Actuators B: Chemical, 2017, 251, 842-850.	4.0	31
692	Preparation of layered double hydroxides using boron mud and red mud industrial wastes and adsorption mechanism to phosphate. Water and Environment Journal, 2017, 31, 145-157.	1.0	31
693	Reconstructed chitosan with alkylamine for enhanced gene delivery by promoting endosomal escape. Carbohydrate Polymers, 2020, 227, 115339.	5.1	31
694	A hollow dual-core PCF-SPR sensor with gold layers on the inner and outer surfaces of the thin cladding. Results in Optics, 2020, 1, 100004.	0.9	31
695	A Quantitative Bacteria Monitoring and Killing Platform Based on Electron Transfer from Bacteria to a Semiconductor. Advanced Materials, 2020, 32, e2003616.	11.1	31
696	Enhanced interfacial adhesion and osseointegration of anodic TiO2 nanotube arrays on ultra-fine-grained titanium and underlying mechanisms. Acta Biomaterialia, 2020, 106, 360-375.	4.1	31
697	Artificial synapses with a sponge-like double-layer porous oxide memristor. NPG Asia Materials, 2021, 13, .	3.8	31
698	In situ construction of Î <sup>3</sup> -MoC/VN heterostructured electrocatalysts with strong electron coupling for highly efficient hydrogen evolution reaction. Chemical Engineering Journal, 2021, 416, 129130.	6.6	31
699	Hybrid photovoltaic-triboelectric nanogenerators for simultaneously harvesting solar and mechanical energies. Nano Energy, 2021, 89, 106376.	8.2	31
700	Separation of plasma implantation of oxygen to form silicon on insulator. Applied Physics Letters, 1997, 70, 1748-1750.	1.5	30
701	Charging of dielectric substrate materials during plasma immersion ion implantation. Nuclear Instruments & Methods in Physics Research B, 2002, 187, 485-491.	0.6	30
702	Effects of pretreatment by ion implantation and interlayer on adhesion between aluminum substrate and TiN film. Thin Solid Films, 2005, 493, 152-159.	0.8	30

#	Article	IF	CITATIONS
703	Synthesis and optical properties of germanium nanorod array fabricated on porous anodic alumina and Si-based templates. Applied Physics Letters, 2005, 86, 021111.	1.5	30
704	Hemocompatibility of lanthanum oxide films fabricated by dual plasma deposition. Thin Solid Films, 2006, 515, 1219-1222.	0.8	30
705	Control of interfacial silicate between HfO2 and Si by high concentration ozone. Applied Physics Letters, 2006, 88, 072903.	1.5	30
706	Corrosion resistance of ZrO <sub>2</sub> –Zr-coated biodegradable surgical magnesium alloy. Journal of Materials Research, 2008, 23, 312-319.	1.2	30
707	Surface-Dependent Self-Assembly of Conducting Polypyrrole Nanotube Arrays in Template-Free Electrochemical Polymerization. ACS Applied Materials & Interfaces, 2014, 6, 10946-10951.	4.0	30
708	Genetic effects of an air discharge plasma on <i>Staphylococcus aureus</i> at the gene transcription level. Applied Physics Letters, 2015, 106, .	1.5	30
709	Porous Dual‣ayered MoO <sub><i>x</i></sub> Nanotube Arrays with Highly Conductive TiN Cores for Supercapacitors. ChemElectroChem, 2015, 2, 512-517.	1.7	30
710	Effects of high concentration of Benzotriazole on corrosion behavior of nanostructured titania-alumina composite coating deposited on Al 2024 by sol-gel method. Surface and Coatings Technology, 2017, 321, 36-44.	2.2	30
711	InSe Nanosheets for Efficient NIR-II-Responsive Drug Release. ACS Applied Materials & Interfaces, 2019, 11, 27521-27528.	4.0	30
712	Improving the performance of light-emitting diodes via plasmonic-based strategies. Journal of Applied Physics, 2020, 127, .	1.1	30
713	A Comparison of Defect States in Tantalum Pentoxide (Ta2O5) Films after Rapid Thermal Annealing inO2orN2Oby Zero-Bias Thermally Stimulated Current Spectroscopy. Japanese Journal of Applied Physics, 1996, 35, 2599-2604.	0.8	29
714	Effects of the auxiliary electrode radius during plasma immersion ion implantation of a small cylindrical bore. Applied Physics Letters, 1997, 71, 1035-1037.	1.5	29
715	Direct current plasma implantation using a grounded conducting grid. Journal of Applied Physics, 2000, 87, 4094-4097.	1.1	29
716	Enhancement of implantation energy using a conducting grid in plasma immersion ion implantation of dielectric/polymeric materials. Review of Scientific Instruments, 2003, 74, 3697-3700.	0.6	29
717	Nucleation and growth of calcium–phosphate on Ca-implanted titanium surface. Surface Science, 2006, 600, 651-656.	0.8	29
718	Vacuum electron field emission from SnO2 nanowhiskers annealed in N2 and O2 atmospheres. Applied Physics Letters, 2006, 88, 013109.	1.5	29
719	Vascular lumen simulation and highly-sensitive nitric oxide detection using three-dimensional gelatin chip coupled to TiC/C nanowire arrays microelectrode. Lab on A Chip, 2012, 12, 4249.	3.1	29
720	Water-Sensitive High-Frequency Molecular Vibrations in Self-Assembled Diphenylalanine Nanotubes. Journal of Physical Chemistry C, 2012, 116, 9793-9799.	1.5	29

#	Article	IF	CITATIONS
721	Dual-emitting nanocomposites derived from rare-earth compound nanotubes for ratiometric fluorescence sensing applications. Nanoscale, 2013, 5, 1629.	2.8	29
722	Synthesis of hollow rare-earth compound nanoparticles by a universal sacrificial template method. CrystEngComm, 2014, 16, 6141-6148.	1.3	29
723	Facet-engineered CeO <sub>2</sub> /graphene composites for enhanced NO <sub>2</sub> gas-sensing. Journal of Materials Chemistry C, 2017, 5, 6973-6981.	2.7	29
724	Core-shell CoMoO4@Ni(OH)2 on ordered macro-porous electrode plate for high-performance supercapacitor. Electrochimica Acta, 2018, 283, 538-547.	2.6	29
725	Spatially controlled synthesis of superlattice-like SnS/nitrogen-doped graphene hybrid nanobelts as high-rate and durable anode materials for sodium-ion batteries. Journal of Materials Chemistry A, 2019, 7, 27475-27483.	5.2	29
726	Ni <sub>3</sub> S <sub>2</sub> Nanocomposite Structures Doped with Zn and Co as Long-Lifetime, High-Energy-Density, and Binder-Free Cathodes in Flexible Aqueous Nickel-Zinc Batteries. ACS Applied Materials & Interfaces, 2021, 13, 34292-34300.	4.0	29
727	Improved corrosion and wear resistance of micro-arc oxidation coatings on the 2024 aluminum alloy by incorporation of quasi-two-dimensional sericite microplates. Applied Surface Science, 2022, 585, 152693.	3.1	29
728	Applications of plasma immersion ion implantation in microelectronics — a brief review. Surface and Coatings Technology, 2001, 136, 151-156.	2.2	28
729	Molybdenum–carbon film fabricated using metal cathodic arc and acetylene dual plasma deposition. Surface and Coatings Technology, 2004, 186, 112-117.	2.2	28
730	Early apatite deposition and osteoblast growth on plasma-sprayed dicalcium silicate coating. Journal of Biomedical Materials Research - Part A, 2005, 74A, 356-365.	2.1	28
731	Effects of NH3, O2, and N2 co-implantation on Cu out-diffusion and antimicrobial properties of copper plasma-implanted polyethylene. Applied Surface Science, 2007, 253, 8981-8985.	3.1	28
732	Applications of plasma-based technology to microelectronics and biomedical engineering. Surface and Coatings Technology, 2009, 203, 2793-2798.	2.2	28
733	Recent applications of plasma-based ion implantation and deposition to microelectronic, nano-structured, and biomedical materials. Surface and Coatings Technology, 2010, 204, 2853-2863.	2.2	28
734	Tunable Silver Nanocap Superlattice Arrays for Surface-Enhanced Raman Scattering. Journal of Physical Chemistry C, 2011, 115, 24328-24333.	1.5	28
735	Carbonâ€Nanotubeâ€Based Stimuliâ€Responsive Controlledâ€Release System. Chemistry - A European Journal, 2011, 17, 4454-4459.	1.7	28
736	Ultrathin Amorphous Alumina Nanoparticles with Quantum-Confined Oxygen-Vacancy-Induced Blue Photoluminescence as Fluorescent Biological Labels. Journal of Physical Chemistry C, 2012, 116, 2356-2362.	1.5	28
737	N-doped SnO2 nanocrystals with green emission dependent upon mutual effects of nitrogen dopant and oxygen vacancy. Acta Materialia, 2013, 61, 7342-7347.	3.8	28
738	Specific wave interface and its formation during magnetic pulse welding. Applied Physics Letters, 2014, 105, 221901.	1.5	28

#	Article	IF	CITATIONS
739	Sensitive and Robust Colorimetric Sensing of Sulfide Anion by Plasmonic Nanosensors Based on Quick Crystal Growth. Plasmonics, 2014, 9, 11-16.	1.8	28
740	Removal of organic pollutants from super heavy oil wastewater by lignite activated coke. Colloids and Surfaces A: Physicochemical and Engineering Aspects, 2014, 447, 120-130.	2.3	28
741	Antibacterial and mechanical properties of honeycomb ceramic materials incorporated with silver and zinc. Materials & Design, 2014, 59, 461-465.	5.1	28
742	Antibacterial and osteoinductive capability of orthopedic materials via cation–π interaction mediated positive charge. Journal of Materials Chemistry B, 2015, 3, 733-737.	2.9	28
743	Effects of cerium ion implantation on the corrosion behavior of magnesium in different biological media. Surface and Coatings Technology, 2016, 306, 6-10.	2.2	28
744	Lactose-Functionalized Gold Nanorods for Sensitive and Rapid Serological Diagnosis of Cancer. ACS Applied Materials & Interfaces, 2016, 8, 5813-5820.	4.0	28
745	Self-passivating carbon film as bipolar plate protective coating in polymer electrolyte membrane fuel cell. International Journal of Hydrogen Energy, 2016, 41, 5783-5792.	3.8	28
746	Gypsum blocks produced from TiO <sub>2</sub> production by-products. Environmental Technology (United Kingdom), 2016, 37, 1094-1100.	1.2	28
747	Corrosion behavior of reactive sputtered Ti/TiN nanostructured coating and effects of intermediate titanium layer on self-healing properties. Surface and Coatings Technology, 2017, 326, 156-164.	2.2	28
748	Construction of perfluorohexane/IR780@liposome coating on Ti for rapid bacteria killing under permeable near infrared light. Biomaterials Science, 2018, 6, 2460-2471.	2.6	28
749	Vertical kinetically oriented MoS <sub>2</sub> –Mo <sub>2</sub> N heterostructures on carbon cloth: a highly efficient hydrogen evolution electrocatalyst. Sustainable Energy and Fuels, 2020, 4, 2201-2207.	2.5	28
750	Simultaneous application of diamond-like carbon coating and surface amination on polyether ether ketone: Towards superior mechanical performance and osseointegration. Smart Materials in Medicine, 2021, 2, 219-228.	3.7	28
751	Recent progress and perspective of cobalt-based catalysts for water splitting: design and nanoarchitectonics. Materials Today Energy, 2022, 23, 100911.	2.5	28
752	Surface and interface control of black phosphorus. CheM, 2022, 8, 632-662.	5.8	28
753	Improvement of tribological properties of 9Cr18 bearing steel using metal and nitrogen plasma-immersion ion implantation. Surface and Coatings Technology, 1999, 115, 234-238.	2.2	27
754	Experimental investigation of the electrical characteristics and initiation dynamics of pulsed high-voltage glow discharge. Journal Physics D: Applied Physics, 2001, 34, 354-359.	1.3	27
755	Electrical properties of AlN thin films prepared by ion beam enhanced deposition. Surface and Coatings Technology, 2005, 196, 130-134.	2.2	27
756	Investigation of plasma hydrogenation and trapping mechanism for layer transfer. Applied Physics Letters, 2005, 86, 031904.	1.5	27

#	Article	IF	CITATIONS
757	Nitrogen plasma-implanted nickel titanium alloys for orthopedic use. Surface and Coatings Technology, 2007, 201, 5607-5612.	2.2	27
758	Graded phase structure in the surface layer of NiTi alloy processed by surface severe plastic deformation. Scripta Materialia, 2011, 64, 1011-1014.	2.6	27
759	Recent developments in optofluidic-surface-enhanced Raman scattering systems: Design, assembly, and advantages. Journal of Materials Research, 2011, 26, 170-185.	1.2	27
760	Achieving significantly enhanced visible-light photocatalytic efficiency using a polyelectrolyte: the composites of exfoliated titania nanosheets, graphene, and poly(diallyl-dimethyl-ammonium chloride). Nanoscale, 2015, 7, 14002-14009.	2.8	27
761	Effects of Atmospheric-Pressure Nonthermal Nitrogen and Air Plasma on Bacteria Inactivation. IEEE Transactions on Plasma Science, 2016, 44, 2699-2707.	0.6	27
762	Ultrahigh quantum efficiency photodetector and ultrafast reversible surface wettability transition of square In2O3 nanowires. Nano Research, 2017, 10, 2772-2781.	5.8	27
763	Excellent adhered thick diamond-like carbon coatings by optimizing hetero-interfaces with sequential highly energetic Cr and C ion treatment. Journal of Alloys and Compounds, 2018, 735, 155-162.	2.8	27
764	Antibacterial and Cytocompatible Nanoengineered Silk-Based Materials for Orthopedic Implants and Tissue Engineering. ACS Applied Materials & amp; Interfaces, 2019, 11, 31605-31614.	4.0	27
765	Flexible Surface-Enhanced Raman Scattering Chip: A Universal Platform for Real-Time Interfacial Molecular Analysis with Femtomolar Sensitivity. ACS Applied Materials & Interfaces, 2020, 12, 54174-54180.	4.0	27
766	Stepwise 3D-spatio-temporal magnesium cationic niche: Nanocomposite scaffold mediated microenvironment for modulating intramembranous ossification. Bioactive Materials, 2021, 6, 503-519.	8.6	27
767	Surface plasmon resonance sensor based on U-shaped photonic quasi-crystal fiber. Applied Optics, 2021, 60, 1761.	0.9	27
768	Hydrogen permeation behavior and mechanism of multi-layered graphene coatings and mitigation of hydrogen embrittlement of pipe steel. Applied Surface Science, 2022, 573, 151529.	3.1	27
769	The importance of bias pulse rise time for determining shallow implanted dose in plasma immersion ion implantation. Applied Physics Letters, 2003, 82, 1827-1829.	1.5	26
770	Origin of the 370-nm luminescence in Si oxide nanostructures. Applied Physics Letters, 2005, 86, 201906.	1.5	26
771	Water plasma implantation/oxidation of magnesium alloys for corrosion resistance. Nuclear Instruments & Methods in Physics Research B, 2006, 242, 300-302.	0.6	26
772	Silver fractal networks for surface-enhanced Raman scattering substrates. Applied Surface Science, 2008, 254, 5399-5402.	3.1	26
773	Infrared reflection by alumina films produced on aluminum alloy by plasma electrolytic oxidation. Materials Chemistry and Physics, 2009, 114, 398-401.	2.0	26
774	Tailoring light emission properties of organic emitter by coupling to resonance-tuned silver nanoantenna arrays. Applied Physics Letters, 2009, 95, .	1.5	26

#	Article	IF	CITATIONS
775	Corrosion behavior of DLC-coated NiTi alloy in the presence of serum proteins. Diamond and Related Materials, 2010, 19, 1230-1234.	1.8	26
776	Fabrication, properties, and cytocompatibility of ZrC film on electropolished NiTi shape memory alloy. Materials Science and Engineering C, 2011, 31, 423-427.	3.8	26
777	Surfaced-enhanced cellular fluorescence imaging. Progress in Surface Science, 2012, 87, 23-45.	3.8	26
778	In situ probing of intracellular pH by fluorescence from inorganic nanoparticles. Biomaterials, 2013, 34, 9183-9189.	5.7	26
779	Tribological properties of polyimide coatings filled with PTFE and surfaceâ€modified nanoâ€Si <sub>3</sub> N <sub>4</sub> . Journal of Applied Polymer Science, 2014, 131, .	1.3	26
780	Glucose oxidase immobilization platform based on ZnO nanowires supported by silicon nanowires for glucose biosensing. Microelectronic Engineering, 2016, 149, 153-158.	1.1	26
781	In situ Synthesis of V <sub>2</sub> O <sub>3</sub> â€Intercalated Nâ€doped Graphene Nanobelts from VO <sub><i>x</i></sub> â€Amine Hybrid as Highâ€Performance Anode Material for Alkaliâ€Ion Batteries. ChemElectroChem, 2018, 5, 1387-1393.	1.7	26
782	Calcium phosphate coating on biomedical WE43 magnesium alloy pretreated with a magnesium phosphate layer for corrosion protection. Surface and Coatings Technology, 2020, 401, 126248.	2.2	26
783	In situ Synthesizing Carbon-Based Film by Tribo-Induced Catalytic Degradation of Poly-α-Olefin Oil for Reducing Friction and Wear. Langmuir, 2020, 36, 10555-10564.	1.6	26
784	Sandwich-Structured Transition Metal Oxide/Graphene/Carbon Nanotube Composite Yarn Electrodes for Flexible Two-Ply Yarn Supercapacitors. Industrial & Engineering Chemistry Research, 2020, 59, 5752-5759.	1.8	26
785	Bioactive phospho-therapy with black phosphorus for <i>in vivo</i> tumor suppression. Theranostics, 2020, 10, 4720-4736.	4.6	26
786	Plasma Engineering of Basal Sulfur Sites on MoS <sub>2</sub> @Ni <sub>3</sub> S <sub>2</sub> Nanorods for the Alkaline Hydrogen Evolution Reaction. Advanced Science, 2022, 9, e2104774.	5.6	26
787	Interface Polarization Strengthened Microwave Catalysis of MoS <sub>2</sub> /FeS/Rhein for the Therapy of Bacteriaâ€Infected Osteomyelitis. Advanced Functional Materials, 2022, 32, .	7.8	26
788	Semiconductor applications of plasma immersion ion implantation. Plasma Physics and Controlled Fusion, 2003, 45, 555-570.	0.9	25
789	Hybrid processes based on plasma immersion ion implantation: a brief review. Surface and Coatings Technology, 2004, 186, 190-195.	2.2	25
790	Bioconductivity and mechanical properties of plasma-sprayed dicalcium silicate/zirconia composite coating. Materials Science and Engineering C, 2005, 25, 509-515.	3.8	25
791	Room-temperature electrosynthesized ZnO thin film with strong (002) orientation and its optical properties. Applied Surface Science, 2006, 252, 2973-2977.	3.1	25
792	Enhanced and tunable blue luminescence from CdS nanocrystal–polymer composites. Scripta Materialia, 2006, 55, 1123-1126.	2.6	25

#	Article	IF	CITATIONS
793	Surface antibacterial characteristics of plasma-modified polyethylene. Biopolymers, 2006, 83, 62-68.	1.2	25
794	Hemocompatibility and antibacterial properties of lanthanum oxide films synthesized by dual plasma deposition. Journal of Biomedical Materials Research - Part A, 2008, 87A, 1027-1033.	2.1	25
795	Mechanical properties of Al2O3/Al bi-layer coated AZ91 magnesium alloy. Thin Solid Films, 2009, 517, 5357-5360.	0.8	25
796	Influence of N2 partial pressure on mechanical properties of (Ti,Al)N films deposited by reactive magnetron sputtering. Vacuum, 2009, 83, 1057-1059.	1.6	25
797	Diffusion-controlled formation mechanism of dual-phase structure during Al induced crystallization of SiGe. Applied Physics Letters, 2012, 100, .	1.5	25
798	Effect of processing conditions on poly(butylene succinate) foam materials. Journal of Applied Polymer Science, 2012, 126, 756-761.	1.3	25
799	Silver Nanovoid Arrays for Surface-Enhanced Raman Scattering. Langmuir, 2012, 28, 8799-8803.	1.6	25
800	Progress in direct-current plasma immersion ion implantation and recent applications of plasma immersion ion implantation and deposition. Surface and Coatings Technology, 2013, 229, 2-11.	2.2	25
801	Microstructure and surface properties of chromium-doped diamond-like carbon thin films fabricated by high power pulsed magnetron sputtering. Applied Surface Science, 2013, 276, 31-36.	3.1	25
802	Investigation of activated oxygen molecules on the surface of Y2O3 nanocrystals by Raman scattering. Journal of Applied Physics, 2013, 114, .	1.1	25
803	Hydrothermal synthesis of perovskite-type MTiO <sub>3</sub> (M = Zn, Co,) Tj ETQq1 1 0.784314 rgBT /Overlocl 2014, 16, 10280-10285.	k 10 Tf 50 1.3	347 Td (Ni) 25
804	Asymmetrical Supercapacitor Composed of Thin Co(OH)2 Nanoflakes on Three-Dimensional Ni/Si Microchannel Plates with Superior Electrochemical Performance. Electrochimica Acta, 2014, 149, 18-27.	2.6	25
805	Effects of external stress on biodegradable orthopedic materials: A review. Bioactive Materials, 2016, 1, 77-84.	8.6	25
806	The modulation of stem cell behaviors by functionalized nanoceramic coatings on Ti-based implants. Bioactive Materials, 2016, 1, 65-76.	8.6	25
807	Long-term antibacterial characteristics and cytocompatibility of titania nanotubes loaded with Au nanoparticles without photocatalytic effects. Applied Surface Science, 2017, 414, 230-237.	3.1	25
808	Wrinkled Single-Crystalline Germanium Nanomembranes for Stretchable Photodetectors. IEEE Transactions on Electron Devices, 2017, 64, 1985-1990.	1.6	25
809	A Highly Sensitive SPR Sensors Based on Two Parallel PCFs for Low Refractive Index Detection. IEEE Photonics Journal, 2018, 10, 1-10.	1.0	25
810	Enhanced corrosion resistance, antibacterial properties, and biocompatibility by hierarchical hydroxyapatite/ciprofloxacin-calcium phosphate coating on nitrided NiTi alloy. Materials Science and Engineering C, 2021, 118, 111524.	3.8	25

#	Article	IF	CITATIONS
811	Ultra-short and dual-core photonic crystal fiber polarization splitter composed of metal and gallium arsenide. Optik, 2021, 226, 165779.	1.4	25
812	Corrosion Behavior and Biocompatibility of Diamond-like Carbon-Coated Zinc: An In Vitro Study. ACS Omega, 2021, 6, 9843-9851.	1.6	25
813	Waste-glass-derived silicon/CNTs composite with strong Si-C covalent bonding for advanced anode materials in lithium-ion batteries. Applied Surface Science, 2021, 563, 150280.	3.1	25
814	A high-performance electrocatalyst composed of nickel clusters encapsulated with a carbon network on TiN nanaowire arrays for the oxygen evolution reaction. Applied Surface Science, 2021, 567, 150779.	3.1	25
815	The electrical, thermal, and thermoelectric properties of black phosphorus. APL Materials, 2020, 8, .	2.2	25
816	Defect states responsible for leakage current in Ta2O5films on Si due to Si contamination from the substrate. Journal of Applied Physics, 1996, 79, 8841-8843.	1.1	24
817	Microcavity engineering by plasma immersion ion implantation. Materials Chemistry and Physics, 1998, 57, 1-16.	2.0	24
818	Sample stage induced dose and energy nonuniformity in plasma immersion ion implantation of silicon. Applied Physics Letters, 1998, 73, 202-204.	1.5	24
819	Accurate determination of pulsed current waveform in plasma immersion ion implantation processes. Journal of Applied Physics, 1999, 86, 3567-3570.	1.1	24
820	Improvement of interfacial and dielectric properties of sputtered Ta2O5 thin films by substrate biasing and the underlying mechanism. Journal of Applied Physics, 2005, 97, 114106.	1.1	24
821	Photoluminescence from 8-hydroxy quinoline aluminum embedded in porous anodic alumina membrane. Applied Physics Letters, 2005, 87, 151910.	1.5	24
822	XPS and biocompatibility studies of titania film on anodized NiTi shape memory alloy. Journal of Materials Science: Materials in Medicine, 2009, 20, 223-228.	1.7	24
823	Synthesis and properties of fluorineâ€containing amphiphilic graft copolymer P(HFMA)â€gâ€P(SPEG). Journal of Polymer Science Part A, 2009, 47, 4895-4907.	2.5	24
824	Nonenzymatic glucose sensor based on over-oxidized polypyrrole modified Pd/Si microchannel plate electrode. Biosensors and Bioelectronics, 2011, 26, 2579-2584.	5.3	24
825	Persistent photoconductivity in ZnO nanostructures induced by surface oxygen vacancy. Physica Status Solidi - Rapid Research Letters, 2012, 6, 117-119.	1.2	24
826	Biological response of endothelial cells to diamondâ€like carbonâ€coated NiTi alloy. Journal of Biomedical Materials Research - Part A, 2012, 100A, 496-506.	2.1	24
827	Interface analysis of inorganic films on polyimide with atomic oxygen exposure. Surface and Coatings Technology, 2013, 216, 121-126.	2.2	24
828	Resonant Raman scattering from CdS nanocrystals enhanced by interstitial Mn. Applied Physics Letters, 2013, 102, .	1.5	24

#	Article	IF	CITATIONS
829	Multifunctional cationic polymer decorated and drug intercalated layered silicate (NLS) for early gastric cancer prevention. Biomaterials, 2014, 35, 3298-3308.	5.7	24
830	Surface modification of biomedical magnesium alloy wires by micro-arc oxidation. Transactions of Nonferrous Metals Society of China, 2014, 24, 1058-1064.	1.7	24
831	Plasmon-induced broadband fluorescence enhancement on Al-Ag bimetallic substrates. Scientific Reports, 2014, 4, 6014.	1.6	24
832	Temperature and strain-rate effects on the deformation behaviors of nano-crystalline graphene sheets. European Physical Journal B, 2015, 88, 1.	0.6	24
833	Tuning of electronic states and magnetic polarization in monolayered MoS2 by codoping with transition metals and nonmetals. Journal of Materials Science, 2016, 51, 9514-9525.	1.7	24
834	Optical Identification of Topological Defect Types in Monolayer Arsenene by First-Principles Calculation. Journal of Physical Chemistry C, 2016, 120, 24917-24924.	1.5	24
835	Three-dimensional homo-nanostructured MnO <sub>2</sub> /nanographene membranes on a macroporous electrically conductive network for high performance supercapacitors. Journal of Materials Chemistry A, 2016, 4, 11317-11329.	5.2	24
836	Protein-assisted assembly of mesoporous nanocrystals and carbon nanotubes for self-supporting high-performance sodium electrodes. Journal of Materials Chemistry A, 2017, 5, 2749-2758.	5.2	24
837	Intertwined Nitrogenâ€Doped Carbon Nanotubes for Highâ€Rate and Longâ€Life Sodiumâ€Ion Battery Anodes. ChemElectroChem, 2017, 4, 2542-2546.	1.7	24
838	Investigation of nano-structured Zirconium oxide film on Ti6Al4V substrate to improve tribological properties prepared by PIII&D. Applied Surface Science, 2017, 394, 586-597.	3.1	24
839	Interconnected nanoporous carbon structure delivering enhanced mass transport and conductivity toward exceptional performance in supercapacitor. Journal of Power Sources, 2019, 435, 226811.	4.0	24
840	Stability and Repeatability of a Karst-like Hierarchical Porous Silicon Oxide-Based Memristor. ACS Applied Materials & Interfaces, 2019, 11, 21734-21740.	4.0	24
841	Hierarchical MoS <sub>2</sub> @Nâ€Doped Carbon Hollow Spheres with Enhanced Performance in Sodium Dualâ€lon Batteries. ChemElectroChem, 2019, 6, 661-667.	1.7	24
842	Rapid and scalable production of high-quality phosphorene by plasma–liquid technology. Chemical Communications, 2020, 56, 221-224.	2.2	24
843	Hierarchical micro-flowers self-assembled from SnS monolayers and nitrogen-doped graphene lamellar nanosheets as advanced anode for lithium-ion battery. Electrochimica Acta, 2020, 331, 135292.	2.6	24
844	Facile Synthesis of MnO <sub>2</sub> /Ti <sub>3</sub> C <sub>2</sub> T <sub>x</sub> /CC as Positive Electrode of All‣olid‣tate Flexible Asymmetric Supercapacitor. ChemistrySelect, 2020, 5, 14768-14775.	0.7	24
845	High-performance multi-dimensional nitrogen-doped N+MnO2@TiC/C electrodes for supercapacitors. Electrochimica Acta, 2021, 370, 137716.	2.6	24
846	A novel self-branching MnCo2O4/ nanographene hybrid composites on macroporous electrically conductive network as bifunctional electrodes for boosting miniature supercapacitors and sodium ion batteries. Journal of Alloys and Compounds, 2020, 846, 155720.	2.8	24

#	Article	IF	CITATIONS
847	Direct temperature monitoring for semiconductors in plasma immersion ion implantation. Review of Scientific Instruments, 2000, 71, 2839-2842.	0.6	23
848	Damage in hydrogen plasma implanted silicon. Journal of Applied Physics, 2001, 90, 1735-1739.	1.1	23
849	Solvent effect on light-emitting property of Si nanocrystals. Physics Letters, Section A: General, Atomic and Solid State Physics, 2005, 334, 447-452.	0.9	23
850	Self-assembled growth and enhanced blue emission of SiOxNy-capped silicon nanowire arrays. Applied Physics Letters, 2005, 86, 193111.	1.5	23
851	Bioactivity of plasma implanted biomaterials. Nuclear Instruments & Methods in Physics Research B, 2006, 242, 1-7.	0.6	23
852	Enhancement of corrosion resistance of AISI 420 stainless steels by nitrogen and silicon plasma immersion ion implantation. Surface and Coatings Technology, 2007, 201, 4879-4883.	2.2	23
853	Effects of Ti transition layer on stability of silver/titanium dioxide multilayered structure. Thin Solid Films, 2007, 515, 3146-3150.	0.8	23
854	Dispersion of multi-stream instability in quantum magnetized hot plasmas. Physics Letters, Section A: General, Atomic and Solid State Physics, 2008, 372, 2676-2683.	0.9	23
855	Enhancement of ductility in Mg–3Al–1Zn alloy with tilted basal texture by electropulsing. Journal of Materials Research, 2009, 24, 3674-3679.	1.2	23
856	A novel hydrothermal route to synthesize solid SnO2 nanospheres and their photoluminescence property. Applied Physics A: Materials Science and Processing, 2009, 97, 581-585.	1.1	23
857	Mechanical and optical characteristics of multilayer inorganic films on polyimide for anti-atomic-oxygen erosion. Applied Surface Science, 2012, 258, 5810-5814.	3.1	23
858	Preparation and electrochemistry of Pd–Ni/Si nanowire nanocomposite catalytic anode for direct ethanol fuel cell. Dalton Transactions, 2012, 41, 5055.	1.6	23
859	Controlled Fabrication of Core–Shell TiO <sub>2</sub> /C and TiC/C Nanofibers on Ti Foils and Their Field-Emission Properties. ACS Applied Materials & Interfaces, 2012, 4, 1037-1042.	4.0	23
860	Ex situ and in situ evaluation of carbon ion-implanted stainless steel bipolar plates in polymer electrolyte membrane fuel cells. Journal of Power Sources, 2012, 199, 207-213.	4.0	23
861	Surface-induced structural transformation in nanowires. Materials Science and Engineering Reports, 2013, 74, 173-209.	14.8	23
862	Enhanced Photodegradation of Methyl Orange Synergistically by Microcrystal Facet Cutting and Flexible Electrically-Conducting Channels. Journal of Physical Chemistry C, 2014, 118, 28063-28068.	1.5	23
863	Electronic structure and magnetism in <i>g</i> -C4N3 controlled by strain engineering. Applied Physics Letters, 2015, 106, .	1.5	23
864	Polyimide composites composed of covalently bonded BaTiO <sub>3</sub> @GO hybrids with high dielectric constant and low dielectric loss. RSC Advances, 2016, 6, 86817-86823.	1.7	23

#	Article	IF	CITATIONS
865	Development of novel implants with self-antibacterial performance through in-situ growth of 1D ZnO nanowire. Colloids and Surfaces B: Biointerfaces, 2016, 141, 623-633.	2.5	23
866	Preparation of multi-layer graphene on nickel-coated silicon microchannel plates by a hydrothermal carbonization procedure and its improved field emission properties. Journal of Materials Chemistry C, 2016, 4, 2079-2087.	2.7	23
867	Fabrication of irregular-layer-free and diameter-tunable Ni–Ti–O nanopores by anodization of NiTi alloy. Electrochemistry Communications, 2017, 76, 10-14.	2.3	23
868	Influence of dynamic compressive loading on the in vitro degradation behavior of pure PLA and Mg/PLA composite. Acta Biomaterialia, 2017, 64, 269-278.	4.1	23
869	Selective and high-sensitive label-free detection of ascorbic acid by carbon nitride quantum dots with intense fluorescence from lone pair states. Talanta, 2019, 196, 530-536.	2.9	23
870	Corrosion behavior of functionally graded and self-healing nanostructured TiO2–Al2O3 - Benzotriazole coatings deposited on AA 2024-T3 by the sol-gel method. Materials Chemistry and Physics, 2020, 240, 122233.	2.0	23
871	Stability and Sensing Enhancement by Nanocubic CeO <sub>2</sub> with {100} Polar Facets on Graphene for NO <sub>2</sub> at Room Temperature. ACS Applied Materials & Interfaces, 2020, 12, 4722-4731.	4.0	23
872	Robust and durable surperhydrophobic F-DLC coating for anti-icing in aircrafts engineering. Surface and Coatings Technology, 2020, 404, 126468.	2.2	23
873	Needle-like CoO nanowire composites with NiO nanosheets on carbon cloth for hybrid flexible supercapacitors and overall water splitting electrodes. RSC Advances, 2020, 10, 37489-37499.	1.7	23
874	Wafer-scale growth of single-crystal graphene on vicinal Ge(001) substrate. Nano Today, 2020, 34, 100908.	6.2	23
875	Nanopatterned silk-coated AZ31 magnesium alloy with enhanced antibacterial and corrosion properties. Materials Science and Engineering C, 2020, 116, 111173.	3.8	23
876	Large-scale and low-cost synthesis of in situ generated SiC/C nano-composites from rice husks for advanced electromagnetic wave absorption applications. Surface and Coatings Technology, 2021, 406, 126641.	2.2	23
877	Uniform cobalt nanoparticles-decorated biscuit-like VN nanosheets by in situ segregation for Li-ion batteries and oxygen evolution reaction. Applied Surface Science, 2021, 536, 147982.	3.1	23
878	TiO2 film supported by vertically aligned gold nanorod superlattice array for enhanced photocatalytic hydrogen evolution. Chemical Engineering Journal, 2021, 417, 127900.	6.6	23
879	A multifunctional antibacterial coating on bone implants for osteosarcoma therapy and enhanced osteointegration. Chemical Engineering Journal, 2022, 428, 131155.	6.6	23
880	Dynamic active sites on plasma engraved Ni hydroxide for enhanced electro-catalytic urea oxidation. Journal of Energy Chemistry, 2022, 71, 150-158.	7.1	23
881	Nucleation mechanism of SPIMOX (separation by plasma implantation of oxygen). Surface and Coatings Technology, 1996, 85, 60-63.	2.2	22
882	Vacuum arc plasma transport through a magnetic duct with a biased electrode at the outer wall. Review of Scientific Instruments, 1999, 70, 3329-3331.	0.6	22

#	Article	IF	CITATIONS
883	Modeling of incident particle energy distribution in plasma immersion ion implantation. Journal of Applied Physics, 2000, 88, 4961-4966.	1.1	22
884	Wall sheath and optimal bias in magnetic filters for vacuum arc plasma sources. Applied Physics Letters, 2002, 80, 365-367.	1.5	22
885	Hybrid evaporation: Clow discharge source for plasma immersion ion implantation. Review of Scientific Instruments, 2003, 74, 4301-4304.	0.6	22
886	Thermal stability of diamondlike carbon buried layer fabricated by plasma immersion ion implantation and deposition in silicon on insulator. Journal of Applied Physics, 2005, 98, 053502.	1.1	22
887	Fabrication and field emission property of a Si nanotip array. Nanotechnology, 2006, 17, 5573-5576.	1.3	22
888	Hard nanocomposite Ti–Si–N films prepared by DC reactive magnetron sputtering using Ti–Si mosaic target. Surface and Coatings Technology, 2007, 201, 6824-6827.	2.2	22
889	Effects of water plasma immersion ion implantation on surface electrochemical behavior of NiTi shape memory alloys in simulated body fluids. Applied Surface Science, 2007, 253, 3154-3159.	3.1	22
890	Tunable emission from composite polymer nanoparticles based on resonance energy transfer. Thin Solid Films, 2008, 516, 6287-6292.	0.8	22
891	Tribological properties of graded diamond-like carbon films on Ti ion-implanted aluminum substrate. Diamond and Related Materials, 2008, 17, 1844-1849.	1.8	22
892	3D ordered NiO/silicon MCP array electrode materials for electrochemical supercapacitors. Materials Research Bulletin, 2009, 44, 1920-1925.	2.7	22
893	Reversible phase transformation in graphene nano-ribbons: Lattice shearing based mechanism. Acta Materialia, 2011, 59, 6783-6789.	3.8	22
894	Suppressed primary osteoblast functions on nanoporous titania surface. Journal of Biomedical Materials Research - Part A, 2011, 96A, 100-107.	2.1	22
895	Interface dipole engineering in metal gate/high-k stacks. Science Bulletin, 2012, 57, 2872-2878.	1.7	22
896	Wear mechanism and tribological characteristics of porous NiTi shape memory alloy for bone scaffold. Journal of Biomedical Materials Research - Part A, 2013, 101A, 2586-2601.	2.1	22
897	Supercapacitor Electrodes Based on Hierarchical Mesoporous MnO <i><sub>x</sub></i> /Nitrided TiO <sub>2</sub> Nanorod Arrays on Carbon Fiber Paper. Advanced Materials Interfaces, 2015, 2, 1400446.	1.9	22
898	Effects of silver plasma immersion ion implantation on the surface characteristics and cytocompatibility of titanium nitride films. Surface and Coatings Technology, 2015, 279, 166-170.	2.2	22
899	Anodic growth of ultra-long Ni-Ti-O nanopores. Electrochemistry Communications, 2016, 71, 28-32.	2.3	22
900	Recent advances in cell-mediated nanomaterial delivery systems for photothermal therapy. Journal of Materials Chemistry B, 2018, 6, 1296-1311.	2.9	22

#	Article	IF	CITATIONS
901	Surface functionalization of biomaterials by plasma and ion beam. Surface and Coatings Technology, 2018, 336, 2-8.	2.2	22
902	Magnetron-sputtered fluorocarbon polymeric film on magnesium for corrosion protection. Surface and Coatings Technology, 2018, 352, 437-444.	2.2	22
903	Enhancement of mechanical properties and corrosion resistance of NiTi alloy by carbon plasma immersion ion implantation. Surface and Coatings Technology, 2019, 365, 52-57.	2.2	22
904	Hierarchical binder-free MnO2/TiO2 composite nanostructure on flexible seed graphite felt for high-performance supercapacitors. Vacuum, 2020, 181, 109648.	1.6	22
905	A tailored positively-charged hydrophobic surface reduces the risk of implant associated infections. Acta Biomaterialia, 2020, 114, 421-430.	4.1	22
906	A composite coating with physical interlocking and chemical bonding on WE43 magnesium alloy for corrosion protection and cytocompatibility enhancement. Surface and Coatings Technology, 2021, 412, 127078.	2.2	22
907	Surface plasmon resonance sensor based onÂeccentric core photonic quasi-crystal fiberÂwith indium tin oxide. Applied Optics, 2019, 58, 6848.	0.9	22
908	Plasma modified and tailored defective electrocatalysts for water electrolysis and hydrogen fuel cells. EcoMat, 2022, 4, .	6.8	22
909	Modeling of the relationship between implantation parameters and implantation dose during plasma immersion ion implantation. Physics Letters, Section A: General, Atomic and Solid State Physics, 2000, 277, 42-46.	0.9	21
910	Self-assembled growth and green emission of gold nanowhiskers. Applied Physics Letters, 2005, 87, 223115.	1.5	21
911	Effects of plasma immersion ion nitridation on dielectric properties of HfO2. Applied Physics Letters, 2007, 90, 122901.	1.5	21
912	Structure and wear properties of NiTi modified by nitrogen plasma immersion ion implantation. Materials Science & Engineering A: Structural Materials: Properties, Microstructure and Processing, 2007, 444, 192-197.	2.6	21
913	Electromagnetic drift waves in nonuniform quantum magnetized electron–positron–ion plasmas. Journal of Physics A: Mathematical and Theoretical, 2008, 41, 115501.	0.7	21
914	Microstructure and mechanical properties of CrN films fabricated by high power pulsed magnetron discharge plasma immersion ion implantation and deposition. Applied Surface Science, 2011, 258, 242-246.	3.1	21
915	High-sensitivity biosensors fabricated by tailoring the localized surface plasmon resonance property of core–shell gold nanorods. Analytica Chimica Acta, 2011, 683, 242-247.	2.6	21
916	Growth of tin oxide nanorods induced by nanocube-oriented coalescence mechanism. Applied Physics Letters, 2011, 98, 133102.	1.5	21
917	Group velocity of extraordinary waves in superdense magnetized quantum plasma with spin-1/2 effects. Physics of Plasmas, 2012, 19, .	0.7	21
918	Effect of plasma CVD operating temperature on nanomechanical properties of TiC nanostructured coating investigated by atomic force microscopy. Materials Research Bulletin, 2012, 47, 2200-2205.	2.7	21

#	Article	IF	CITATIONS
919	Functionalization of biomedical materials using plasma and related technologies. Applied Surface Science, 2014, 310, 11-18.	3.1	21
920	Competitive Reaction Pathway for Siteâ€selective Conjugation of Raman Dyes to Hotspots on Gold Nanorods for Greatly Enhanced SERS Performance. Small, 2014, 10, 4012-4019.	5.2	21
921	Characterization of carbon ion implantation induced graded microstructure and phase transformation in stainless steel. Materials Characterization, 2015, 106, 11-19.	1.9	21
922	Selfâ€5upporting and Binderâ€Free Anode Film Composed of Beaded Streamâ€Like Li <sub>4</sub> Ti <sub>5</sub> O <sub>12</sub> Nanoparticles for Highâ€Performance Lithiumâ€Ion Batteries. ChemElectroChem, 2016, 3, 1301-1305.	1.7	21
923	Facile synthesis of porous iron oxide/graphene hybrid nanocomposites and potential application in electrochemical energy storage. New Journal of Chemistry, 2017, 41, 13553-13559.	1.4	21
924	Oriented MoS <sub>2</sub> Nanoflakes on Nâ€Doped Carbon Nanosheets Derived from Dodecylamineâ€Intercalated MoO <sub>3</sub> for Highâ€Performance Lithiumâ€Ion Battery Anodes. ChemElectroChem, 2018, 5, 1350-1356.	1.7	21
925	High-ion-energy and low-temperature deposition of diamond-like carbon (DLC) coatings with pulsed kV bias. Surface and Coatings Technology, 2019, 365, 152-157.	2.2	21
926	Formation of self-layered hydrothermal coating on magnesium aided by titanium ion implantation: Synergistic control of corrosion resistance and cytocompatibility. Surface and Coatings Technology, 2020, 401, 126251.	2.2	21
927	Strain-enhanced power conversion efficiency of a BP/SnSe van der Waals heterostructure. Physical Chemistry Chemical Physics, 2020, 22, 14787-14795.	1.3	21
928	Graphene Quantum Dot-Decorated Vertically Oriented Graphene/Germanium Heterojunctions for Near-Infrared Photodetectors. ACS Applied Nano Materials, 2020, 3, 6915-6924.	2.4	21
929	Electrochemical stability, corrosion behavior, and biological properties of Ni–Ti–O nanoporous layers anodically on NiTi alloy. Corrosion Science, 2021, 179, 109104.	3.0	21
930	Selective inhibition effects on cancer cells and bacteria of Ni–Ti–O nanoporous layers grown on biomedical NiTi alloy by anodization. Rare Metals, 2022, 41, 78-85.	3.6	21
931	Programmed surface on poly(aryl-ether-ether-ketone) initiating immune mediation and fulfilling bone regeneration sequentially. Innovation(China), 2021, 2, 100148.	5.2	21
932	A lithium-doped surface inspires immunomodulatory functions for enhanced osteointegration through PI3K/AKT signaling axis regulation. Biomaterials Science, 2021, 9, 8202-8220.	2.6	21
933	Separation by plasma implantation of oxygen (SPIMOX) operational phase space. IEEE Transactions on Plasma Science, 1997, 25, 1128-1135.	0.6	20
934	Dose and energy uniformity over inner surface in plasma immersion ion implantation. Journal of Applied Physics, 1998, 84, 1859-1862.	1.1	20
935	Characterization of III nitride materials and devices by secondary ion mass spectrometry. Journal of Vacuum Science & Technology an Official Journal of the American Vacuum Society B, Microelectronics Processing and Phenomena, 1998, 16, 197.	1.6	20
936	Hybrid elevated-temperature, low/high-voltage plasma immersion ion implantation of AISI304 stainless steel. Surface and Coatings Technology, 2001, 135, 178-183.	2.2	20

#	Article	IF	CITATIONS
937	Low-frequency Raman scattering of Ge and Si nanocrystals in silica matrix. Journal of Applied Physics, 2005, 98, 064303.	1.1	20
938	Formation of apatite on hydrogenated amorphous silicon (a-Si:H) film deposited by plasma-enhanced chemical vapor deposition. Materials Chemistry and Physics, 2007, 101, 124-128.	2.0	20
939	Role of interface dipole in metal gate/high-k effective work function modulation by aluminum incorporation. Applied Physics Letters, 2009, 94, .	1.5	20
940	Oxygen vacancy density-dependent transformation from infrared to Raman active vibration mode in SnO_2 nanostructures. Optics Letters, 2011, 36, 4296.	1.7	20
941	Influence of Structure Parameters and Crystalline Phase on the Photocatalytic Activity of TiO <sub>2</sub> Nanotube Arrays. Journal of Nanoscience and Nanotechnology, 2011, 11, 11200-11205.	0.9	20
942	Tunable electroluminescence from polymer-passivated 3C-SiC quantum dot thin films. Applied Physics Letters, 2012, 101, 123110.	1.5	20
943	Design and preparation of novel fluorescent polyimides containing <i>ortho</i> -linked units and pyridine moieties. Designed Monomers and Polymers, 2012, 15, 389-404.	0.7	20
944	Sensitive and simultaneous detection of different disease markers using multiplexed gold nanorods. Analytica Chimica Acta, 2012, 755, 108-114.	2.6	20
945	Quasi-seeded growth, phase transformation, and size tuning of multifunctional hexagonal NaLnF <sub>4</sub> (Ln = Y, Gd, Yb) nanocrystalsvia in situcation-exchange reaction. Journal of Materials Chemistry, 2012, 22, 2254-2262.	6.7	20
946	Thermal degradation and flame retarding characteristics of polypropylene composites incorporated with boron mud. Composites Science and Technology, 2013, 85, 131-135.	3.8	20
947	WO3 nanoparticles decorated core–shell TiC–C nanofiber arrays for high sensitive and non-enzymatic photoelectrochemical biosensing. Chemical Communications, 2013, 49, 7091.	2.2	20
948	Surface electromagnetic wave equations in a warm magnetized quantum plasma. Physics of Plasmas, 2014, 21, 072114.	0.7	20
949	Tensile loading induced phase transition and rippling in single-layer MoS 2. Applied Surface Science, 2017, 404, 180-187.	3.1	20
950	Monolithic Hierarchical Carbon Assemblies Embedded with Mesoporous NaTi2(PO4)3 Nanocrystals for Flexible High-Performance Sodium Anodes. Electrochimica Acta, 2017, 254, 328-336.	2.6	20
951	Cellular response to nano-structured Zr and ZrO2 alloyed layers on Ti-6Al-4V. Materials Science and Engineering C, 2018, 90, 523-530.	3.8	20
952	Nickel/Multi-walled Carbon Nanotube Nanocomposite Synthesized in Supercritical Fluid as Efficient Lubricant Additive for Mineral Oil. Tribology Letters, 2018, 66, 1.	1.2	20
953	Flexible Nb <sub>4</sub> N <sub>5</sub> /rGO Electrode for High-Performance Solid State Supercapacitors. Journal of Nanoscience and Nanotechnology, 2018, 18, 30-38.	0.9	20
954	Roles of membrane protein damage and intracellular protein damage in death of bacteria induced by atmospheric-pressure air discharge plasmas. RSC Advances, 2018, 8, 21139-21149.	1.7	20

#	Article	IF	CITATIONS
955	Graphite felt incorporated with MoS2/rGO for electrochemical detoxification of high-arsenic fly ash. Chemical Engineering Journal, 2020, 382, 122763.	6.6	20
956	Hollow Spheres Consisting of SnS Nanosheets Conformally Coated with Sâ€Doped Carbon for Advanced Lithiumâ€∲Sodiumâ€ion Battery Anodes. ChemElectroChem, 2020, 7, 914-921.	1.7	20
957	Electronic Modulation between Tungsten Nitride and Cobalt Dopants for Enhanced Hydrogen Evolution Reaction at a Wide Range of pH. ChemCatChem, 2020, 12, 2962-2966.	1.8	20
958	Dynamic mixing deposition/implantation in a plasma immersion configuration. Journal of Vacuum Science and Technology A: Vacuum, Surfaces and Films, 1999, 17, 3255-3259.	0.9	19
959	Effects of tube length and radius for inner surface plasma immersion ion implantation using an auxiliary electrode. IEEE Transactions on Plasma Science, 1999, 27, 225-238.	0.6	19
960	Electrochemical corrosion properties of AISI304 steel treated by low-temperature plasma immersion ion implantation. Scripta Materialia, 2000, 43, 417-422.	2.6	19
961	Plasma nitridation and microstructure of high-k ZrO2 thin films fabricated by cathodic arc deposition. Journal of Crystal Growth, 2005, 277, 422-427.	0.7	19
962	Experimental investigation of hybrid-evaporation-glow discharge plasma immersion ion implantation. Journal of Applied Physics, 2005, 97, 113301.	1.1	19
963	Improved stability of plasma-sprayed dicalcium silicate/zirconia composite coating. Thin Solid Films, 2006, 515, 1214-1218.	0.8	19
964	Oxygen plasma treatment to restrain nickel out-diffusion from porous nickel titanium orthopedic materials. Surface and Coatings Technology, 2007, 201, 4893-4896.	2.2	19
965	In situ growth of aligned CdS nanowire arrays on Cd foil and their optical and electron field emission properties. Journal of Applied Physics, 2008, 104, 014312.	1.1	19
966	Green dielectric materials composed of natural graphite minerals and biodegradable polymer. RSC Advances, 2012, 2, 8793.	1.7	19
967	Corrosion behavior of chromium and oxygen plasma-modified magnesium in sulfate solution and simulated body fluid. Applied Surface Science, 2012, 258, 8273-8278.	3.1	19
968	Fluorine-containing pH-responsive core/shell microgel particles: preparation, characterization, and their applications in controlled drug release. Colloid and Polymer Science, 2012, 290, 349-357.	1.0	19
969	Evidence of atomically resolved 6×6 buffer layer with long-range order and short-range disorder during formation of graphene on 6H-SiC by thermal decomposition. Applied Physics Letters, 2013, 102, .	1.5	19
970	Effect of surface mechanical attrition treatment of titanium using alumina balls: surface roughness, contact angle and apatite forming ability. Frontiers of Materials Science, 2013, 7, 285-294.	1.1	19
971	Observation of inactivation ofBacillus sbtilisspores under exposures of oxygen added argon atmospheric pressure plasma jet. Japanese Journal of Applied Physics, 2014, 53, 110310.	0.8	19
972	Trifunctional Polymeric Nanocomposites Incorporated with Fe <sub>3</sub> O <sub>4</sub> /lodine-Containing Rare Earth Complex for Computed X-ray Tomography, Magnetic Resonance, and Optical Imaging. ACS Applied Materials & Interfaces, 2015, 7, 24523-24532.	4.0	19

#	Article	IF	CITATIONS
973	Electrochemiluminescent Spinâ€Polarized Modulation by Magnetic Ions and Surface Plasmon Coupling. Angewandte Chemie - International Edition, 2016, 55, 2017-2021.	7.2	19
974	Dominant Factors Governing the Electron Transfer Kinetics and Electrochemical Biosensing Properties of Carbon Nanofiber Arrays. ACS Applied Materials & Interfaces, 2016, 8, 28872-28879.	4.0	19
975	Lowâ€Temperature Synthesis of Mesoporous SiC Hollow Spheres by Magnesiothermic Reduction. Journal of the American Ceramic Society, 2016, 99, 1859-1861.	1.9	19
976	Enhanced corrosion resistance and biocompatibilty of PMMA-coated ZK60 magnesium alloy. Materials Letters, 2016, 173, 178-181.	1.3	19
977	In situ fabrication of Ni nanoparticles on N-doped TiO <sub>2</sub> nanowire arrays by nitridation of NiTiO <sub>3</sub> for highly sensitive and enzyme-free glucose sensing. Journal of Materials Chemistry B, 2017, 5, 1779-1786.	2.9	19
978	Enhancement of high-temperature strength of Ni-based films by addition of nano-multilayers and incorporation of W. Acta Materialia, 2017, 133, 55-67.	3.8	19
979	Copolymer P(BS-co-LA) Enhanced Compatibility of PBS/PLA Composite. Journal of Polymers and the Environment, 2018, 26, 3060-3068.	2.4	19
980	Tantalum nitride films for corrosion protection of biomedical Mg-Y-RE alloy. Journal of Alloys and Compounds, 2018, 764, 947-958.	2.8	19
981	Simultaneous texturing and conductivity tailoring of mesoporous NaTi2(PO4)3 nanocrystals by gadolinium doping for enhanced Na storage. Electrochimica Acta, 2019, 309, 177-186.	2.6	19
982	Corrosion protection and enhanced biocompatibility of biomedical Mg-Y-RE alloy coated with tin dioxide. Surface and Coatings Technology, 2019, 357, 78-82.	2.2	19
983	Ultrathin carbon layer-encapsulated TiN nanotubes array with enhanced capacitance and electrochemical stability for supercapacitors. Applied Surface Science, 2020, 503, 144293.	3.1	19
984	Enhanced Peltier Effect in Wrinkled Graphene Constriction by Nanoâ€Bubble Engineering. Small, 2020, 16, e1907170.	5.2	19
985	Comparative study of TiAlN coatings deposited by different high-ionization physical vapor deposition techniques. Ceramics International, 2020, 46, 10814-10819.	2.3	19
986	A zinc-doped coating prepared on the magnesium alloy by plasma electrolytic oxidation for corrosion protection. Surface and Coatings Technology, 2022, 433, 128148.	2.2	19
987	Effects of cathode materials and arc current on optimal bias of a cathodic arc through a magnetic duct. Applied Physics Letters, 2002, 80, 3700-3702.	1.5	18
988	Fabrication of SOI structure with AlN film as buried insulator by Ion-Cut process. Applied Surface Science, 2002, 199, 287-292.	3.1	18
989	Effects and mechanisms of nitrogen incorporation into hafnium oxide by plasma immersion implantation. Journal of Vacuum Science & Technology B, 2007, 25, 1853.	1.3	18
990	Silicon-induced DNA damage pathway and its modulation by titanium plasma immersion ion implantation. Biomaterials, 2008, 29, 544-550.	5.7	18

#	Article	IF	CITATIONS
991	Electrostatic drift waves in nonuniform quantum magnetized plasmas. Physics of Plasmas, 2008, 15, 082103.	0.7	18
992	Surface-enhanced Raman scattering from silver nanostructures with different morphologies. Applied Physics A: Materials Science and Processing, 2010, 100, 83-88.	1.1	18
993	Extraction of organic materials from red water by metal-impregnated lignite activated carbon. Journal of Hazardous Materials, 2011, 197, 352-360.	6.5	18
994	An undercutting model of atomic oxygen for multilayer silica/alumina films fabricated by plasma immersion implantation and deposition on polyimide. Applied Surface Science, 2011, 257, 9158-9163.	3.1	18
995	UV-blue photoluminescence from close-packed SiC nanocrystal film. Applied Physics Letters, 2011, 98, .	1.5	18
996	Electrochemical Characteristics of Discrete, Uniform, and Monodispersed Hollow Mesoporous Carbon Spheres in Double‣ayered Supercapacitors. Chemistry - an Asian Journal, 2013, 8, 2627-2633.	1.7	18
997	Electrochemical analysis of nickel electrode deposited on silicon microchannel plate. Electrochimica Acta, 2013, 90, 344-349.	2.6	18
998	Effects of carbon dioxide plasma immersion ion implantation on the electrochemical properties of AZ31 magnesium alloy in physiological environment. Applied Surface Science, 2013, 286, 257-260.	3.1	18
999	First-principles calculation of the band structure, electronic states, and optical properties of Cr-doped ZnS double-wall nanotubes. Computational Materials Science, 2015, 101, 1-7.	1.4	18
1000	Plasma and ion-beam modification of metallic biomaterials for improved anti-bacterial properties. Surface and Coatings Technology, 2016, 306, 140-146.	2.2	18
1001	Hafnium-implanted WE43 magnesium alloy for enhanced corrosion protection and biocompatibility. Surface and Coatings Technology, 2016, 306, 11-15.	2.2	18
1002	A sandwich-type electrochemical immunosensor based on the biotin- streptavidin-biotin structure for detection of human immunoglobulin G. Scientific Reports, 2016, 6, 22694.	1.6	18
1003	Boundary and Elastohydrodynamic Lubrication Behaviors of Nano-CuO/Reduced Graphene Oxide Nanocomposite as an Efficient Oil-Based Additive. Langmuir, 2019, 35, 10322-10333.	1.6	18
1004	Titania-zinc phosphate/nanocrystalline zinc composite coatings for corrosion protection of biomedical WE43 magnesium alloy. Surface and Coatings Technology, 2021, 410, 126940.	2.2	18
1005	In situ sample temperature measurement in plasma immersion ion implantation. Review of Scientific Instruments, 1999, 70, 2818-2821.	0.6	17
1006	Contamination issues in hydrogen plasma immersion ion implantation of silicon—a brief review. Surface and Coatings Technology, 2002, 156, 244-252.	2.2	17
1007	Silicon carbide formation by methane plasma immersion ion implantation into silicon. Journal of Vacuum Science & Technology an Official Journal of the American Vacuum Society B, Microelectronics Processing and Phenomena, 2003, 21, 1375.	1.6	17
1008	Improvement of adhesion strength of amorphous carbon films on tungsten ion implanted 321 stainless steel substrate. Diamond and Related Materials, 2006, 15, 952-957.	1.8	17

#	Article	IF	CITATIONS
1009	Effects of external magnetic field on propagation of electromagnetic wave in uniform magnetized plasma slabs. Computer Physics Communications, 2006, 175, 545-552.	3.0	17
1010	Mechanism of mechanical property enhancement in nitrogen and titanium implanted 321 stainless steel. Materials Science & Engineering A: Structural Materials: Properties, Microstructure and Processing, 2006, 425, 1-6.	2.6	17
1011	In vitro biocompatibility of titanium-nickel alloy with titanium oxide film by H2O2 oxidation. Transactions of Nonferrous Metals Society of China, 2007, 17, 553-557.	1.7	17
1012	Behavior of endothelial cells on micro-patterned titanium oxide fabricated by plasma immersion ion implantation and deposition and plasma etching. Surface and Coatings Technology, 2007, 201, 6874-6877.	2.2	17
1013	Platelet activation behavior on nitrogen plasma-implanted silicon. Materials Science and Engineering C, 2007, 27, 928-932.	3.8	17
1014	Catalysis of dispersed silver particles on directional etching of silicon. Applied Surface Science, 2008, 254, 3061-3066.	3.1	17
1015	Corrosion behavior of ZnO nanosheets on brass substrate in NaCl solutions. Materials Chemistry and Physics, 2009, 115, 439-443.	2.0	17
1016	Biocompatibility of silver and copper plasma doped polyethylene. Surface and Coatings Technology, 2009, 203, 2550-2553.	2.2	17
1017	Excitation and recombination photodynamics in colloidal cubic SiC nanocrystals. Applied Physics Letters, 2010, 97, .	1.5	17
1018	Controllable Growth of Conical and Cylindrical TiO <sub>2</sub> –Carbon Core–Shell Nanofiber Arrays and Morphologically Dependent Electrochemical Properties. Chemistry - A European Journal, 2011, 17, 14552-14558.	1.7	17
1019	Low-frequency Raman scattering of bioinspired self-assembled diphenylalanine nanotubes/microtubes. Optics Express, 2012, 20, 5119.	1.7	17
1020	Optical properties and chemical structures of Kapton-H film after proton irradiation by immersion in a hydrogen plasma. Applied Surface Science, 2012, 258, 3829-3834.	3.1	17
1021	Novel anionic fluorine-containing amphiphilic self-assembly polymer micelles for potential application in protein drug carrier. Journal of Fluorine Chemistry, 2012, 141, 21-28.	0.9	17
1022	Concentration- and time-dependent response of human gingival fibroblasts to fibroblast growth factor 2 immobilized on titanium dental implants. International Journal of Nanomedicine, 2012, 7, 1965.	3.3	17
1023	Electronic states and photoluminescence of TiO2 nanotubes with adsorbed surface oxygen. Applied Physics Letters, 2012, 100, 121904.	1.5	17
1024	Structure and magnetic properties of soft organic ZnAl-LDH/polyimide electromagnetic shielding composites. Journal of Materials Science, 2012, 47, 2033-2039.	1.7	17
1025	Improved corrosion resistance of Mg-Y-RE alloy coated with niobium nitride. Thin Solid Films, 2014, 572, 85-90.	0.8	17
1026	Size-dependent deformation behavior of nanocrystalline graphene sheets. Materials Science and Engineering B: Solid-State Materials for Advanced Technology, 2015, 198, 95-101.	1.7	17

#	Article	IF	CITATIONS
1027	Corrosion resistance of praseodymium-ion-implanted TiN coatings in blood and cytocompatibility with vascular endothelial cells. Vacuum, 2015, 117, 73-80.	1.6	17
1028	Removal of organic pollutants from red water by magnetic-activated coke. Desalination and Water Treatment, 2015, 54, 2710-2722.	1.0	17
1029	Zinc Electrodeposition on Polycrystalline Copper: Electrochemical Study of Early-Stage Growth Mechanism. Journal of Physical Chemistry C, 2017, 121, 3938-3946.	1.5	17
1030	Inherent Chemotherapeutic Anti ancer Effects of Lowâ€Dimensional Nanomaterials. Chemistry - A European Journal, 2019, 25, 10995-11006.	1.7	17
1031	High-Efficiency Dual-Frequency Reflective Linear Polarization Converter Based on Metasurface for Microwave Bands. Applied Sciences (Switzerland), 2019, 9, 1910.	1.3	17
1032	Formation of ultra-small Mn3O4 nanoparticles trapped in nanochannels of hollow carbon spheres by nanoconfinement with excellent supercapacitor performance. International Journal of Hydrogen Energy, 2019, 44, 13675-13683.	3.8	17
1033	Excellent Lubricating Ability of Functionalization Graphene Dispersed in Perfluoropolyether for Titanium Alloy. ACS Applied Nano Materials, 2019, 2, 1391-1401.	2.4	17
1034	Improved Load-Bearing Capacity and Tribological Properties of PTFE Coatings Induced by Surface Texturing and the Addition of GO. Tribology Letters, 2021, 69, 1.	1.2	17
1035	Improving exposure of anodically ordered Ni–Ti–O and corrosion resistance and biological properties of NiTi alloys by substrate electropolishing. Rare Metals, 2021, 40, 3575-3587.	3.6	17
1036	Plasma-activated interfaces for biomedical engineering. Bioactive Materials, 2021, 6, 2134-2143.	8.6	17
1037	Ag as Cocatalyst and Electron-Hole Medium in CeO2 QDs/Ag/Ag2Se Z-scheme Heterojunction Enhanced the Photo-Electrocatalytic Properties of the Photoelectrode. Nanomaterials, 2020, 10, 253.	1.9	17
1038	Versatile Phenolâ€Incorporated Nanoframes for In Situ Antibacterial Activity Based on Oxidative and Physical Damages. Advanced Functional Materials, 2022, 32, .	7.8	17
1039	Surface metal contamination on silicon wafers after hydrogen plasma immersion ion implantation. Nuclear Instruments & Methods in Physics Research B, 1999, 155, 75-78.	0.6	16
1040	Enhancement of process efficacy using seed plasma in pulsed high-voltage glow-discharge plasma implantation. Physics Letters, Section A: General, Atomic and Solid State Physics, 2002, 303, 67-71.	0.9	16
1041	Deformation behavior of titanium nitride film prepared by plasma immersion ion implantation and deposition. Surface and Coatings Technology, 2002, 156, 170-175.	2.2	16
1042	Title is missing!. Journal of Materials Science Letters, 2002, 21, 1611-1614.	0.5	16
1043	Synthesis of beta gallium oxide nano-ribbons from gallium arsenide by plasma immersion ion implantation and rapid thermal annealing. Chemical Physics Letters, 2003, 382, 573-577.	1.2	16
1044	Microstructure and crystallinity of porous silicon and epitaxial silicon layers fabricated on p[sup +] porous silicon. Journal of Vacuum Science & Technology an Official Journal of the American Vacuum Society B, Microelectronics Processing and Phenomena, 2003, 21, 168.	1.6	16

#	Article	IF	CITATIONS
1045	Formation of silicon-on-diamond by direct bonding of plasma-synthesized diamond-like carbon to silicon. Applied Physics Letters, 2004, 85, 2532-2534.	1.5	16
1046	Preparation of GaN thin film and Ga2O3 nanoribbons by plasma immersion ion implantation of N into GaAs. Journal of Applied Physics, 2004, 95, 8178-8184.	1.1	16
1047	Cu oxide nanowire array grown on Si-based SiO2 nanoscale islands via nanochannels. Acta Materialia, 2004, 52, 5051-5055.	3.8	16
1048	Co-doping effects and electrical transport in In–N doped zinc oxide. Chemical Physics Letters, 2006, 432, 352-355.	1.2	16
1049	Control of stress and delamination in single and multi-layer carbon thin films prepared by cathodic arc and RF plasma deposition and implantation. Surface and Coatings Technology, 2006, 200, 6405-6408.	2.2	16
1050	In situ fabrication of alumina nanotube array and photoluminescence. Applied Physics Letters, 2006, 89, 073114.	1.5	16
1051	Optical and mechanical properties of alumina films fabricated on Kapton polymer by plasma immersion ion implantation and deposition using different biases. Applied Surface Science, 2007, 253, 9483-9488.	3.1	16
1052	Effects of anodic oxidation in H2SO4 electrolyte on the biocompatibility of NiTi shape memory alloy. Materials Letters, 2008, 62, 3512-3514.	1.3	16
1053	Recent Progress in Fabrication of Anisotropic Nanostructures for Surface- Enhanced Raman Spectroscopy. Recent Patents on Nanotechnology, 2009, 3, 10-20.	0.7	16
1054	Nanocrystalline titanium nitride films prepared by electrophoretic deposition. Surface and Coatings Technology, 2009, 204, 418-422.	2.2	16
1055	Aligned silver nanorod arrays for surface-enhanced Raman spectroscopy. Physica B: Condensed Matter, 2009, 404, 1523-1526.	1.3	16
1056	Phase transformation and size tuning in controlled-growth of nanocrystals via self-seeded nucleation with preferential thermodynamic stability. Chemical Communications, 2011, 47, 12544.	2.2	16
1057	Dual Ti and C ion-implanted stainless steel bipolar plates in polymer electrolyte membrane fuel cells. Surface and Coatings Technology, 2012, 206, 2914-2921.	2.2	16
1058	Fluorine-containing thermo-sensitive core/shell microgel particles: Preparation, characterization, and their applications in controlled drug release. Journal of Fluorine Chemistry, 2012, 135, 75-82.	0.9	16
1059	Synergistic effect of chloride ion and albumin on the corrosion of pure magnesium. Frontiers of Materials Science, 2014, 8, 244-255.	1.1	16
1060	Substitutional doping of Ag into epitaxial graphene on 6H-SiC substrates during thermal decomposition. Carbon, 2016, 104, 233-240.	5.4	16
1061	Fabrication and enhanced supercapacitance of hollow nanostructured MoS2 prepared by a CATB-assisted hydrothermal process. Materials Letters, 2016, 184, 96-99.	1.3	16
1062	Smart polymeric particle encapsulated gadolinium oxide and europium: theranostic probes for magnetic resonance/optical imaging and antitumor drug delivery. Journal of Materials Chemistry B, 2016, 4, 1100-1107.	2.9	16

PAUL CHU

#	Article	IF	CITATIONS
1063	Porous Materials Composed of Flue Gas Desulfurization Gypsum and Textile Fiber Wastes. Waste and Biomass Valorization, 2017, 8, 203-207.	1.8	16
1064	Preparation and effectiveness of slowâ€release silicon fertilizer by sintering with iron ore tailings. Environmental Progress and Sustainable Energy, 2018, 37, 1011-1019.	1.3	16
1065	Air-stable n-doped black phosphorus transistor by thermal deposition of metal adatoms. Nanotechnology, 2019, 30, 135201.	1.3	16
1066	Black phosphorus: Versatile twoâ€dimensional materials in cancer therapies. View, 2021, 2, 20200043.	2.7	16
1067	Neural network-based multiobjective optimization algorithm for nonlinear beam dynamics. Physical Review Accelerators and Beams, 2020, 23, .	0.6	16
1068	Size-dependent flame retardancy of black phosphorus nanosheets. Nanoscale, 2022, 14, 2599-2604.	2.8	16
1069	A silicate-loaded MgAl LDH self-healing coating on biomedical Mg alloys for corrosion retardation and cytocompatibility enhancement. Surface and Coatings Technology, 2022, 439, 128442.	2.2	16
1070	Thickness uniformity of silicon-on-insulator fabricated by plasma immersion ion implantation and ion cut. IEEE Transactions on Plasma Science, 1999, 27, 633-636.	0.6	15
1071	Comparison between the different implantation orders in H+and He+coimplantation. Journal Physics D: Applied Physics, 2001, 34, 477-482.	1.3	15
1072	Multiple ion-focusing effects in plasma immersion ion implantation. Applied Physics Letters, 2002, 81, 3744-3746.	1.5	15
1073	Effects of assistant anode on planar inductively coupled magnetized argon plasma in plasma in in plasma immersion ion implantation. Journal of Applied Physics, 2003, 93, 5883-5887.	1.1	15
1074	Influence of ion energies on the surface morphology of carbon films. Surface and Coatings Technology, 2005, 196, 241-245.	2.2	15
1075	Effects of O2 and H2O plasma immersion ion implantation on surface chemical composition and surface energy of poly vinyl chloride. Applied Surface Science, 2006, 252, 7884-7889.	3.1	15
1076	Influence of substrate bias on the composition of SiC thin films fabricated by PECVD and underlying mechanism. Surface and Coatings Technology, 2007, 201, 6777-6780.	2.2	15
1077	Hydrogen plasma surface activation of silicon for biomedical applications. New Biotechnology, 2007, 24, 113-117.	2.7	15
1078	In vitro corrosion behavior of TiN layer produced on orthopedic nickel–titanium shape memory alloy by nitrogen plasma immersion ion implantation using different frequencies. Surface and Coatings Technology, 2008, 202, 2463-2466.	2.2	15
1079	Nano-Scale Surface Morphology, Wettability and Osteoblast Adhesion on Nitrogen Plasma-Implanted NiTi Shape Memory Alloy. Journal of Nanoscience and Nanotechnology, 2009, 9, 3449-3454.	0.9	15
1080	Synthesis and Growth Mechanism of Quasialigned Ultrafine ZnS Nanowire Arrays Fabricated Directly on Zinc Foils. Journal of Physical Chemistry C, 2009, 113, 5520-5525.	1.5	15

PAUL CHU

#	Article	IF	CITATIONS
1081	Surface mechanical attrition treatment induced phase transformation behavior in NiTi shape memory alloy. Journal of Alloys and Compounds, 2009, 482, 298-301.	2.8	15
1082	DLC deposition inside tubes using hollow cathode discharge plasma immersion ion implantation and deposition. Surface and Coatings Technology, 2010, 204, 2909-2912.	2.2	15
1083	Fabrication and Photocatalytic Activity of Nanoporous WO <sub>3</sub> Film. Nanoscience and Nanotechnology Letters, 2010, 2, 51-57.	0.4	15
1084	Fast Preparation of LiFePO <sub>4</sub> Nanoparticles for Lithium Batteries by Microwave-Assisted Hydrothermal Method. Journal of Nanoscience and Nanotechnology, 2010, 10, 980-986.	0.9	15
1085	Longitudinal optical phonon–plasmon coupling in luminescent 3C–SiC nanocrystal films. Optics Letters, 2010, 35, 4024.	1.7	15
1086	Control of cathodic arc spot motion under external magnetic field. Vacuum, 2013, 91, 20-23.	1.6	15
1087	Atomic layer deposition of platinum thin films on anodic aluminium oxide templates as surface-enhanced Raman scattering substrates. Vacuum, 2013, 89, 257-260.	1.6	15
1088	Fabrication of highly ordered porous nickel oxide anode materials and their electrochemical characteristics in lithium storage. Journal of Alloys and Compounds, 2014, 594, 65-69.	2.8	15
1089	Electrodeposition of nanostructured MnO2 electrode on three-dimensional nickel/silicon microchannel plates for miniature supercapacitors. Materials Letters, 2014, 126, 116-118.	1.3	15
1090	High-quality, single-layered epitaxial graphene fabricated on 6H-SiC (0001) by flash annealing in Pb atmosphere and mechanism. Nanotechnology, 2015, 26, 105708.	1.3	15
1091	Robust Electrodes Based on Coaxial TiC/C-MnO <sub>2</sub> Core/Shell Nanofiber Arrays with Excellent Cycling Stability for High-Performance Supercapacitors. Small, 2015, 11, 1847-1856.	5.2	15
1092	Hybrid Co(OH)2/nano-graphene/Ni nano-composites on silicon microchannel plates for miniature supercapacitors. Materials Letters, 2016, 172, 40-43.	1.3	15
1093	Multiband Hot Photoluminescence from Nanocavity-Embedded Silicon Nanowire Arrays with Tunable Wavelength. Nano Letters, 2017, 17, 1552-1558.	4.5	15
1094	Fabrication of Ni-Ti-O nanoporous film on NiTi alloy in ethylene glycol containing NaCl. Surface and Coatings Technology, 2017, 321, 136-145.	2.2	15
1095	Comparison of the Effects Induced by Plasma Generated Reactive Species and H <sub>2</sub> O <sub>2</sub> on Lactate Dehydrogenase (LDH) Enzyme. IEEE Transactions on Plasma Science, 2018, 46, 2742-2752.	0.6	15
1096	Template growth of Au/Ag nanocomposites on phosphorene for sensitive SERS detection of pesticides. Nanotechnology, 2019, 30, 275604.	1.3	15
1097	Highly active cobalt-doped nickel sulfide porous nanocones for high-performance quasi-solid-state zinc-ion batteries. Journal of Energy Chemistry, 2022, 66, 237-249.	7.1	15
1098	Tuning Superhydrophobic Materials with Negative Surface Energy Domains. Research, 2019, 2019, 1391804.	2.8	15

#	Article	IF	CITATIONS
1099	A dual functional chondro-inductive chitosan thermogel with high shear modulus and sustained drug release for cartilage tissue engineering. International Journal of Biological Macromolecules, 2022, 205, 638-650.	3.6	15
1100	Determination of trace metallic impurities on 200-mm silicon wafers by time-of-flight secondary-ion-mass spectroscopy. Journal of Vacuum Science & Technology an Official Journal of the American Vacuum Society B, Microelectronics Processing and Phenomena, 1997, 15, 1908.	1.6	14
1101	Enhancement of surface properties of 45# carbon steel using plasma immersion ion implantation. Thin Solid Films, 1997, 311, 190-195.	0.8	14
1102	Hybrid simulation of sheath and ion dynamics of plasma implantation into ring-shaped targets. Journal Physics D: Applied Physics, 2001, 34, 1091-1099.	1.3	14
1103	Investigation of low-pressure elevated-temperature plasma immersion ion implantation of AISI 304 stainless steel. Journal of Vacuum Science and Technology A: Vacuum, Surfaces and Films, 2001, 19, 1008-1012.	0.9	14
1104	Effects of bias voltage on the corrosion resistance of titanium nitride thin films fabricated by dynamic plasma immersion ion implantation-deposition. Journal of Vacuum Science and Technology A: Vacuum, Surfaces and Films, 2002, 20, 160-164.	0.9	14
1105	Corrosion resistance of AISI304 stainless steel treated by hybrid elevated-temperature, low-voltage/high-voltage nitrogen plasma immersion ion implantation. Materials Science & Engineering A: Structural Materials: Properties, Microstructure and Processing, 2002, 326, 348-354.	2.6	14
1106	Relaxed silicon–germanium-on-insulator substrates by oxygen implantation into pseudomorphic silicon germanium/silicon heterostructure. Applied Physics Letters, 2003, 82, 2452-2454.	1.5	14
1107	Influence of thickness and dielectric properties on implantation efficacy in plasma immersion ion implantation of insulators. Journal of Applied Physics, 2004, 95, 3319-3323.	1.1	14
1108	Surface and corrosion characteristics of carbon plasma implanted and deposited nickel-titanium alloy. Journal of Vacuum Science and Technology A: Vacuum, Surfaces and Films, 2005, 23, 525-530.	0.9	14
1109	Effects of nitrogen ion implantation and implantation energy on surface properties and adhesion strength of TiN films deposited on aluminum by magnetron sputtering. Materials Science & Engineering A: Structural Materials: Properties, Microstructure and Processing, 2006, 415, 140-144.	2.6	14
1110	Spontaneous reorientation of bimetal multilayer nanowires. Applied Physics Letters, 2007, 91, 253114.	1.5	14
1111	Improvement of interfacial and microstructure properties of high-k ZrO2 thin films fabricated by filtered cathodic arc deposition using nitrogen incorporation. Surface and Coatings Technology, 2007, 201, 8282-8285.	2.2	14
1112	Effects of tungsten pre-implanted layer on corrosion and electrochemical characteristics of amorphous carbon films on stainless steel. Diamond and Related Materials, 2008, 17, 1738-1742.	1.8	14
1113	Nanocrystal-induced line narrowing of surface acoustic phonons in the Raman spectra of embedded <mml:math display="inline" xmlns:mml="http://www.w3.org/1998/Math/MathML"><mml:mrow><mml:msub><mml:mrow><mml:mtext>Ge</mml:mtext></mml:mrow><mml:mi>x&lt; nanocrystals. Physical Review B, 2008, 78, .</mml:mi></mml:msub></mml:mrow></mml:math>	/ <mark>1:1</mark> /mml:mi>·	
1114	Effects of ozone oxidation on interfacial and dielectric properties of thin HfO2 films. Journal of Applied Physics, 2008, 104, 054117.	1.1	14
1115	Raman investigation of oxidation mechanism of silicon nanowires. Applied Physics Letters, 2009, 95, .	1.5	14
1116	Nickel release behavior and surface characteristics of porous NiTi shape memory alloy modified by different chemical processes. Journal of Biomedical Materials Research - Part A, 2009, 89A, 483-489.	2.1	14

#	Article	IF	CITATIONS
1117	Corrosion resistance of TiN coated biomedical nitinol under deformation. Materials Science and Engineering C, 2009, 29, 1599-1603.	3.8	14
1118	Nano-networks have better adsorption capability than nano-rods. Nano Communication Networks, 2010, 1, 257-263.	1.6	14
1119	Activation of mitogen-activated protein kinases cellular signal transduction pathway in mammalian cells induced by silicon carbide nanowires. Biomaterials, 2010, 31, 7856-7862.	5.7	14
1120	Three-dimensional supercapacitors composed of Ba0.65Sr0.35TiO3 (BST)/NiSi2/silicon microchannel plates. Materials Science and Engineering B: Solid-State Materials for Advanced Technology, 2011, 176, 387-392.	1.7	14
1121	Electron field emission enhanced by geometric and quantum effects from nanostructured AlGaN/GaN quantum wells. Applied Physics Letters, 2011, 98, 152110.	1.5	14
1122	Effect of high fluence Au ion irradiation on nanocrystalline tungsten film. Journal of Nuclear Materials, 2013, 442, 189-194.	1.3	14
1123	Multi-functional honeycomb ceramic materials produced from bauxite residues. Materials & Design, 2014, 59, 333-338.	5.1	14
1124	Irradiation effects on multilayered W/ZrO 2 film under 4 MeV Au ions. Journal of Nuclear Materials, 2014, 455, 86-90.	1.3	14
1125	Enhanced cytocompatibility and reduced genotoxicity of polydimethylsiloxane modified by plasma immersion ion implantation. Colloids and Surfaces B: Biointerfaces, 2016, 148, 139-146.	2.5	14
1126	Microstructure evolution in the fusion zone of laser-welded Mg–Gd–Y–Zr alloy during solution and aging treatment. Materials Characterization, 2016, 118, 486-493.	1.9	14
1127	Recent advances in anti-infection surfaces fabricated on biomedical implants by plasma-based technology. Surface and Coatings Technology, 2017, 312, 2-6.	2.2	14
1128	Carbon nanodots-based nanocomposites with enhanced photocatalytic performance and photothermal effects. Applied Physics Letters, 2017, 111, .	1.5	14
1129	Highly Luminescent and Stable Siâ€Based CsPbBr 3 Quantum Dot Thin Films Prepared by Glow Discharge Plasma with Realâ€Time and In Situ Diagnosis. Advanced Functional Materials, 2018, 28, 1805214.	7.8	14
1130	Hard and adherent a-C:H gradient coatings by stress engineering. Journal of Alloys and Compounds, 2018, 765, 921-926.	2.8	14
1131	Highly sensitive PCF-SPR biosensor for hyperthermia temperature monitoring. Journal of Optics (India), 2018, 47, 288-294.	0.8	14
1132	Investigation of corrosion mechanism of NiTi modified by carbon plasma immersion ion implantation (C-PIII) by electrochemical impedance spectroscopy. Journal of Alloys and Compounds, 2019, 790, 1067-1075.	2.8	14
1133	Lithium ion trapping mechanism of SiO2 in LiCoO2 based memristors. Scientific Reports, 2019, 9, 5081.	1.6	14
1134	Modification of Layered Graphitic Carbon Nitride by Nitrogen Plasma for Improved Electrocatalytic Hydrogen Evolution. Nanomaterials, 2019, 9, 568.	1.9	14

#	Article	IF	CITATIONS
1135	Recent Progress in Electrode Materials for Nonaqueous Lithium-Ion Capacitors. Journal of Nanoscience and Nanotechnology, 2020, 20, 2652-2667.	0.9	14
1136	A Biomimetic Nanoâ€Engineered Platform for Functional Tissue Engineering of Cartilage Superficial Zone. Advanced Healthcare Materials, 2021, 10, e2001018.	3.9	14
1137	Activating Carbon Nitride by BP@Ni for the Enhanced Photocatalytic Hydrogen Evolution and Selective Benzyl Alcohol Oxidation. ACS Applied Materials & amp; Interfaces, 2021, 13, 50988-50995.	4.0	14
1138	Plasma functionalized MoSe <sub>2</sub> for efficient nonenzymatic sensing of hydrogen peroxide in ultraâ€wide pH range. SmartMat, 2022, 3, 491-502.	6.4	14
1139	Diamond-like carbon coating and surface grafting of osteoprotegerin and alendronate on polyetheretherketone to ameliorate the mechanical performance and osseointegration simultaneously. Composites Part B: Engineering, 2022, 236, 109815.	5.9	14
1140	A highly sensitive D-type photonic crystal fiber infrared sensor with indium tin oxide based on surface plasmon resonance. Modern Physics Letters B, 2022, 36, .	1.0	14
1141	Plasmon-enhanced hydrogen evolution on Pt-anchored titanium nitride nanowire arrays. Applied Surface Science, 2022, 598, 153745.	3.1	14
1142	General synthesis of nanostructured Mo2C electrocatalysts using a carbon template for electrocatalytic applications. Carbon, 2022, 197, 238-245.	5.4	14
1143	Plasma immersion ion implantation for SOI synthesis: SIMOX and ion-cut. Journal of Electronic Materials, 1998, 27, 1059-1066.	1.0	13
1144	Efficacy of high-frequency, low-voltage plasma immersion ion implantation of a bar-shaped target. Journal of Applied Physics, 2000, 88, 2221-2225.	1.1	13
1145	Profile control in BF3 plasma doping. Journal of Applied Physics, 2000, 88, 3198-3201.	1.1	13
1146	Energy distribution and depth profile in BF3 plasma doping. Surface and Coatings Technology, 2001, 136, 146-150.	2.2	13
1147	Epitaxial growth of CoSi2 film by Co/a-Si/Ti/Si(100) multilayer solid state reaction. Journal of Applied Physics, 2001, 89, 2641-2648.	1.1	13
1148	Influence of temperature and ion kinetic energy on surface morphology of CeO2 films prepared by dual plasma deposition. Materials Science & Engineering A: Structural Materials: Properties, Microstructure and Processing, 2002, 336, 75-80.	2.6	13
1149	Two-dimensional particle-in-cell plasma immersion ion implantation simulation of gear/windmill geometry in cylindrical co-ordinates along the (r–î) plane. Surface and Coatings Technology, 2002, 156, 97-102.	2.2	13
1150	Improved planar radio frequency inductively coupled plasma configuration in plasma immersion ion implantation. Review of Scientific Instruments, 2003, 74, 2704-2708.	0.6	13
1151	Mechanism of apatite formation on hydrogen plasma-implanted single-crystal silicon. Applied Physics Letters, 2004, 85, 3623-3625.	1.5	13
1152	Effects of mesh-assisted carbon plasma immersion ion implantation on the surface properties of insulating silicon carbide ceramics. Journal of Vacuum Science and Technology A: Vacuum, Surfaces and Films, 2004, 22, 356-360.	0.9	13

#	Article	IF	CITATIONS
1153	Formation of Si-based nano-island array on porous anodic alumina. Acta Materialia, 2004, 52, 5633-5637.	3.8	13
1154	Light emission from as-prepared and oxidized Si nanowires with diameters of 5–15nm. Journal of Crystal Growth, 2005, 285, 620-626.	0.7	13
1155	Improvement on corrosion resistance of NiTi orthopedic materials by carbon plasma immersion ion implantation. Nuclear Instruments & Methods in Physics Research B, 2006, 242, 270-274.	0.6	13
1156	Luminescent amorphous alumina nanoparticles in toluene solution. Journal of Physics Condensed Matter, 2006, 18, 9937-9942.	0.7	13
1157	Fabrication of silicon-on-SiO2/diamondlike-carbon dual insulator using ion cutting and mitigation of self-heating effects. Applied Physics Letters, 2006, 88, 142108.	1.5	13
1158	New plasma surface-treated memory alloys: Towards a new generation of "smart―orthopaedic materials. Materials Science and Engineering C, 2008, 28, 454-459.	3.8	13
1159	Synthesis, growth mechanism, and light-emission properties of twisted SiO2 nanobelts and nanosprings. Journal of Chemical Physics, 2008, 129, 164702.	1.2	13
1160	Effects of long pulse width and high pulsing frequency on surface superhydrophobicity of polytetrafluoroethylene in quasi-direct-current plasma immersion ion implantation. Journal of Applied Physics, 2009, 105, 053302.	1.1	13
1161	Nanomechanical properties and microstructure of ZrO2/Al2O3 plasma sprayed coatings. Materials Science & Engineering A: Structural Materials: Properties, Microstructure and Processing, 2009, 518, 185-189.	2.6	13
1162	Fabrication and optical properties of C/β-SiC/Si hybrid rolled-up microtubes. Journal of Applied Physics, 2009, 105, 016103.	1.1	13
1163	Surface treatment of NiTi shape memory alloy by modified advanced oxidation process. Transactions of Nonferrous Metals Society of China, 2009, 19, 575-580.	1.7	13
1164	Capacitive humidity sensing behavior of ordered Ni/Si microchannel plate nanocomposites. Sensors and Actuators A: Physical, 2010, 160, 48-53.	2.0	13
1165	Synthesis and characterization of fluorescent copolymer containing rare earth metal complex and its interaction with DNA. Journal of Polymer Science Part A, 2010, 48, 5961-5967.	2.5	13
1166	Ultralow-threshold field emission from oriented nanostructured GaN films on Si substrate. Applied Physics Letters, 2010, 96, 092101.	1.5	13
1167	Twinning Ge0.54Si0.46 nanocrystal growth mechanism in amorphous SiO2 films. Applied Physics Letters, 2010, 96, .	1.5	13
1168	Identification of local silicon cluster nanostructures inside SixGe1â^'x alloy nanocrystals by Raman spectroscopy. Chemical Communications, 2010, 46, 5539.	2.2	13
1169	Arrays of nanofibers composed of a TiC core and a carbon coating for sensitive electrochemical detection of hydrazine. Mikrochimica Acta, 2011, 175, 137-143.	2.5	13
1170	In vitro corrosion inhibition on biomedical shape memory alloy by plasma-polymerized allylamine film. Materials Letters, 2012, 89, 51-54.	1.3	13

#	Article	IF	CITATIONS
1171	Synthesis and characterization of novel organosiliconâ€modified polyurethane. Journal of Applied Polymer Science, 2012, 125, 1486-1492.	1.3	13
1172	Improved in vitro and in vivo biocompatibility of dual plasma modified titanium alloy. Surface and Coatings Technology, 2013, 229, 130-134.	2.2	13
1173	Structure and properties of TiC/Ti coatings fabricated on NiTi by plasma immersion ion implantation and deposition. Vacuum, 2013, 89, 238-243.	1.6	13
1174	Crystallization Effects of Nanocrystalline GaN Films on Field Emission. Journal of Physical Chemistry C, 2013, 117, 1518-1523.	1.5	13
1175	Size-dependent elastic modulus of single-layer MoS2 nano-sheets. Journal of Materials Science, 2016, 51, 6850-6859.	1.7	13
1176	An electrochemical immunosensor comprising thionin/silver nanoparticles decorated KIT-6 for ultrasensitive detection of squamous cell carcinoma antigen. RSC Advances, 2016, 6, 6932-6938.	1.7	13
1177	Unusual anti-bacterial behavior and corrosion resistance of magnesium alloy coated with diamond-like carbon. RSC Advances, 2016, 6, 14756-14762.	1.7	13
1178	Highly efficient field emission from ZnO nanorods and nanographene hybrids on a macroporous electric conductive network. Journal of Materials Chemistry C, 2017, 5, 9296-9305.	2.7	13
1179	Effects of diamond-like carbon film on the corrosion behavior of NdFeB permanent magnet. Surface and Coatings Technology, 2017, 312, 66-74.	2.2	13
1180	Highly efficient field emission from indium-doped ZnO nanostructure on nanographene/macroporous electric conductive network. Materials Letters, 2018, 222, 25-28.	1.3	13
1181	Effects of Benzotriazole on nano-mechanical properties of zirconia–alumina–Benzotriazole nanocomposite coating deposited on Al 2024 by the sol–gel method. Applied Physics A: Materials Science and Processing, 2019, 125, 1.	1.1	13
1182	Co3O4 and Co(OH)2 loaded graphene on Ni foam for high-performance supercapacitor electrode. Ionics, 2019, 25, 1783-1792.	1.2	13
1183	Abrasion and erosion behavior of DLC-coated oil-well tubings in a heavy oil/sand environment. Surface and Coatings Technology, 2019, 357, 379-383.	2.2	13
1184	Study of TiAlN coatings deposited by continuous high power magnetron sputtering (C-HPMS). Surface and Coatings Technology, 2020, 402, 126315.	2.2	13
1185	Enhanced discharge and surface properties of TiSiCN coatings deposited by pulse-enhanced vacuum arc evaporation. Surface and Coatings Technology, 2020, 403, 126413.	2.2	13
1186	Reducing Migration of Sintered Ag for Power Devices Operating at High Temperature. IEEE Transactions on Power Electronics, 2020, 35, 12646-12650.	5.4	13
1187	Articular cartilage inspired bilayer coating on Ti6Al4V alloy with low friction and high load-bearing properties. Applied Surface Science, 2020, 515, 146065.	3.1	13
1188	Substitution of quartz and clay with fly ash in the production of architectural ceramics: A mechanistic study. Ceramics International, 2021, 47, 12514-12525.	2.3	13

#	Article	IF	CITATIONS
1189	Insights into enhancement of photocatalytic properties of g-C3N4 by local electric field induced by polarization of MgO(111). Journal of Environmental Chemical Engineering, 2021, 9, 105922.	3.3	13
1190	The Superiority of N 2O Plasma Annealing over O 2 Plasma Annealing for Amorphous Tantalum Pentoxide (Ta 2O 5) Films. Japanese Journal of Applied Physics, 1998, 37, L435-L437.	0.8	12
1191	Mechanism of enhanced plasma transport of vacuum arc plasma through curved magnetic ducts. Journal of Vacuum Science and Technology A: Vacuum, Surfaces and Films, 1999, 17, 3074-3076.	0.9	12
1192	Nickel precipitation at nanocavities in separation by implantation of oxygen. Journal of Vacuum Science and Technology A: Vacuum, Surfaces and Films, 2000, 18, 2249.	0.9	12
1193	Nitrogen depth profiles in plasma implanted stainless steel. Physics Letters, Section A: General, Atomic and Solid State Physics, 2002, 299, 577-580.	0.9	12
1194	Low vacuum MEVVA titanium and nitrogen co-ion implantation into D2 steel substrates. Surface and Coatings Technology, 2004, 185, 264-267.	2.2	12
1195	Determination of nitrogen-related defects in N-implanted ZnO films by dynamic cathodoluminescence. Nuclear Instruments & Methods in Physics Research B, 2005, 237, 307-311.	0.6	12
1196	Microwave-cut silicon layer transfer. Applied Physics Letters, 2005, 87, 224103.	1.5	12
1197	Optical emission from nano-poly[2-methoxy-5-(2′-ethyl-hexyloxy)-p-phenylene vinylene] arrays. Journal of Applied Physics, 2005, 98, 074304.	1.1	12
1198	Silicon layer transfer using plasma hydrogenation. Applied Physics Letters, 2005, 87, 111910.	1.5	12
1199	Nitrogen binding behavior in ZnO films with time-resolved cathodoluminescence. Applied Surface Science, 2006, 252, 8131-8134.	3.1	12
1200	Silver nanocrystal superlattices: Self-assembly and optical emission. Applied Physics Letters, 2006, 88, 143111.	1.5	12
1201	Effects of magnetic field gradient on ion beam current in cylindrical Hall ion source. Journal of Applied Physics, 2007, 102, 123305.	1.1	12
1202	Growth of pinhole-free ytterbium silicide film by solid-state reaction on Si(001) with a thin amorphous Si interlayer. Journal of Applied Physics, 2007, 102, 033508.	1.1	12
1203	Polarized Raman scattering of Ge nanocrystals embedded in a-SiO2. Applied Physics Letters, 2007, 90, 081909.	1.5	12
1204	Behavior of human umbilical vein endothelial cells on micro-patterned amorphous hydrogenated carbon films produced by plasma immersion ion implantation & deposition and plasma etching. Diamond and Related Materials, 2007, 16, 550-557.	1.8	12
1205	Effects of plasma treatment on bioactivity of TiO2 coatings. Surface and Coatings Technology, 2007, 201, 6878-6881.	2.2	12
1206	Effects of aluminum incorporation on hafnium oxide film using plasma immersion ion implantation. Microelectronics Reliability, 2008, 48, 1765-1768.	0.9	12

#	Article	IF	CITATIONS
1207	In vitro bioactivity and osteoblast response on chemically modified biomedical porous NiTi synthesized by capsule-free hot isostatic pressing. Surface and Coatings Technology, 2008, 202, 2458-2462.	2.2	12
1208	Electrochemical Stability of Orthopedic Porous NiTi Shape Memory Alloys Treated by Different Surface Modification Techniques. Journal of the Electrochemical Society, 2009, 156, C187.	1.3	12
1209	Low energy-consumption plasma electrolytic oxidation based on grid cathode. Review of Scientific Instruments, 2010, 81, 103504.	0.6	12
1210	Microstructure and tribological properties of ternary BCN thin films with different carbon contents. Diamond and Related Materials, 2010, 19, 1225-1229.	1.8	12
1211	Novel plasma immersion ion implantation and deposition hardware and technique based on high power pulsed magnetron discharge. Review of Scientific Instruments, 2011, 82, 033511.	0.6	12
1212	Cross-linked polystyrene microspheres as density-reducing agent in drilling fluid. Journal of Petroleum Science and Engineering, 2011, 78, 529-533.	2.1	12
1213	A Localized Surface Plasmon Resonance Biosensor Based on Integrated Controllable Au2S/AuAgS-Coated Gold Nanorods Composite. Plasmonics, 2011, 6, 1-9.	1.8	12
1214	Conversion of strain state from biaxial to uniaxial in strained silicon. Applied Physics Letters, 2011, 98,	1.5	12
1215	Photoluminescence induced by twinning interface in CdS nanocrystals. Applied Physics Letters, 2012, 100, 171911.	1.5	12
1216	Three-dimensional numerical investigation of electron transport with rotating spoke in a cylindrical anode layer Hall plasma accelerator. Physics of Plasmas, 2012, 19, .	0.7	12
1217	Preparation of Fe3O4/poly(styrene-butyl acrylate-[2-(methacryloxy)ethyl]trimethylammonium) Tj ETQq1 1 0.784 Magnetism and Magnetic Materials, 2012, 324, 1410-1418.	314 rgBT / 1.0	Overlock 10 12
1218	Antimicrobial effects of oxygen plasma modified medical grade Ti–6Al–4V alloy. Vacuum, 2013, 89, 271-279.	1.6	12
1219	Effects of chromium ion implantation voltage on the corrosion resistance and cytocompatibility of dual chromium and oxygen plasma-ion-implanted biodegradable magnesium. Surface and Coatings Technology, 2013, 235, 875-880.	2.2	12
1220	Properties of carbon film deposited on stainless steel by close field unbalanced magnetron sputter ion plating. Thin Solid Films, 2013, 531, 320-327.	0.8	12
1221	Carbon-Doped TiO <sub>2</sub> Nanotube Array Platform for Visible Photocatalysis. Nanoscience and Nanotechnology Letters, 2013, 5, 1251-1257.	0.4	12
1222	Three-dimensional nanoscale Co3O4 electrode on ordered Ni/Si microchannel plates for electrochemical supercapacitors. Materials Letters, 2014, 132, 405-408.	1.3	12
1223	Discharge current modes of high power impulse magnetron sputtering. AIP Advances, 2015, 5, .	0.6	12
1224	Deposition of diamond-like carbon films on interior surface of long and slender quartz glass tube by enhanced glow discharge plasma immersion ion implantation. Surface and Coatings Technology, 2015, 265, 218-221.	2.2	12

#	Article	IF	CITATIONS
1225	Magnetic, fluorescent, and thermo-responsive poly(MMA-NIPAM-Tb(AA) <sub>3</sub> Phen)/Fe <sub>3</sub> O <sub>4</sub> multifunctional nanospheres prepared by emulsifier-free emulsion polymerization. Journal of Biomaterials Applications, 2015, 30, 201-211.	1.2	12
1226	Analysis of a highly birefringent asymmetric photonic crystal fibre based on a surface plasmon resonance sensor. Journal of Modern Optics, 2016, 63, 1189-1195.	0.6	12
1227	Effects of Laser Shock Processing on Fatigue Crack Growth in Ti-17 Titanium Alloy. Journal of Materials Engineering and Performance, 2017, 26, 813-821.	1.2	12
1228	Imaging and motion of cathode group spots during pulse-enhanced vacuum arc evaporation. Vacuum, 2017, 139, 37-43.	1.6	12
1229	Mechanism of <scp>M</scp> <i><sub>x</sub></i> <scp>O</scp> <sub><i>y</i></sub> nanoparticles/ <scp>CNT</scp> s for catalytic carbonization of polyethylene and application to flame retardancy. Journal of Applied Polymer Science, 2017, 134, 45233.	1.3	12
1230	Enhancement of Ferromagnetism in Nonmagnetic Metal Oxide Nanoparticles by Facet Engineering. Small, 2017, 13, 1602951.	5.2	12
1231	Electrocatalytic hydrogen evolution of palladium nanoparticles electrodeposited on nanographene coated macroporous electrically conductive network. International Journal of Hydrogen Energy, 2018, 43, 2171-2183.	3.8	12
1232	Dealkalization of Red Mud by Carbide Slag and Flue Gas. Clean - Soil, Air, Water, 2018, 46, 1700634.	0.7	12
1233	Discharge and Deposition Characteristics of High-Power Impulse Magnetron Sputtering Using Various Target Materials. IEEE Transactions on Plasma Science, 2019, 47, 193-198.	0.6	12
1234	A quasi-2D material CePO4 and the self-lubrication in micro-arc oxidized coatings on Al alloy. Tribology International, 2019, 138, 157-165.	3.0	12
1235	Multifunctional nitrogen-doped nanoporous carbons derived from metal–organic frameworks for efficient CO <sub>2</sub> storage and high-performance lithium-ion batteries. New Journal of Chemistry, 2019, 43, 10405-10412.	1.4	12
1236	Hollow cathode effect modified time-dependent global model and high-power impulse magnetron sputtering discharge and transport in cylindrical cathode. Journal of Applied Physics, 2019, 125, .	1.1	12
1237	Effects of Ti, Ni, and Dual Ti/Ni Plasma Immersion Ion Implantation on the Corrosion and Wear Properties of Magnesium Alloy. Coatings, 2020, 10, 313.	1.2	12
1238	3D urchin-like NiCo2O4 coated with carbon nanospheres prepared on flexible graphite felt for efficient bifunctional electrocatalytic water splitting. Journal of Materials Science, 2021, 56, 9961-9973.	1.7	12
1239	Graphene-mediated ferromagnetic coupling in the nickel nano-islands/graphene hybrid. Science Advances, 2021, 7, .	4.7	12
1240	In vitro and in vivo antibacterial performance of Zr & O PIII magnesium alloys with high concentration of oxygen vacancies. Bioactive Materials, 2021, 6, 3049-3061.	8.6	12
1241	Atomistic Observation of the Local Phase Transition in MoTe <sub>2</sub> for Application in Homojunction Photodetectors. Small, 2022, 18, e2200913.	5.2	12
1242	Combined impurity gettering effects of helium-induced cavities and oxygen precipitates created by plasma immersion ion implantation. Thin Solid Films, 1997, 300, 64-67.	0.8	11

#	Article	IF	CITATIONS
1243	Properties of titanium nitride fabricated on stainless steel by plasma-based ion implantation/deposition. Materials Science & Engineering A: Structural Materials: Properties, Microstructure and Processing, 2000, 282, 164-169.	2.6	11
1244	Dynamic nitrogen and titanium plasma ion implantation/deposition at different bias voltages. Thin Solid Films, 2001, 390, 139-144.	0.8	11
1245	Target temperature simulation during fast-pulsing plasma immersion ion implantation. Journal Physics D: Applied Physics, 2001, 34, 1639-1645.	1.3	11
1246	Plasma transport in magnetic duct filter. Journal Physics D: Applied Physics, 2002, 35, 3176-3180.	1.3	11
1247	Current control for magnetized plasma in direct-current plasma-immersion ion implantation. Applied Physics Letters, 2003, 82, 2014-2016.	1.5	11
1248	Anode double layer in magnetized radio frequency inductively coupled hydrogen plasma. Journal of Applied Physics, 2003, 94, 1390-1395.	1.1	11
1249	Implantation dynamics of plasma implantation into insulating strips. Journal Physics D: Applied Physics, 2004, 37, 50-54.	1.3	11
1250	Two-dimensional numerical simulation of non-uniform plasma immersion ion implantation. Surface and Coatings Technology, 2004, 186, 47-52.	2.2	11
1251	Linear ion source with magnetron hollow cathode discharge. Review of Scientific Instruments, 2005, 76, 113502.	0.6	11
1252	Local vibration at the surface of a Ge nanocrystal embedded in a silicon oxide matrix. Journal of Applied Physics, 2006, 99, 014301.	1.1	11
1253	The effect of N+-implanted aluminum substrate on the mechanical properties of TiN films. Surface and Coatings Technology, 2006, 200, 2672-2678.	2.2	11
1254	Optical emission from the aggregated state in poly [2-methoxy-5-(2′-ethyl-hexyloxy)-p-phenylene vinylene]. Journal of Vacuum Science and Technology A: Vacuum, Surfaces and Films, 2006, 24, 202-205.	0.9	11
1255	Nitrogen Incorporation into Hafnium Oxide Films by Plasma Immersion Ion Implantation. Japanese Journal of Applied Physics, 2007, 46, 3234-3238.	0.8	11
1256	Microstructure and visible-photoluminescence of titanium dioxide thin films fabricated by dual cathodic arc and nitrogen plasma deposition. Surface and Coatings Technology, 2007, 201, 4897-4900.	2.2	11
1257	Characteristics of end Hall ion source with magnetron hollow cathode discharge. Nuclear Instruments & Methods in Physics Research B, 2007, 257, 796-800.	0.6	11
1258	Ab initio determination of lattice dynamics and thermodynamics of $\hat{I}^2$ - BC2N. Solid State Communications, 2008, 146, 69-72.	0.9	11
1259	Investigation of plasma distribution in electron-focused electric field enhanced glow discharge plasma immersion ion implantation. Journal of Applied Physics, 2008, 104, 043303.	1.1	11
1260	Bonding strength of fluorinated and hydrogenated surfactant to bovine serum albumin. Journal of Fluorine Chemistry, 2009, 130, 870-877.	0.9	11

#	Article	IF	CITATIONS
1261	Optical and vibrational properties of 2H-, 4H-, and 6H-AlN: First-principle calculations. Journal of Applied Physics, 2009, 105, 083511.	1.1	11
1262	Influence of GeSi interfacial layer on Ge–Ge optical phonon mode in SiO2 films embedded with Ge nanocrystals. Applied Physics Letters, 2009, 95, .	1.5	11
1263	Interfacial adhesion measurement of a ceramic coating on metal substrate. Journal of Coatings Technology Research, 2010, 7, 391-398.	1.2	11
1264	Chemical combustion synthesis and up-conversion properties of Er3+ doped Yb3Al5O12 powder. Optical Materials, 2010, 32, 1188-1192.	1.7	11
1265	Hybrid plasma surface modification and ion implantation of biopolymers. Surface and Coatings Technology, 2010, 204, 2892-2897.	2.2	11
1266	Inverse Hall–Petch relationship in the nanostructured TiO2: Skin-depth energy pinning versus surface preferential melting. Journal of Applied Physics, 2010, 108, 073503.	1.1	11
1267	Magnetorotational instability in a two-fluid model. Plasma Physics and Controlled Fusion, 2011, 53, 065021.	0.9	11
1268	Adsorption of polyvinyl alcohol from wastewater by sintered porous red mud. Water Science and Technology, 2012, 65, 2055-2060.	1.2	11
1269	Hydrothermal Growth Mechanism of Controllable Hydrophilic Titanate Nanostructures on Medical NiTi Shape Memory Alloy. Journal of Materials Engineering and Performance, 2012, 21, 2600-2606.	1.2	11
1270	3C-SiC nanocrystals/TiO2 nanotube heterostructures with enhanced photocatalytic performance. Applied Physics Letters, 2014, 104, .	1.5	11
1271	General Properties of Bulk SiC. Engineering Materials and Processes, 2014, , 7-114.	0.2	11
1272	Rare-earth-incorporated polymeric vector for enhanced gene delivery. Biomaterials, 2014, 35, 479-488.	5.7	11
1273	Fabrication and photoelectrochemical study of vertically oriented TiO 2 /Ag/SiNWs arrays. Journal of Alloys and Compounds, 2015, 635, 112-117.	2.8	11
1274	Selective growth of Pb islands on graphene/SiC buffer layers. Journal of Applied Physics, 2015, 117, 065304.	1.1	11
1275	Synthesis, microstructure, and electronic band structure properties of nanocrystalline neodymium-doped bismuth titanate ferroelectric films fabricated by the sol–gel method. Materials Research Bulletin, 2015, 61, 238-244.	2.7	11
1276	Communication between nitric oxide synthase and positively-charged surface and bone formation promotion. Colloids and Surfaces B: Biointerfaces, 2016, 148, 354-362.	2.5	11
1277	Three-dimensional flexible carbon electrode for symmetrical supercapacitors. Materials Letters, 2016, 185, 193-196.	1.3	11
1278	Simultaneous arsenate and alkali removal from alkaline wastewater by in-situ formation of Zn–Al layered double hydroxide. Microporous and Mesoporous Materials, 2016, 227, 137-143.	2.2	11

#	Article	IF	CITATIONS
1279	Praseodymium-surface-modified magnesium alloy: Retardation of corrosion in artificial hand sweat. Materials Letters, 2016, 163, 85-89.	1.3	11
1280	Self-assembly and enhanced visible-light-driven photocatalytic activity of reduced graphene oxide-Bi2WO6 photocatalysts. Nanotechnology Reviews, 2017, 6, 505-516.	2.6	11
1281	Environmentally friendly wollastonite@TiO2 composite particles prepared by a mechano-chemical method. Particuology, 2018, 40, 105-112.	2.0	11
1282	Barrier Reduction of Lithium Ion Tunneling through Graphene with Hybrid Defects: Firstâ€Principles Calculations. Advanced Theory and Simulations, 2018, 1, 1700009.	1.3	11
1283	Vertically distributed VO <sub>2</sub> nanoplatelets on hollow spheres with enhanced thermochromic properties. Journal of Materials Chemistry C, 2018, 6, 7896-7904.	2.7	11
1284	Spontaneous single-crystal to single-crystal transition with self-healing cracks involving solvent exchange. CrystEngComm, 2019, 21, 1102-1106.	1.3	11
1285	EIS and noise study of zirconia-alumina- benzotriazole nano-composite coating applied on Al2024 by the sol-gel method. Journal of Alloys and Compounds, 2020, 816, 152662.	2.8	11
1286	From Octahedron Crystals to 2D Silicon Nanosheets: Facet‣elective Cleavage and Biophotonic Applications. Small, 2020, 16, e2003594.	5.2	11
1287	Fabrication of Bimetallic Oxides (MCo2O4: M=Cu, Mn) on Ordered Microchannel Electro-Conductive Plate for High-Performance Hybrid Supercapacitors. Sustainability, 2021, 13, 9896.	1.6	11
1288	Enhanced Hydroxyapatite Growth and Osteogenic Activity on Polydopamine Coated Ti Implants. Nanoscience and Nanotechnology Letters, 2015, 7, 233-239.	0.4	11
1289	Topochemical Synthesis of Copper Phosphide Nanoribbons for Flexible Optoelectronic Memristors. Advanced Functional Materials, 0, , 2110900.	7.8	11
1290	Commercialization of Electric Vehicles in Hong Kong. Energies, 2022, 15, 942.	1.6	11
1291	Origin of superior pseudocapacitive mechanism of transition metal nitrides. Journal of Energy Chemistry, 2022, 69, 561-568.	7.1	11
1292	In-Situ and controllable construction of Mo2N embedded Mo2C nanobelts as robust electrocatalyst for superior pH-universal hydrogen evolution reaction. Journal of Alloys and Compounds, 2022, 918, 165611.	2.8	11
1293	Inner surface ion implantation using deflecting electric field. Nuclear Instruments & Methods in Physics Research B, 1998, 143, 306-310.	0.6	10
1294	Boron segregation in As-implanted Si caused by electric field and transient enhanced diffusion. Applied Physics Letters, 1998, 72, 1709-1711.	1.5	10
1295	Floating low-temperature radio-frequency plasma oxidation of polycrystalline silicon-germanium. Applied Physics Letters, 1998, 73, 360-362.	1.5	10
1296	Quasi-direct current plasma immersion ion implantation. Applied Physics Letters, 2001, 79, 3044-3046.	1.5	10

#	Article	IF	CITATIONS
1297	Experimental investigation of electron oscillation inside the filter of a vacuum arc plasma source. Applied Physics Letters, 2001, 78, 422-424.	1.5	10
1298	Metallic contamination in hydrogen plasma immersion ion implantation of silicon. Journal of Applied Physics, 2001, 90, 3743-3749.	1.1	10
1299	Time Dependence of Phosphorus Diffusion and Dose Loss during Postimplantation Annealing at Low Temperatures. Japanese Journal of Applied Physics, 2002, 41, 1220-1223.	0.8	10
1300	Characteristics and polarization-enhanced model of wurtzite aluminum nitride thin films synthesized on Si(100) substrates by pulsed laser deposition. Journal of Applied Physics, 2003, 94, 1934-1940.	1.1	10
1301	Plasma immersion ion implantation of industrial gears. Surface and Coatings Technology, 2004, 186, 260-264.	2.2	10
1302	Strain relaxation mechanism in SiGe-on-insulator fabricated by Ge condensation. Journal of Crystal Growth, 2005, 281, 275-280.	0.7	10
1303	Relaxed SiGe-on-insulator fabricated by dry oxidation of sandwiched Si/SiGe/Si structure. Materials Science and Engineering B: Solid-State Materials for Advanced Technology, 2005, 124-125, 153-157.	1.7	10
1304	Formation mechanism of individual alumina nanotubes wrapping metal (Cu and Fe) nanowires. Journal of Crystal Growth, 2006, 289, 295-298.	0.7	10
1305	Si-based solid blue emitters from 3C-SiC nanocrystals. Applied Physics A: Materials Science and Processing, 2006, 82, 485-487.	1.1	10
1306	Enhanced electron field emission from oriented columnar AlN and mechanism. Applied Physics Letters, 2006, 88, 251103.	1.5	10
1307	Activation volume and incipient plastic deformation of uniaxially-loaded gold nanowires at very high strain rates. Nanotechnology, 2007, 18, 455702.	1.3	10
1308	Effects of pulsing frequency on shape recovery and investigation of nickel out-diffusion after mechanical bending of nitrogen plasma implanted NiTi shape memory alloys. Surface and Coatings Technology, 2007, 201, 8286-8290.	2.2	10
1309	Characteristics of phosphorus-doped diamond-like carbon films synthesized by plasma immersion ion implantation and deposition (PIII and D). Surface and Coatings Technology, 2007, 201, 6643-6646.	2.2	10
1310	Surface Stability of Platinum Nanoparticles Surrounded by High-Index Facets. Journal of Physical Chemistry C, 2008, 112, 3247-3251.	1.5	10
1311	Structure and mechanical properties of diamondlike carbon films produced by hollow-cathode plasma deposition. Journal of Vacuum Science and Technology A: Vacuum, Surfaces and Films, 2008, 26, 1149-1153.	0.9	10
1312	Impact energy and retained dose uniformity in enhanced glow discharge plasma immersion ion implantation. Applied Physics Letters, 2009, 95, 061503.	1.5	10
1313	Lowâ€Frequency Raman Scattering from Nanocrystals Caused by Coherent Excitation of Phonons. Small, 2009, 5, 2823-2826.	5.2	10
1314	Intracellular chromosome breaks on silicon surface. Biomaterials, 2009, 30, 2661-2665.	5.7	10

#	Article	IF	CITATIONS
1315	Structure and gas-barrier properties of amorphous hydrogenated carbon films deposited on inner walls of cylindrical polyethylene terephthalate by plasma-enhanced chemical vapor deposition. Applied Surface Science, 2009, 255, 3983-3988.	3.1	10
1316	Surface Structures and Osteoblast Activity on Biomedical Polytetrafluoroethylene Treated by Longâ€Pulse, Highâ€Frequency Oxygen Plasma Immersion Ion Implantation. Advanced Engineering Materials, 2010, 12, B163.	1.6	10
1317	Fermi-Level Pinning at Metal/High-\$k\$ Interface Influenced by Electron State Density of Metal Gate. IEEE Electron Device Letters, 2010, 31, 1101-1103.	2.2	10
1318	Photoluminescence from colloids containing aluminum hydroxide nanocrystals with uniform size. Applied Physics Letters, 2010, 97, 121901.	1.5	10
1319	Optimization of Optoelectronic Plasmonic Structures. Plasmonics, 2011, 6, 319-325.	1.8	10
1320	Fabrication method of parallel mesoporous carbon nanotubes. Colloids and Surfaces A: Physicochemical and Engineering Aspects, 2011, 377, 150-155.	2.3	10
1321	Magnetorotational instability in a collisionless plasma with heat flux vector and an isotropic plasma with self-gravitational effect. Physics of Plasmas, 2011, 18, .	0.7	10
1322	Wear Properties of Porous NiTi Orthopedic Shape Memory Alloy. Journal of Materials Engineering and Performance, 2012, 21, 2622-2627.	1.2	10
1323	Geodesic acoustic modes in toroidally rotating tokamaks with an arbitrary β. Physics of Plasmas, 2013, 20, 072504.	0.7	10
1324	Surface and interference co-enhanced Raman scattering from indium tin oxide nanocap arrays. Applied Surface Science, 2013, 280, 343-348.	3.1	10
1325	Direct imprint of nanostructures in metals using porous anodic alumina stamps. Nanotechnology, 2013, 24, 255303.	1.3	10
1326	Bio-tribological properties and cytocompatibility of Ti–Si–N coatings. Vacuum, 2015, 115, 50-57.	1.6	10
1327	Enhanced cytocompatibility of silver-containing biointerface by constructing nitrogen functionalities. Applied Surface Science, 2015, 349, 327-332.	3.1	10
1328	Supermolecular theranostic capsules for pH-sensitive magnetic resonance imaging and multi-responsive drug delivery. Journal of Materials Chemistry B, 2015, 3, 8499-8507.	2.9	10
1329	Graded metal carbon protein binding films prepared by hybrid cathodic arc — Glow discharge plasma assisted chemical vapor deposition. Surface and Coatings Technology, 2015, 265, 222-234.	2.2	10
1330	Theoretical Assessment of Localized Surface Plasmon Resonance Properties of Au-Interlayer-Ag Multilayered Nanoshells. Plasmonics, 2016, 11, 1589-1595.	1.8	10
1331	Morphology-controlled synthesis and electron field emission properties of ZnSe nanowalls. RSC Advances, 2017, 7, 10631-10637.	1.7	10
1332	Localized surface plasmon resonance properties of Ag nanorod arrays on graphene-coated Au substrate. Optics Communications, 2017, 402, 216-220.	1.0	10

#	Article	IF	CITATIONS
1333	Porous nanopeapod Pd catalyst with excellent stability and efficiency. Chemical Communications, 2017, 53, 740-742.	2.2	10
1334	ldentification of Lattice Oxygen in Few-Layer Black Phosphorous Exfoliated in Ultrahigh Vacuum and Largely Improved Ambipolar Field-Effect Mobilities by Hydrogenation and Phosphorization. ACS Applied Materials & Interfaces, 2017, 9, 39804-39811.	4.0	10
1335	Improved interfacial adhesion between TiAlN/DLC multi-layered coatings by controlling the morphology via bias. Surface and Coatings Technology, 2017, 331, 15-20.	2.2	10
1336	Control of multidrug-resistant planktonic <i>Acinetobacter baumannii</i> : biocidal efficacy study by atmospheric-pressure air plasma. Plasma Science and Technology, 2018, 20, 065513.	0.7	10
1337	Hexagonal VO <sub>2</sub> particles: synthesis, mechanism and thermochromic properties. RSC Advances, 2018, 8, 10064-10071.	1.7	10
1338	In situ formation of porous TiO2 nanotube array with MgTiO3 nanoparticles for enhanced photocatalytic activity. Surface and Coatings Technology, 2019, 365, 222-226.	2.2	10
1339	Nano-mechanical properties of zirconia-alumina-benzotriazole nano-composite coating deposited on Al2024 by the sol-gel method. Thin Solid Films, 2019, 689, 137417.	0.8	10
1340	Al2O3 coating for densification of SiC ceramics and sintering kinetics. Surface and Coatings Technology, 2019, 374, 603-609.	2.2	10
1341	Facile mass production of self-supported two-dimensional transition metal oxides for catalytic applications. Chemical Communications, 2019, 55, 11406-11409.	2.2	10
1342	A high-birefringent photonic quasi-crystal fiber with two elliptical air holes. Optik, 2019, 184, 10-15.	1.4	10
1343	Selfâ€Regulated Superâ€Hydrophobic Cu/CuO Electrode Film Deposited by Oneâ€Step Highâ€Power Sputtering. Advanced Electronic Materials, 2020, 6, 1900891.	2.6	10
1344	Zirconium-based nanostructured coating on the Mg-4Y-3RE alloy for corrosion retardation. Chemical Physics Letters, 2020, 756, 137824.	1.2	10
1345	Ambipolar Plasmonâ€Enhanced Photodetector Built on Germanium Nanodots Array/Graphene Hybrid. Advanced Materials Interfaces, 2020, 7, 2001122.	1.9	10
1346	Enhanced Osteogenic Differentiation of Human Mesenchymal Stem Cells on Amine-Functionalized Titanium Using Humidified Ammonia Supplied Nonthermal Atmospheric Pressure Plasma. International Journal of Molecular Sciences, 2020, 21, 6085.	1.8	10
1347	Investigation of Indenter-Size-Dependent Nanoplasticity of Silicon by Molecular Dynamics Simulation. ACS Applied Electronic Materials, 2020, 2, 3039-3047.	2.0	10
1348	Dynamic changes of hydrophobic behavior during icing. Surface and Coatings Technology, 2020, 397, 126043.	2.2	10
1349	Cost-effective liquid-junction solar devices with plasma-implanted Ni/TiN/CNF hierarchically structured nanofibers. Journal of Electroanalytical Chemistry, 2021, 887, 115167.	1.9	10
1350	Cationic Alternating Polypeptide Fixed on Polyurethane at Multiple Sites for Excellent Antibacterial and Antifouling Properties. Langmuir, 2021, 37, 10657-10667.	1.6	10

#	Article	IF	CITATIONS
1351	Porous manganese dioxide nanosheets on modified graphite felt for cathodes in high-capacity flexible Zinc-MnO2 batteries. Vacuum, 2021, 191, 110353.	1.6	10
1352	High-sensitivity SPR sensor based on the eightfold eccentric core PQF with locally coated indium tin oxide. Applied Optics, 2020, 59, 6484.	0.9	10
1353	Magnesium cationic cue enriched interfacial tissue microenvironment nurtures the osseointegration of gamma-irradiated allograft bone. Bioactive Materials, 2022, 10, 32-47.	8.6	10
1354	Porous Mo2C-Mo3N2 heterostructure/rGO with synergistic functions as polysulfides regulator for high-performance lithium sulfur batteries. Chemical Engineering Journal, 2022, 433, 133629.	6.6	10
1355	Sodium alginate coating on biodegradable high-purity magnesium with a hydroxide/silane transition layer for corrosion retardation. Colloids and Surfaces A: Physicochemical and Engineering Aspects, 2022, 642, 128647.	2.3	10
1356	Pulsed sheath dynamics in a small cylindrical bore with an auxiliary electrode for plasma immersion ion implantation. Physics of Plasmas, 1997, 4, 4431-4434.	0.7	9
1357	Steady-state direct-current plasma immersion ion implantation using an electron cyclotron resonance plasma source. Thin Solid Films, 2001, 390, 145-148.	0.8	9
1358	Low temperature growth of CeO2(111) layer on Si(100) using dual plasma deposition. Materials Science & Engineering A: Structural Materials: Properties, Microstructure and Processing, 2001, 308, 176-179.	2.6	9
1359	Dynamic mixing deposition of niobium nitride films by cathodic arc plasma in ambient nitrogen. Journal of Vacuum Science and Technology A: Vacuum, Surfaces and Films, 2001, 19, 2048-2050.	0.9	9
1360	Optimal duct bias for transport of cathodic-arc plasmas. IEEE Transactions on Plasma Science, 2002, 30, 1602-1605.	0.6	9
1361	Influence of bias voltage on the tribological properties of titanium nitride films fabricated by dynamic plasma ion implantation/deposition. Surface and Coatings Technology, 2002, 161, 232-236.	2.2	9
1362	Flexible system for multiple plasma immersion ion implantation-deposition processes. Review of Scientific Instruments, 2003, 74, 5137-5140.	0.6	9
1363	Synthesis of aluminum nitride films by plasma immersion ion implantation–deposition using hybrid gas–metal cathodic arc gun. Review of Scientific Instruments, 2004, 75, 719-724.	0.6	9
1364	Microstructure investigation of BaxSr1â^'xTiO3 thin film grown on porous silicon substrate. Materials Science in Semiconductor Processing, 2004, 7, 253-258.	1.9	9
1365	Growth and visible photoluminescence of highly oriented (100) zinc oxide film synthesized on silicon by plasma immersion ion implantation. Materials Science in Semiconductor Processing, 2004, 7, 459-462.	1.9	9
1366	Si–N–O Films Synthesized by Plasma Immersion Ion Implantation and Deposition (PIII&D) for Blood-Contacting Biomedical Applications. IEEE Transactions on Plasma Science, 2006, 34, 1160-1165.	0.6	9
1367	Oxygen Plasma Ion Implantation of Biomedical Titanium Alloy. IEEE Transactions on Plasma Science, 2006, 34, 1235-1240.	0.6	9
1368	Nucleation and growth of amorphous carbon film on tungsten-implanted stainless steel substrates. Diamond and Related Materials, 2006, 15, 1580-1584.	1.8	9

#	Article	IF	CITATIONS
1369	Resonant electron transfer and luminescent enhancement in a toluene suspension of Si nanocrystals. Journal of Chemical Physics, 2006, 125, 054713.	1.2	9
1370	Oxidation suppression in ytterbium silicidation by Tiâ^•TiN bicapping layer. Journal of Vacuum Science and Technology A: Vacuum, Surfaces and Films, 2007, 25, 285-289.	0.9	9
1371	Microstructure and tribological properties of Cu–Zn/TiN multilayers fabricated by dual magnetron sputtering. Surface and Coatings Technology, 2007, 202, 189-193.	2.2	9
1372	Mechanical properties, bioactivity and corrosion resistance of oxygen and sodium plasma treated nickel titanium shape memory alloy. Surface and Coatings Technology, 2007, 202, 1308-1312.	2.2	9
1373	The role of strain in hydrogenation induced cracking in Siâ^•Si1â~'xGexâ^•Si structures. Applied Physics Letters, 2008, 93, 041909.	1.5	9
1374	Interface-induced pseudoelastic behavior in Bi-metal multilayer nanowires. Applied Physics Letters, 2008, 92, 123103.	1.5	9
1375	Dependence of photoluminescence of ZnO/Zn0.85Mg0.15O multi-quantum wells on barrier width. Physics Letters, Section A: General, Atomic and Solid State Physics, 2009, 373, 3281-3284.	0.9	9
1376	Magnetorotational instability in dissipative dusty plasmas. Physics of Plasmas, 2009, 16, 122107.	0.7	9
1377	Microstructure, mechanical properties, and blood compatibility of zirconium nitride deposited on nickel–titanium shape memory alloy. Surface and Coatings Technology, 2010, 204, 2841-2845.	2.2	9
1378	Origin of flat-band voltage sharp roll-off in metal gate/high-k/ultrathin- SiO2/Si p-channel metal-oxide-semiconductor stacks. Applied Physics Letters, 2010, 97, 132908.	1.5	9
1379	Size-independent low-frequency Raman scattering in Ge-nanocrystal-embedded SiO_2 films. Optics Letters, 2010, 35, 1022.	1.7	9
1380	High-energy heavy ion beam annealing effect on ion beam synthesis of silicon carbide. Surface and Coatings Technology, 2011, 206, 770-774.	2.2	9
1381	Synthesis and Cellular Biocompatibility of Two Nanophase Hydroxyapatite with Different Ca/P Ratio. Journal of Nanoscience and Nanotechnology, 2011, 11, 11069-11073.	0.9	9
1382	Surface Hardening of NiTi Shape Memory Alloy Induced by the NanoStructured Layer After Surface Mechanical Attrition Treatment. Journal of Nanoscience and Nanotechnology, 2011, 11, 10954-10957.	0.9	9
1383	Osteoblast differentiation and disinfection induced by nitrogen plasma-treated surfaces. Bio-Medical Materials and Engineering, 2011, 21, 75-82.	0.4	9
1384	Electrochemical behaviour of TiO <sub>2</sub> nanotube on titanium in artificial saliva containing bovine serum albumin. Corrosion Engineering Science and Technology, 2012, 47, 167-169.	0.7	9
1385	Interference effects on indium tin oxide enhanced Raman scattering. Journal of Applied Physics, 2012, 111, .	1.1	9
1386	Oxidation behavior of Ti–B–C–N coatings deposited by reactive magnetron sputtering. Vacuum, 2012, 86, 1505-1512.	1.6	9

#	Article	IF	CITATIONS
1387	Anode properties and morphology evolution of three-dimensional lithium-ion battery electrodes comprising Ni-coated Si microchannel plates. Journal of Alloys and Compounds, 2013, 563, 186-191.	2.8	9
1388	Electronic structures and optical properties induced by silicon twin boundaries: The first-principle calculation. Physics Letters, Section A: General, Atomic and Solid State Physics, 2015, 379, 1384-1390.	0.9	9
1389	Nitrogen-doped multilayered nanographene derived from Ni <sub>3</sub> C with efficient electron field emission. Journal of Materials Chemistry C, 2016, 4, 9251-9260.	2.7	9
1390	Ink Dispersion on Qianlong Xuan Paper with Improved Ink Expression. Journal of Materials Science and Technology, 2016, 32, 182-188.	5.6	9
1391	Vertically-oriented few-layer graphene supported by silicon microchannel plates as a counter electrode in dye-sensitized solar cells. Organic Electronics, 2017, 45, 74-80.	1.4	9
1392	Freestanding Nanoengineered [001] Preferentially Oriented TiO <sub>2</sub> Nanosheetsâ^'Graphene Planarly Aligned Nanohybrids with Enhanced Li‣torage Properties. ChemElectroChem, 2017, 4, 2819-2825.	1.7	9
1393	K <sub>2</sub> MgSi <sub>3</sub> O <sub>8</sub> in Slow-Release Mineral Fertilizer Prepared by Sintering of By-Product of Red Mud-Based Flocculant. Environmental Engineering Science, 2018, 35, 829-835.	0.8	9
1394	NiFeP nanoflakes composite with CoP on carbon cloth as flexible and durable electrocatalyst for efficient overall water splitting. Nanotechnology, 2019, 30, 485402.	1.3	9
1395	Enhanced oxygen-induced properties of bulk oxygenated amorphous carbon films deposited with an anode layer ion source. Vacuum, 2019, 169, 108915.	1.6	9
1396	N-doped TiO <sub>2</sub> nanotube arrays with uniformly embedded Co <sub>x</sub> P nanoparticles for high-efficiency hydrogen evolution reaction. RSC Advances, 2019, 9, 11676-11682.	1.7	9
1397	Stimulus-responsive electrochemiluminescence from self-assembled block copolymer and nonpolar carbon quantum dot composite nanospheres. Carbon, 2019, 147, 532-539.	5.4	9
1398	Activation of graphitic carbon nitride by surface discharge plasma treatment for enhanced photocatalysis. Vacuum, 2019, 159, 235-238.	1.6	9
1399	Insight into the overpotentials of electrocatalytic hydrogen evolution on black phosphorus decorated with metal clusters. Electrochimica Acta, 2020, 358, 136902.	2.6	9
1400	In-Situ Synthesis of Heterostructured Carbon-Coated Co/MnO Nanowire Arrays for High-Performance Anodes in Asymmetric Supercapacitors. Molecules, 2020, 25, 3218.	1.7	9
1401	Design of bimetal-coated photonic crystal fiber filter based on surface plasmon resonance. Results in Optics, 2020, 1, 100027.	0.9	9
1402	High-Potential surface on zirconia ceramics for bacteriostasis and biocompatibility. Colloids and Surfaces B: Biointerfaces, 2020, 193, 111074.	2.5	9
1403	Crystalline Red Phosphorus Nanoribbons: Largeâ€Scale Synthesis and Electrochemical Nitrogen Fixation. Angewandte Chemie, 2020, 132, 14489-14493.	1.6	9
1404	Silicon monophosphides with controlled size and crystallinity for enhanced lithium anodic performance. Nanoscale, 2021, 13, 51-58.	2.8	9

#	Article	IF	CITATIONS
1405	High efficient co-doping in plasma electrolytic oxidation to obtain long-term self-lubrication on Ti6Al4V. Tribology International, 2021, 160, 107018.	3.0	9
1406	MXene Coatings: Novel Hydrogen Permeation Barriers for Pipe Steels. Nanomaterials, 2021, 11, 2737.	1.9	9
1407	Balancing the biocompatibility and bacterial resistance of polypyrrole by optimized silver incorporation. Materials Science and Engineering C, 2022, 134, 112701.	3.8	9
1408	Effects of acid treatment and plasma micromachining on the surface properties of carbon fibers. Applied Surface Science, 2022, 592, 153261.	3.1	9
1409	Subnanometer MoP clusters confined in mesoporous carbon (CMK-3) as superior electrocatalytic sulfur hosts for high-performance lithium-sulfur batteries. Chemical Engineering Journal, 2022, 446, 137050.	6.6	9
1410	Construction of α-MnO2 on Carbon Fibers Modified with Carbon Nanotubes for Ultrafast Flexible Supercapacitors in Ionic Liquid Electrolytes with Wide Voltage Windows. Nanomaterials, 2022, 12, 2020.	1.9	9
1411	Analysis of surface particles by time-of-flight secondary ion mass spectrometry. Materials Chemistry and Physics, 1996, 43, 87-94.	2.0	8
1412	High oxygen and carbon contents in GaAs epilayers grown below a critical substrate temperature by molecular beam epitaxy. Applied Physics Letters, 1996, 68, 841-843.	1.5	8
1413	Long term reproducibility of secondary ion mass spectroscopy measurements in silicon. Journal of Vacuum Science & Technology an Official Journal of the American Vacuum Society B, Microelectronics Processing and Phenomena, 1996, 14, 3321.	1.6	8
1414	Process window and mechanism of surface property enhancement of 9Cr18 steel using plasma immersion ion implantation. Journal of Vacuum Science & Technology an Official Journal of the American Vacuum Society B, Microelectronics Processing and Phenomena, 1999, 17, 851.	1.6	8
1415	Preparation of gallium nitride (GaN) and related compounds by plasma immersion ion implantation and rapid thermal annealing. Surface and Coatings Technology, 2001, 136, 142-145.	2.2	8
1416	Ignition and dynamics of high-voltage glow discharge plasma implantation. Nuclear Instruments & Methods in Physics Research B, 2006, 242, 275-278.	0.6	8
1417	Surface modification of W9Cr4V2Mo high-temperature bearing steel by rare earth ion implantation. Surface and Coatings Technology, 2006, 201, 4357-4360.	2.2	8
1418	Biomimetic deposition process of an apatite coating on NiTi shape memory alloy. Materials Letters, 2006, 60, 3002-3006.	1.3	8
1419	Optical and electrical properties of single-ion transport light-emitting electrochemical cells. Journal of Applied Physics, 2006, 99, 064505.	1.1	8
1420	Corrosion resistance and antithrombogenic behavior of La and Nd ion implanted stainless steels. Journal of Vacuum Science and Technology A: Vacuum, Surfaces and Films, 2006, 24, 1790-1794.	0.9	8
1421	Interfacial compound suppression and dielectric properties enhancement of F–N codoped ZrO2 thin films. Applied Physics Letters, 2007, 90, 082906.	1.5	8
1422	Effects of electron-focusing electric field upon enhanced glow discharge plasma ion implantation. Surface and Coatings Technology, 2007, 201, 6516-6519.	2.2	8

#	Article	IF	CITATIONS
1423	In vitro evaluation of diamond-like carbon coatings with a Si/SiCx interlayer on surgical NiTi alloy. Nuclear Instruments & Methods in Physics Research B, 2007, 257, 132-135.	0.6	8
1424	Fabrication of graded TiN coatings on nitinol occluders and effects on in vivo nickel release. Bio-Medical Materials and Engineering, 2008, 18, 387-393.	0.4	8
1425	Theoretical investigation of sheath expansion and implant fluence uniformity in enhanced glow discharge plasma immersion ion implantation. Applied Physics Letters, 2008, 93, 091501.	1.5	8
1426	Syntheses and Growth Mechanisms of 3 <i>C</i> -SiC Nanostructures from Carbon and Silicon Powders. Journal of Nanoscience and Nanotechnology, 2009, 9, 6648-6654.	0.9	8
1427	Facile synthesis of hollow and porous nickel microspheres by low temperature molecular self-assembly. Solid State Sciences, 2011, 13, 438-443.	1.5	8
1428	Uniformity enhancement of incident dose on concave surface in plasma immersion ion implantation assisted by beam-line ion source. Surface and Coatings Technology, 2011, 206, 2021-2024.	2.2	8
1429	Superelastic Porous NiTi with Adjustable Porosities Synthesized by Powder Metallurgical Method. Journal of Materials Engineering and Performance, 2012, 21, 2553-2558.	1.2	8
1430	Three-dimensional particle-in-cell simulation of discharge characteristics in cylindrical anode layer hall plasma accelerator. Physics of Plasmas, 2012, 19, .	0.7	8
1431	High temperature oxidation of Cr–N coatings prepared by high power pulsed magnetron sputtering – Plasma immersion ion implantation & deposition. Vacuum, 2014, 108, 66-70.	1.6	8
1432	Luminescence properties of Lu3M5O12:Eu3+ (MÂ=ÂAl, Ga) and effects of Bi3+ co-dopant. Journal of Sol-Gel Science and Technology, 2015, 76, 43-49.	1.1	8
1433	Ordered-standing nickel hydroxide microchannel arrays: Synthesis and application for highly sensitive non-enzymatic glucose sensors. Microelectronic Engineering, 2015, 133, 11-15.	1.1	8
1434	Fabrication of nanocomposite electrode based on Bi4Nd Ti3O12 perovskite supported by silicon microchannel plates for high performance electrochemical capacitors. Journal of Alloys and Compounds, 2015, 619, 748-753.	2.8	8
1435	Drawing-fabrication of multifarious nanoplasmonic platform on PLLA paper for optimized SERS performance. Journal of Raman Spectroscopy, 2016, 47, 687-691.	1.2	8
1436	Cold atmospheric-pressure air plasma treatment of C6 glioma cells: effects of reactive oxygen species in the medium produced by the plasma on cell death. Plasma Science and Technology, 2017, 19, 025503.	0.7	8
1437	EFFECT OF INHIBITOR AGENTS ADDITION ON CORROSION RESISTANCE PERFORMANCE OF TITANIA SOL–GEL COATINGS APPLIED ON 304 STAINLESS STEEL. Surface Review and Letters, 2017, 24, 1750055.	0.5	8
1438	Tunable magnetic coupling in Mn-doped monolayer MoS <sub>2</sub> under lattice strain. Journal of Physics Condensed Matter, 2018, 30, 215801.	0.7	8
1439	Effects of silica and Ag on the electrochemical behavior of titania-based nanocomposite coatings deposited on 2024 aluminum alloy by the sol-gel method. Journal of Alloys and Compounds, 2018, 739, 92-100.	2.8	8
1440	Multi-wavelength unidirectional forward scattering in the visible range in an all-dielectric silicon hollow nanodisk. Applied Optics, 2018, 57, 4771.	0.9	8

#	Article	IF	CITATIONS
1441	Effects of ion flux density and energy on the composition of TiNx thin films prepared by magnetron sputtering with an anode layer ion source. Surface and Coatings Technology, 2019, 365, 58-64.	2.2	8
1442	Inconel 718 treated with two-stage solution and aging processes: microstructure evolution and enhanced properties. Materials Research Express, 2019, 6, 075803.	0.8	8
1443	Mediated Drug Release from Nanovehicles by Black Phosphorus Quantum Dots for Efficient Therapy of Chronic Obstructive Pulmonary Disease. Angewandte Chemie, 2020, 132, 20749-20757.	1.6	8
1444	Carbon-encapsulated nanosphere-assembled MoS2 nanosheets with large interlayer distance for flexible lithium-ion batteries. Journal of Solid State Electrochemistry, 2021, 25, 1657-1665.	1.2	8
1445	Subsurface intercalation activating basal plane of black phosphorus for nitrogen reduction. Journal of Energy Chemistry, 2021, 60, 293-299.	7.1	8
1446	Black Phosphorus: An Effective Feedstock for the Synthesis of Phosphorus-Based Chemicals. CCS Chemistry, 2019, 1, 166-172.	4.6	8
1447	Highly Sensitive Dual-core Photonic Crystal Fiber Based on a Surface Plasmon Resonance Sensor with Gold Film. Plasmonics, 2022, 17, 543-550.	1.8	8
1448	MXene nanofibers confining MnO <sub><i>x</i></sub> nanoparticles: a flexible anode for high-speed lithium ion storage networks. Dalton Transactions, 2022, 51, 1423-1433.	1.6	8
1449	Efficient coupling of MnO <sub>2</sub> /TiN on carbon cloth positive electrode and Fe <sub>2</sub> O <sub>3</sub> /TiN on carbon cloth negative electrode for flexible ultra-fast hybrid supercapacitors. RSC Advances, 2021, 11, 35726-35736.	1.7	8
1450	Fan-shape Mn-doped CoO/C microspheres for high lithium-ion storage capacity. Journal of Alloys and Compounds, 2022, 903, 163980.	2.8	8
1451	Near-infrared photonic artificial synapses based on organic heterojunction phototransistors. Applied Physics Letters, 2022, 120, .	1.5	8
1452	On the formation of solid state crystallized intrinsic polycrystalline germanium thin films. Journal of Materials Research, 1997, 12, 2548-2551.	1.2	7
1453	Improvement of the wear and corrosion resistance of oil pump materials using plasma immersion ion implantation. Surface and Coatings Technology, 1998, 98, 897-900.	2.2	7
1454	Computed electron oscillation inside the duct of a vacuum arc source. Journal of Applied Physics, 1999, 85, 6381-6384.	1.1	7
1455	Chemical structure modification of silicone surfaces by plasma immersion ion implantation. Journal of Materials Science Letters, 2000, 19, 1883-1885.	0.5	7
1456	Effects of plasma excitation power, sample bias, and duty cycle on the structure and surface properties of amorphous carbon thin films fabricated on AISI440 steel by plasma immersion ion implantation. Journal of Vacuum Science and Technology A: Vacuum, Surfaces and Films, 2000, 18, 2164.	0.9	7
1457	Hydrogen-induced surface blistering of sample chuck materials in hydrogen plasma immersion ion implantation. Journal of Vacuum Science and Technology A: Vacuum, Surfaces and Films, 2001, 19, 2301-2306.	0.9	7
1458	Guiding effects of electric and magnetic fields on the plasma output of a cathodic arc magnetic filter. Journal of Applied Physics, 2001, 89, 672-675.	1.1	7

#	Article	IF	CITATIONS
1459	Improvement of nitrogen retained dose using ammonia as a precursor in nitrogen plasma immersion ion implantation of silicon. Journal of Vacuum Science and Technology A: Vacuum, Surfaces and Films, 2005, 23, 1346-1349.	0.9	7
1460	Fabrication of rutile TiO2 thin films by low-temperature, bias-assisted cathodic arc deposition and their dielectric properties. Journal of Materials Research, 2006, 21, 844-850.	1.2	7
1461	Dependence of ion sheath collapse on secondary electron emission in plasma immersion ion implantation. Applied Physics Letters, 2007, 90, 131503.	1.5	7
1462	Structure and topographies of diamond-like carbon films produced on tungsten pre-implanted stainless steel substrate by plasma immersion ion implantation and deposition. Diamond and Related Materials, 2007, 16, 1490-1499.	1.8	7
1463	Plasma processing of AISI 304 stainless steel using radio frequency hollow cathode discharge. Surface and Coatings Technology, 2007, 201, 8650-8653.	2.2	7
1464	Fabrication of highly (1000) oriented textured zinc oxide films by metal cathodic arc and oxygen dual plasma deposition and their optical properties. Surface and Coatings Technology, 2007, 201, 8348-8351.	2.2	7
1465	Luminescence properties of ultrasmall amorphous Si nanoparticles with sizes smaller than 2nm. Journal of Crystal Growth, 2007, 304, 476-480.	0.7	7
1466	Experimental investigation of discharge characteristics in enhanced glow discharge plasma immersion ion implantation. Physics Letters, Section A: General, Atomic and Solid State Physics, 2008, 372, 6183-6186.	0.9	7
1467	Investigation of plasma immersion ion implantation of nickel-titanium rod by multiple-grid particle-in-cell simulation. Journal of Applied Physics, 2008, 103, 053308.	1.1	7
1468	Comparison of oxidation resistance of copper treated by beam-line ion implantation and plasma immersion ion implantation. Materials Chemistry and Physics, 2009, 116, 519-522.	2.0	7
1469	Investigation of plasma potential and pulsed discharge characteristics in enhanced glow discharge plasma immersion ion implantation and deposition. Nuclear Instruments & Methods in Physics Research B, 2009, 267, 1696-1700.	0.6	7
1470	Theoretical investigation of plasma immersion ion implantation of cylindrical bore using hollow cathode plasma discharge. Surface and Coatings Technology, 2009, 203, 2727-2730.	2.2	7
1471	Germanium surface hydrophilicity and low-temperature Ge layer transfer by Ge–SiO2 bonding. Journal of Vacuum Science and Technology B:Nanotechnology and Microelectronics, 2010, 28, 769-774.	0.6	7
1472	Hybrid particle-in-cell (PIC) ions and Boltzmann electron distribution simulation of direct-current plasma immersion ion implantation into three-dimensional objects. Journal Physics D: Applied Physics, 2010, 43, 095203.	1.3	7
1473	Analysis of hazardous organic residues from sodium hydrosulfite industry and utilization as raw materials in a novel solid lubricant production. Journal of Hazardous Materials, 2011, 198, 65-69.	6.5	7
1474	Surface carbon layer and visible-light photocatalytic activities of carbon-coated TiO 2 nanotubes synthesized in organic electrolytes. Applied Physics A: Materials Science and Processing, 2011, 105, 703-707.	1.1	7
1475	Multiple-mode excitation in spin-transfer nanocontacts with dynamic polarizer. Applied Physics Letters, 2011, 98, 242506.	1.5	7
1476	Morphology-dependent low-frequency Raman scattering in ultrathin spherical, cubic, and cuboid SnO2 nanocrystals. Applied Physics Letters, 2011, 99, 251902.	1.5	7

#	Article	IF	CITATIONS
1477	<i>In Vitro</i> Degradation and Biocompatibility of WE43, ZK60, and AZ91 Biodegradable Magnesium Alloys. Advanced Materials Research, 0, 287-290, 2008-2014.	0.3	7
1478	Nickel-Palladium Nanoparticles for Nonenzymatic Methanol Detection. Analytical Letters, 2012, 45, 1447-1453.	1.0	7
1479	Tunable fluorescence from patterned silver nano-island arrays for sensitive sub-cell imaging. Journal Physics D: Applied Physics, 2013, 46, 495302.	1.3	7
1480	Control of Surface Degradation on Biodegradable Magnesium Alloys by Plasma-Based Technology. IEEE Transactions on Plasma Science, 2013, 41, 725-730.	0.6	7
1481	Facile synthesis of hollow silica spheres with nanoholes. Dalton Transactions, 2013, 42, 6381.	1.6	7
1482	Mineral wool fibers incorporated with cuprous oxide for visible light photocatalytic inactivation of Escherichia coli. Ceramics International, 2014, 40, 5407-5412.	2.3	7
1483	Dopant-Induced Surface Magnetism in β-SiC Controlled by Dopant Depth. Journal of Physical Chemistry C, 2014, 118, 25429-25433.	1.5	7
1484	Impedance study of adsorption phenomena on three-dimensional nano-nickel electrode deposited on silicon microchannel plate. Electrochimica Acta, 2014, 132, 165-171.	2.6	7
1485	Microporous N-doped carbon film produced by cold atmospheric plasma jet and its cell compatibility. Vacuum, 2014, 108, 27-34.	1.6	7
1486	Manipulation of strain state in silicon nanoribbons by top-down approach. Applied Physics Letters, 2015, 106, .	1.5	7
1487	Effects of Al and N plasma immersion ion implantation on surface microhardness, oxidation resistance and antibacterial characteristics of Cu. Transactions of Nonferrous Metals Society of China, 2015, 25, 1944-1949.	1.7	7
1488	Effects of plasma-generated nitrogen functionalities on the upregulation of osteogenesis of bone marrow-derived mesenchymal stem cells. Journal of Materials Chemistry B, 2015, 3, 1856-1863.	2.9	7
1489	Effects of N <sub>2</sub> /O <sub>2</sub> flow rate on the surface properties and biocompatibility of nano-structured TiO <sub> <i>x</i> </sub> N <sub> <i>y</i> </sub> thin films prepared by high vacuum magnetron sputtering. Chinese Physics B, 2015, 24, 075202.	0.7	7
1490	Paramagnetic, pH and temperature-sensitive polymeric particles for anticancer drug delivery and brain tumor magnetic resonance imaging. RSC Advances, 2015, 5, 87512-87520.	1.7	7
1491	Corrosion resistance of Ti-Si-N coatings in blood and cytocompatibility with vascular endothelial cells. Vacuum, 2016, 128, 45-55.	1.6	7
1492	Microstructure and mechanical properties of (AlTi)xN1-x films by magnetic-field-enhanced high power impulse magnetron sputtering. Journal of Vacuum Science and Technology A: Vacuum, Surfaces and Films, 2017, 35, .	0.9	7
1493	Three-dimensional CoMoO 4 nanorods/nanographene composites on a Ni coated macroporous electrically conductive network with excellent electrochemical performance. Materials Science and Engineering B: Solid-State Materials for Advanced Technology, 2017, 226, 177-187.	1.7	7
1494	Reduction in Chemical Oxygen Demand of TNT Red Water Using Layered Double Hydroxide Prepared from Red Mud and Brucite. Environmental Engineering Science, 2017, 34, 721-730.	0.8	7

#	Article	IF	CITATIONS
1495	Preparation of SnO <sub>2</sub> Nanoparticles Doped With Palladium and Graphene and Application for Ethanol Detection. IEEE Sensors Journal, 2017, 17, 6240-6245.	2.4	7
1496	Discharge and Plasma Characteristics of Pulse-Enhanced Vacuum Arc Evaporation (PEVAE) for Titanium Cathode. IEEE Transactions on Plasma Science, 2018, 46, 2619-2625.	0.6	7
1497	Tunable band offsets in the BP/P <sub>4</sub> O <sub>10</sub> van der Waals heterostructure: first-principles calculations. Physical Chemistry Chemical Physics, 2018, 20, 29931-29938.	1.3	7
1498	Corrosion Behavior and Mechanism of Carbon Ion-Implanted Magnesium Alloy. Coatings, 2020, 10, 734.	1.2	7
1499	Improvement of the Laser-Welded Lap Joint of Dissimilar Mg Alloy and Cu by Incorporation of a Zn Interlayer. Materials, 2020, 13, 2053.	1.3	7
1500	Enhanced Hydrogen Evolution Activity of Phosphorusâ€Rich Tungsten Phosphide by Cobalt Doping: A Comprehensive Study of the Active Sites and Electronic Structure. ChemElectroChem, 2021, 8, 1658-1664.	1.7	7
1501	Optical Anapole Modes in Gallium Phosphide Nanodisk with Forked Slits for Electric Field Enhancement. Nanomaterials, 2021, 11, 1490.	1.9	7
1502	Flexible Supercapacitors Based on CNT/MnO2-BP Composite Yarn Synthesized by In Situ Reduction. Journal of the Electrochemical Society, 2021, 168, 080524.	1.3	7
1503	Three-dimensional nano/micro-structured porous MoP/CNTs microspheres as high-capacity anode for lithium-ion batteries. Journal of Alloys and Compounds, 2021, 872, 159608.	2.8	7
1504	Short-brush NiFeOxHy films and the Pt derivative as high-performance electrode materials for efficient electrocatalytic water splitting. Applied Surface Science, 2022, 574, 151636.	3.1	7
1505	A new technique to optimize the properties of photonic crystal fibers supporting transmission of multiple orbital angular momentum modes. Journal of Optics (India), 2023, 52, 307-316.	0.8	7
1506	Coimplantation of carbon and group II acceptors in GaAs. Applied Physics Letters, 1996, 68, 1135-1137.	1.5	6
1507	Ion mean charge state in a biased vacuum arc plasma duct. IEEE Transactions on Plasma Science, 2000, 28, 2194-2201.	0.6	6
1508	The effect of mesh anode on cathodic arc in focusing magnetic field. Chinese Physics B, 2000, 9, 279-283.	1.3	6
1509	Effects of magnetic field on pulse wave forms in plasma immersion ion implantation in a radio-frequency, inductively coupled plasma. Journal of Applied Physics, 2002, 92, 2284-2289.	1.1	6
1510	Bias voltage influence on surface morphology of titanium nitride synthesized by dynamic nitrogen and titanium plasma immersion ion implantation and deposition. Materials Science & Engineering A: Structural Materials: Properties, Microstructure and Processing, 2002, 337, 236-240.	2.6	6
1511	Controlling synthesis of Ti–O/Ti–N gradient films by PIII. Surface and Coatings Technology, 2002, 156, 208-213.	2.2	6
1512	Fabrication of silicon-on-AlN novel structure and its residual strain characterization. Journal of Crystal Growth, 2002, 244, 27-32.	0.7	6

#	Article	IF	CITATIONS
1513	lon-cutting of Si onto glass by pulsed and direct-current plasma immersion ion implantation. Journal of Vacuum Science & Technology an Official Journal of the American Vacuum Society B, Microelectronics Processing and Phenomena, 2003, 21, 2109.	1.6	6
1514	Fabrication of silicon carbide thin films by plasma immersion ion implantation with self-ignited glow discharge. Thin Solid Films, 2004, 447-448, 153-157.	0.8	6
1515	Simulation of suppression of floating-body effect in partially depleted SOI MOSFET using a Si1â~'xGex dual source structure. Materials Science and Engineering B: Solid-State Materials for Advanced Technology, 2004, 114-115, 264-268.	1.7	6
1516	Catalytic growth of α-FeSi2 and silicon nanowires. Journal of Crystal Growth, 2005, 280, 286-291.	0.7	6
1517	Polycrystalline tubular nanostructures of germanium. Journal of Crystal Growth, 2005, 285, 59-65.	0.7	6
1518	A ground-based radio frequency inductively coupled plasma apparatus for atomic oxygen simulation in low Earth orbit. Review of Scientific Instruments, 2007, 78, 103301.	0.6	6
1519	Annealing behavior and hardness enhancement of amorphous SiCN thin films. Journal of Vacuum Science and Technology A: Vacuum, Surfaces and Films, 2007, 25, 1407.	0.9	6
1520	Particle-in-cell numerical simulation of non-uniform plasma immersion ion implantation. Surface and Coatings Technology, 2007, 201, 5458-5462.	2.2	6
1521	Improvement of electrochemical performance of Si thin film anode by rare-earth La PIII technique. Surface and Coatings Technology, 2007, 201, 6785-6788.	2.2	6
1522	Comparative studies on influence of acetylene to argon flow rate ratios on nano-scratch behavior of a-C:H films produced on steel substrates by plasma immersion ion implantation and deposition. Thin Solid Films, 2007, 516, 252-256.	0.8	6
1523	Chemical and Physical Properties of Copper and Nitrogen Plasma-Implanted Polyethylene. Plasma Processes and Polymers, 2007, 4, 158-164.	1.6	6
1524	Observation of spontaneous pattern with six-fold symmetry in disk-shaped ZnO complex microstructures. Applied Physics A: Materials Science and Processing, 2007, 89, 173-176.	1.1	6
1525	Structure and optical properties of multi-quantum wells grown on Si(111) substrates. Superlattices and Microstructures, 2008, 44, 197-202.	1.4	6
1526	Magnetothermal instability of plasmas in a horizontal magnetic field. Physics of Plasmas, 2009, 16, 102109.	0.7	6
1527	Damping of surface acoustic vibration induced by electrons trapped on SnO2 nanocrystal surface. Applied Physics Letters, 2009, 95, 211903.	1.5	6
1528	Plasma immersion ion implantation of cylindrical bore using self-excited radio-frequency glow discharge. Surface and Coatings Technology, 2010, 204, 2996-2998.	2.2	6
1529	Strain Stability and Carrier Mobility Enhancement in Strained Si on Relaxed SiGe-on-Insulator. Journal of the Electrochemical Society, 2010, 157, H104.	1.3	6
1530	A Specially Designed PLC-Based High-Voltage Pulse Modulator for Plasma Immersion Ion Implantation. IEEE Transactions on Plasma Science, 2010, 38, 3083-3088.	0.6	6

#	Article	IF	CITATIONS
1531	Novel thermoelectric materials based on boron-doped silicon microchannel plates. Materials Letters, 2011, 65, 1618-1620.	1.3	6
1532	Density gradient effects on the magnetorotational instability. Plasma Physics and Controlled Fusion, 2011, 53, 035012.	0.9	6
1533	Improved hydrogen ionization rate in enhanced glow discharge plasma immersion ion implantation by enlarging the interaction path using an insulating tube. Review of Scientific Instruments, 2011, 82, 023503.	0.6	6
1534	Direct and diffuse reflection of electron waves at armchair edges of epitaxial graphene. RSC Advances, 2013, 3, 25735.	1.7	6
1535	Plasma-target surface interaction during non-equilibrium plasma irradiation at atmospheric pressure: Generation of dusty plasma. Laser and Particle Beams, 2014, 32, 69-78.	0.4	6
1536	Multifunctional gold coated rare-earth hydroxide fluoride nanotubes for simultaneous wastewater purification and quantitative pollutant determination. Materials Research Bulletin, 2014, 52, 122-127.	2.7	6
1537	3C-SiC/ZnS heterostructured nanospheres with high photocatalytic activity and enhancement mechanism. AIP Advances, 2015, 5, .	0.6	6
1538	Electrochemical investigation of the corrosion properties of three-dimensional nickel electrodes on silicon microchannel plates. Corrosion Science, 2015, 100, 113-120.	3.0	6
1539	Electrochemical analysis of interface adsorption phenomena on three-dimensional nano-nickel electrode deposited on silicon microchannel plate. Electrochimica Acta, 2016, 194, 253-262.	2.6	6
1540	Fabrication of ordered porous silicon nanowires electrode modified with palladium-nickel nanoparticles and electrochemical characteristics in direct alkaline fuel cell of carbohydrates. Ionics, 2016, 22, 1891-1898.	1.2	6
1541	Utilization of recycled chemical residues from sodium hydrosulfite production in solid lubricant for drilling fluids. Desalination and Water Treatment, 2016, 57, 1804-1813.	1.0	6
1542	Ge@CNFs Anchored on 3D Graphene Foam for Binderâ€Free and Highâ€Efficiency Anodes in Li–Ion Batteries. ChemElectroChem, 2017, 4, 1002-1006.	1.7	6
1543	Morphological control of gold nanorods via thermally driven bi-surfactant growth and application for detection of heavy metal ions. Nanotechnology, 2018, 29, 334001.	1.3	6
1544	Enhanced mechanical and electrochemical properties of TiNx thin films prepared by magnetron sputtering with an anode layer ion source. Surface and Coatings Technology, 2019, 365, 253-260.	2.2	6
1545	Effect of Ti interlayer on corrosion behavior of nanostructured Ti/TiN multilayer coating deposited on TiAl <sub>6</sub> V <sub>4</sub> . Materials and Corrosion - Werkstoffe Und Korrosion, 2019, 70, 2113-2127.	0.8	6
1546	Investigation of the microstructure on the nanoporous carbon based capacitive performance. Microporous and Mesoporous Materials, 2021, 310, 110629.	2.2	6
1547	Functionalised <scp>hâ€BN</scp> as an effective lubricant additive in <scp>PAO</scp> oil for <scp>MoN</scp> coating sliding against <scp>Si<sub>3</sub>N<sub>4</sub></scp> ball. Lubrication Science, 2021, 33, 33-42.	0.9	6
1548	Enhanced corrosion resistance and reduced cytotoxicity of the <scp>AZ91</scp> Mg alloy by plasma nitriding and a hierarchical structure composed of ciprofloxacinâ€loaded polymeric multilayers and calcium phosphate coating. Journal of Biomedical Materials Research - Part A, 2021, 109, 2657-2672.	2.1	6

#	Article	IF	CITATIONS
1549	Enhanced Bioactivity of Biomedical NiTi Through Surface Plasma Polymerization. Nanoscience and Nanotechnology Letters, 2015, 7, 220-225.	0.4	6
1550	Surface-Enhanced Raman Scattering Sensor Based on Silver Dendritic Nanostructures. Sensor Letters, 2010, 8, 395-398.	0.4	6
1551	Stable static zinc-iodine redox battery constructed with graphene quantum dots coated graphite felt. Journal of Power Sources, 2022, 520, 230861.	4.0	6
1552	Investigation on solid phase epitaxy of deposited SiGe film on a Si substrate. Thin Solid Films, 1997, 293, 310-314.	0.8	5
1553	Plasma immersion Ar+ ion implantation induced disorder in strained InGaAsP multiple quantum wells. Electronics Letters, 1998, 34, 817.	0.5	5
1554	Characteristics and design of metal vacuum arc plasma source power supply for pulsed-mode plasma immersion ion implantation. Review of Scientific Instruments, 2000, 71, 4435.	0.6	5
1555	Enhancement of implantation efficiency by grid biasing in radio-frequency inductively coupled plasma direct-current plasma immersion ion implantation. Journal of Vacuum Science & Technology an Official Journal of the American Vacuum Society B, Microelectronics Processing and Phenomena, 2002, 20, 1452.	1.6	5
1556	Surface modification of 2Cr13 oil pump steel by plasma immersion ion implantation–ion beam enhanced deposition (PIII–IBED). Thin Solid Films, 2002, 402, 211-214.	0.8	5
1557	Oxygen profile engineering in silicon by germanium addition and high-temperature annealing. Applied Physics Letters, 2003, 83, 305-307.	1.5	5
1558	Low-temperature photoluminescence of hydrogen Ion and plasma implanted silicon and porous silicon. Journal of Applied Physics, 2004, 96, 248-251.	1.1	5
1559	Plasma hydrogenation of strain-relaxed SiGeâ^•Si heterostructure for layer transfer. Applied Physics Letters, 2004, 85, 4944-4946.	1.5	5
1560	Plasma-Sheath Expansion During Plasma Immersion Ion Implantation of Insulating Materials. IEEE Transactions on Plasma Science, 2004, 32, 792-798.	0.6	5
1561	Self-organized synthesis of micrometer scale silver disks by electroless metal deposition on Si-incorporated diamond-like carbon films. Journal of Crystal Growth, 2005, 284, 470-476.	0.7	5
1562	Self-assembled growth and blue emission of a SiOx-capped (x= 0.5–0.8) silicon nanowire array. Nanotechnology, 2005, 16, 2222-2226.	1.3	5
1563	Photoluminescence and self-interference in germanium-doped silica films. Journal of Applied Physics, 2007, 101, 093503.	1.1	5
1564	Comparative study of mechanical properties of a-C:H films produced on tungsten pre-implanted stainless steel substrate by plasma immersion ion implantation and deposition. Diamond and Related Materials, 2007, 16, 1304-1311.	1.8	5
1565	Evolution mechanism of nanocrystalline tungsten-carbon and effects on tungsten implanted amorphous hydrogenated carbon. Journal of Applied Physics, 2007, 102, 113517.	1.1	5
1566	Effects of pulse parameters on macro-particle production in pulsed cathodic vacuum arc deposition. Surface and Coatings Technology, 2007, 201, 6542-6544.	2.2	5

PAUL CHU

#	Article	IF	CITATIONS
1567	Silicidation of Ni(Yb) Film on Si(001). Journal of Electronic Materials, 2008, 37, 245-248.	1.0	5
1568	Mechanism of apatite formation on silicon suboxide film prepared by pulsed metal vacuum arc deposition. Materials Chemistry and Physics, 2008, 109, 342-346.	2.0	5
1569	Finite element analysis of residual stress and interlayer in hard coating/interlayer/soft substrate system during nanoindentation. Journal of Materials Research, 2008, 23, 1358-1363.	1.2	5
1570	Mechanical properties of tungsten doped amorphous hydrogenated carbon films prepared by tungsten plasma immersion ion implantation. Surface and Coatings Technology, 2009, 203, 2612-2616.	2.2	5
1571	Surface-polarization-induced formation of amorphous foliaceous SiO2 helical nanobelts. Applied Physics Letters, 2009, 94, 253110.	1.5	5
1572	Thermal convective and rotational instability in dissipative magnetohydrodynamics. Physics of Plasmas, 2010, 17, 052102.	0.7	5
1573	Ion focusing in enhanced glow discharge plasma immersion ion implantation of hydrogen and nitrogen into silicon. Journal of Applied Physics, 2010, 108, 033304.	1.1	5
1574	Large-Scale Synthesis of Mullite Nanowires by Molten Salt Method. Journal of Nanoscience and Nanotechnology, 2010, 10, 4792-4796.	0.9	5
1575	Cationic Lanthanide Luminescent Copolymer: Design, Synthesis and Interaction with DNA. Journal of Macromolecular Science - Pure and Applied Chemistry, 2011, 48, 832-839.	1.2	5
1576	Recent Progress in Patterned Silicon Nanowire Arrays: Fabrication, Properties and Applications. Recent Patents on Nanotechnology, 2011, 5, 62-70.	0.7	5
1577	A novel technique to enhance surface properties of DLC films deposited on the inner wall of cylindrical PET barrel by DC-RF hybrid discharge. Surface and Coatings Technology, 2011, 206, 1016-1019.	2.2	5
1578	Preparation, characterization of cationic terbium luminescent copolymer and its interaction with DNA. Colloid and Polymer Science, 2011, 289, 1459-1468.	1.0	5
1579	Theoretical predictions of morphotropic phase boundary in (1â^'x)Na1/2Bi1/2TiO3-xBaTiO3 by first-principle calculations. Applied Physics A: Materials Science and Processing, 2011, 104, 1085-1089.	1.1	5
1580	Uniform starâ€polystyrene nanoparticles prepared by emulsion atom transfer radical polymerization. Polymer International, 2011, 60, 1638-1645.	1.6	5
1581	High voltage pulser with a fast fall-time for plasma immersion ion implantation. Review of Scientific Instruments, 2011, 82, 045102.	0.6	5
1582	Modulation of surface-enhanced Raman spectra by depth selective excitation of embedded indium tin oxide nanoisland arrays. Journal Physics D: Applied Physics, 2011, 44, 215305.	1.3	5
1583	Oxidation resistance of quintuple Ti-Al-Si-C-N coatings and associated mechanism. Journal of Vacuum Science and Technology A: Vacuum, Surfaces and Films, 2012, 30, .	0.9	5
1584	Surface Treatment of Polyethylene Terephthalate Using Plasma Ion Implantation Based on Direct Coupling of RF and High-Voltage Pulse. IEEE Transactions on Plasma Science, 2012, 40, 487-491.	0.6	5

#	Article	IF	CITATIONS
1585	Plasma immersion ion implantation into cylindrical bore using internal inductively-coupled radio-frequency discharge. Surface and Coatings Technology, 2012, 206, 5042-5045.	2.2	5
1586	Direct formation of amine functionality on DLC films and surface cyto-compatibility. Diamond and Related Materials, 2013, 38, 28-31.	1.8	5
1587	Effects of loading mode and orientation on deformation mechanism of graphene nano-ribbons. Applied Physics Letters, 2013, 103, 191906.	1.5	5
1588	Plasmon-Matter Interactions in Optoelectronic Metamaterials with Negative Refractive Index. Plasmonics, 2013, 8, 1309-1315.	1.8	5
1589	Enhanced fluorescence from dye molecules by Au nanoparticles on asymmetric double-stranded DNA and mechanism. Applied Physics Letters, 2014, 104, .	1.5	5
1590	Vascular endothelial cell compatibility of superhard ternary Ti–Si–N coatings with different Si contents. Vacuum, 2014, 106, 53-63.	1.6	5
1591	All-silicon solid films with highly efficient and tunable full-color photoluminescence. Scripta Materialia, 2014, 76, 17-20.	2.6	5
1592	Investigation of organic matter adsorption from TNT red water by modified bamboo charcoal. Desalination and Water Treatment, 2015, 56, 684-694.	1.0	5
1593	Electrochemical characteristics of nano-graphene on a macroporous electrically conductive network prepared by hydrothermal carbonization. Electrochimica Acta, 2016, 215, 515-524.	2.6	5
1594	Dynamic transition in the discharge current between gas-dominant discharge and self-sputtering in high-power impulse magnetron sputtering. Surface and Coatings Technology, 2016, 306, 319-322.	2.2	5
1595	Synthesis, crystal structure and photoluminescence properties of Eu2+-activated RbCaGd(PO4)2 phosphors. RSC Advances, 2016, 6, 11211-11217.	1.7	5
1596	A sensitive non-enzymatic immunosensor composed of silver nanoflowers for squamous cell carcinoma antigen. RSC Advances, 2017, 7, 2242-2248.	1.7	5
1597	Self-assembled bundled TiO2nanowire arrays encapsulated with indium tin oxide for broadband absorption in plasmonic photocatalysis. Physical Chemistry Chemical Physics, 2017, 19, 27059-27064.	1.3	5
1598	Protection against lead-free solder in wave-soldering by Ti/TiC coatings prepared by filtered cathodic arc deposition. Surface and Coatings Technology, 2017, 312, 7-12.	2.2	5
1599	Manganese molybdate nanoflakes on silicon microchannel plates as novel nano energetic material. Royal Society Open Science, 2017, 4, 171229.	1.1	5
1600	Improving of tribology properties of TiAl6V4 with nanostructured Ti/TiN-multilayered coating deposited by high-vacuum magnetron sputtering. Applied Physics A: Materials Science and Processing, 2018, 124, 1.	1.1	5
1601	Pd/ZnO/Ni photoelectrochemical ethanol sensor. Journal of Photochemistry and Photobiology A: Chemistry, 2020, 401, 112785.	2.0	5
1602	Intercalator-assisted plasma-liquid technology: an efficient exfoliation method for few-layer two-dimensional materials. Science China Materials, 2020, 63, 2079-2085.	3.5	5

#	Article	IF	CITATIONS
1603	Complete ablation of resistant tumors with photosensitive black phosphorus quantum dots-based lipid nanocapsules. Chemical Engineering Journal, 2021, 421, 127879.	6.6	5
1604	Field emission from geometrically modulated tungsten-nickel sulfide / graphitic carbon nanobelts on Si microchannel plates. Ceramics International, 2021, 47, 4034-4042.	2.3	5
1605	Effects of hydrogen etching on MnO2 electrode materials for supercapacitors. Surface and Coatings Technology, 2021, 410, 126951.	2.2	5
1606	Effects of the tantalum intermediate layer on the nanomechanical properties and biocompatibility of nanostructured tantalum/tantalum nitride bilayer coating deposited by magnetron sputtering on the nickel titanium alloy. Applied Nanoscience (Switzerland), 2021, 11, 1867-1880.	1.6	5
1607	Degradation of tetracycline in water by gas–liquid plasma in conjunction with rGO-TiO <sub>2</sub> nanocomposite. Plasma Science and Technology, 2021, 23, 115503.	0.7	5
1608	Enhanced discharge of high power pulsed magnetron sputtering coupling with high voltage. Wuli Xuebao/Acta Physica Sinica, 2014, 63, 185207.	0.2	5
1609	Cylindric high power impulse magnetron sputtering source and its discharge characteristics. Wuli Xuebao/Acta Physica Sinica, 2016, 65, 185202.	0.2	5
1610	Carrier-Free Cellular Transport of CRISPR/Cas9 Ribonucleoprotein for Genome Editing by Cold Atmospheric Plasma. Biology, 2021, 10, 1038.	1.3	5
1611	Carbon and group II acceptor coimplantation in GaAs. Journal of Applied Physics, 1998, 84, 4929-4934.	1.1	4
1612	A novel distributed system for plasma immersion ion implanter control and automation. Review of Scientific Instruments, 1998, 69, 1495-1498.	0.6	4
1613	Pure high dose metal ion implantation using the plasma immersion technique. Review of Scientific Instruments, 1999, 70, 4359-4361.	0.6	4
1614	Gettering of Cu by microcavities in bonded/ion-cut silicon-on-insulator and separation by implantation of oxygen. Journal of Applied Physics, 1999, 86, 4214-4219.	1.1	4
1615	Silicon-on-Insulator Structure Fabricated by Electron Beam Evaporation of Si on Porous Si and Epitaxial Layer Transfer. Chinese Physics Letters, 2001, 18, 662-664.	1.3	4
1616	Steady-state direct-current plasma immersion ion implantation using a multipolar magnetic field electron cyclotron resonance plasma source. Journal of Vacuum Science and Technology A: Vacuum, Surfaces and Films, 2001, 19, 2889.	0.9	4
1617	Ion kinetic energy control in dual plasma deposition of thin films. Journal of Vacuum Science and Technology A: Vacuum, Surfaces and Films, 2001, 19, 2851.	0.9	4
1618	Interactions between plasma and ionization gauge in plasma immersion ion implantation. Surface and Coatings Technology, 2003, 169-170, 36-40.	2.2	4
1619	Room-temperature electroluminescence from H-plasma-implanted silicon. Semiconductor Science and Technology, 2003, 18, L55-L58.	1.0	4
1620	Optical emission from silicon-based SiO2 islands fabricated by anodic alumina templates. Journal of Applied Physics, 2004, 96, 1443-1446.	1.1	4

#	Article	IF	CITATIONS
1621	Fabrication of thick, high-quality strained SiGe layer on ultra-thin silicon-on-insulator and modeling of film strain. Materials Science in Semiconductor Processing, 2004, 7, 393-397.	1.9	4
1622	Mo-containing diamond-like carbon films with blue emission. Journal of Crystal Growth, 2005, 281, 538-542.	0.7	4
1623	Transport efficiency of vacuum arc plasma in a curved magnetic filter. Review of Scientific Instruments, 2005, 76, 023303.	0.6	4
1624	Plasma-nitrided high-k polycrystalline nano-array induced by electron irradiation. Nanotechnology, 2006, 17, 4379-4383.	1.3	4
1625	Effects of plasma hydrogenation on low temperature growth of nanocrystalline cubic SiC thin films. Diamond and Related Materials, 2007, 16, 826-830.	1.8	4
1626	Corrosion properties of Fe–24Cr stainless alloy modified by plasma immersion ion implantation in 0.5ÂM sulfuric acid solution. Surface and Coatings Technology, 2007, 201, 6781-6784.	2.2	4
1627	Plasma distribution in the slender bore excited by coaxial rf electrode. Surface and Coatings Technology, 2007, 201, 6651-6654.	2.2	4
1628	Oxygen and sodium plasma-implanted nickel–titanium shape memory alloy: A novel method to promote hydroxyapatite formation and suppress nickel leaching. Nuclear Instruments & Methods in Physics Research B, 2007, 257, 687-691.	0.6	4
1629	Thickness uniformity and surface morphology of Fe, Ti, and Hf films produced by filtered pulsed cathodic arc deposition. Surface and Coatings Technology, 2008, 203, 887-892.	2.2	4
1630	BIOMIMETIC DEPOSITION OF APATITE ON SURFACE CHEMICALLY MODIFIED POROUS NITI SHAPEMEMORY ALLOY. Surface Review and Letters, 2008, 15, 97-104.	0.5	4
1631	In situ characterization of initial growth of HfO2. Applied Physics Letters, 2009, 94, 032904.	1.5	4
1632	Plasma sheath physics and dose uniformity in enhanced glow discharge plasma immersion ion implantation and deposition. Journal of Applied Physics, 2009, 106, 013313.	1.1	4
1633	Direct Growth of Quasi-Aligned Ultrafine ZnS Nanowire Arrays on Conducting Zinc Foils and Their Field Emission Properties. Journal of Nanoscience and Nanotechnology, 2009, 9, 3347-3351.	0.9	4
1634	Special Issue on Plasma-Based Surface Modification and Treatment Technologies. IEEE Transactions on Plasma Science, 2009, 37, 1121-1122.	0.6	4
1635	Field Emission and Optical Properties of ZnO Nanowires Grown Directly on Conducting Brass Substrates. Journal of Nanoscience and Nanotechnology, 2009, 9, 3848-3852.	0.9	4
1636	Trace detection of multiwalled carbon nanotubes using Raman-enhancing silver nanocap arrays. Journal Physics D: Applied Physics, 2010, 43, 455302.	1.3	4
1637	Toughness characteristics of arc enhanced magnetron sputtered SiCN hard films. Surface Engineering, 2010, 26, 571-577.	1.1	4
1638	Magnetothermal instability in weakly magnetized plasmas with anisotropic resistivity and viscosity. Physics of Plasmas, 2010, 17, 042117.	0.7	4

PAUL CHU

#	Article	IF	CITATIONS
1639	Toxicity of Carbon Nanotubes to p21 and hus1 Gene Deficient Mammalian Cells. Journal of Nanoscience and Nanotechnology, 2011, 11, 11001-11005.	0.9	4
1640	Improved tribological properties of TiC with porous nanostructured TiO2 intermediate layer. Materials Chemistry and Physics, 2011, 131, 420-424.	2.0	4
1641	Si–Si optical phonon behavior in localized Si clusters ofÂSi x Ge1â^'x ÂalloyÂnanocrystals. Applied Physics A: Materials Science and Processing, 2011, 103, 361-365.	1.1	4
1642	Diffusion behavior of dual capping layers in TiN/LaN/AlN/HfSiOx/Si stack. Applied Physics Letters, 2011, 99, 131914.	1.5	4
1643	Coupling of Kelvin–Helmholtz instability and buoyancy instability in a thermally laminar plasma. Physics of Plasmas, 2011, 18, .	0.7	4
1644	Tribological behavior of Ti-Al-Si-C-N hard coatings deposited by hybrid arc-enhanced magnetron sputtering. Journal of Vacuum Science and Technology A: Vacuum, Surfaces and Films, 2012, 30, 021501.	0.9	4
1645	Effects of annealing temperature on excitonic emissions from Na-implanted ZnO nanorods. Materials Letters, 2013, 90, 76-78.	1.3	4
1646	Magnetorotational instability in plasmas with mobile dust grains. Physics of Plasmas, 2013, 20, 032102.	0.7	4
1647	Photoluminescence properties of ordered Bi4â^'xNdxTi3O12 matrix supported by 3-dimensional silicon microchannel plate. Journal Physics D: Applied Physics, 2013, 46, 315105.	1.3	4
1648	Microstructure and properties of ZrTiC(N) composite films on NiTi alloy. Surface Engineering, 2014, 30, 860-865.	1.1	4
1649	Passband and defective bands in photonic and quasi-crystals. Journal of the Optical Society of America B: Optical Physics, 2014, 31, 664.	0.9	4
1650	Photonic quantum well composed of photonic crystal and quasicrystal. Optics Communications, 2014, 313, 369-374.	1.0	4
1651	Electronic double layer supercapacitor based on three-dimensional silicon microchannel plates in organic electrolyte. Materials Research Innovations, 2015, 19, 303-309.	1.0	4
1652	Lattice shearing in nano-grained graphene sheets: a molecular dynamics simulation. RSC Advances, 2015, 5, 105194-105199.	1.7	4
1653	Strong phonon–plasmon coupling at the interface of 3C–SiC/metal oxide nanoparticles. Acta Materialia, 2015, 83, 113-119.	3.8	4
1654	<i>In situ</i> plasma fabrication of ceramicâ€ike structure on polymeric implant with enhanced surface hardness, cytocompatibility and antibacterial capability. Journal of Biomedical Materials Research - Part A, 2016, 104, 1102-1112.	2.1	4
1655	<i>d</i> ferromagnetism in black phosphorous oxide caused by surface P-O bonds. Applied Physics Letters, 2016, 108, .	1.5	4
1656	Electrochemical degradation and extraction capability of magnesium wastes in sewage treatment. Materials and Design, 2016, 111, 537-540.	3.3	4

#	Article	IF	CITATIONS
1657	Studies on the surface morphology and hydrophobic property of NiTi thin films under in situ and post annealing various temperatures. Materials Letters, 2016, 183, 244-247.	1.3	4
1658	Effects of pulse voltage and deposition time on the adhesion strength of graded metal/carbon films deposited on bendable stainless steel foils by hybrid cathodic arc – glow discharge plasma assisted chemical vapor deposition. Applied Surface Science, 2016, 366, 535-544.	3.1	4
1659	Tin repellence on wave-soldering stainless steel holders coated with Ti/TiC/DLC. Surface and Coatings Technology, 2017, 320, 614-618.	2.2	4
1660	Analysis of Local Surface Plasmon Resonance in Multilayered Au/Ag/Graphene Nanoshells. Nano, 2017, 12, 1750062.	0.5	4
1661	Effect of Isothermal Temperature on Growth Behavior of Nanostructured Bainite in Laser Cladded Coatings. Materials, 2017, 10, 800.	1.3	4
1662	In Silico Screening and Design of Coating Materials for PEMFC Bipolar Plates. Coatings, 2018, 8, 386.	1.2	4
1663	Localized surface plasmon resonance properties of symmetry-broken Au–ITO–Ag multilayered nanoshells. Applied Physics A: Materials Science and Processing, 2018, 124, 1.	1.1	4
1664	High-performance anode materials based on 3D orderly and vertically macroporous graphene-Si framework for Li-ion batteries. Ionics, 2019, 25, 467-473.	1.2	4
1665	Unique Role of Arginine in Positivelyâ€Charged Surface for Promotion of Antibacterial and Osteogenetic Capabilities. Advanced Materials Interfaces, 2019, 6, 1901414.	1.9	4
1666	Dual-band unidirectional forward scattering of Au–Si sliced nanorod in the visible region. Applied Physics A: Materials Science and Processing, 2019, 125, 1.	1.1	4
1667	Controlled fiberization of dipeptide in merging phases leads to collagen-level strength and opto/electric mechanofunctionalities. Biomaterials, 2019, 208, 1-7.	5.7	4
1668	Wrinkled‧urfaceâ€Induced Memristive Behavior of MoS 2 Wrapped GaN Nanowires. Advanced Electronic Materials, 2020, 6, 2000571.	2.6	4
1669	Gate-tunable two-dimensional superconductivity revealed in flexible wafer-scale hybrid structures. Journal of Materials Chemistry C, 2020, 8, 14605-14610.	2.7	4
1670	A zipped-up tunable metal coordinated cationic polymer for nanomedicine. Journal of Materials Chemistry B, 2020, 8, 1350-1358.	2.9	4
1671	Effects of the target-to-substrate distance on the microstructure and properties of TiN coatings fabricated by pulse-enhanced vacuum arc evaporation. Journal of Adhesion Science and Technology, 2021, 35, 1125-1137.	1.4	4
1672	A cationic alternating copolymer composed of ornithine and glycine with an ordered sequence for enhanced bacterial activity. Polymer Engineering and Science, 2021, 61, 1405-1414.	1.5	4
1673	Investigation of a high-sensitivity surface plasmon resonance sensor based on the eccentric core quasi D-shape photonic quasi-crystal fiber. Journal of Modern Optics, 2021, 68, 555-563.	0.6	4
1674	GaO <i><sub>x</sub></i> @GaN Nanowire Arrays on Flexible Graphite Paper with Tunable Persistent Photoconductivity. ACS Applied Materials & Interfaces, 2021, 13, 41916-41925.	4.0	4

#	Article	IF	CITATIONS
1675	Artificial Synapse Based on Bioâ€Hierarchical Porous Memristor Driven by Multilevelâ€Ions Migration. Advanced Electronic Materials, 2022, 8, .	2.6	4
1676	Formation of Buried Porous Silicon Structure by Hydrogen Plasma Immersion Ion Implantation. Materials Research Society Symposia Proceedings, 1996, 452, 427.	0.1	3
1677	Guiding of plasma by electric field and magnetic field. Chinese Physics B, 2001, 10, 424-428.	1.3	3
1678	Automatically reigniting dc vacuum arc plasma source. Review of Scientific Instruments, 2002, 73, 2971-2973.	0.6	3
1679	Implant damage and redistribution of indium in indium-implanted thin silicon-on-insulator. Materials Science and Engineering B: Solid-State Materials for Advanced Technology, 2004, 114-115, 251-254.	1.7	3
1680	<title>Thermal stability of metal containing diamond-like carbon thin film fabricated by dual plasma deposition</title> . , 2004, 5774, 330.		3
1681	Formation of silicon on plasma synthesized SiOxNy and reaction mechanism. Applied Surface Science, 2005, 243, 89-95.	3.1	3
1682	Anti-Corrosion Properties of Nitrogen and Oxygen Plasma-Implanted Nickel-Titanium Shape Memory Alloy. Solid State Phenomena, 2005, 107, 111-114.	0.3	3
1683	Cr/CrN Compound Films Prepared by Ion Beam Assisted Deposition for Improving the Performance of Bearing Steel. Plasma Science and Technology, 2005, 7, 2959-2961.	0.7	3
1684	Effects of H2O2 pretreatment on surface characteristics and bioactivity of NaOH-treated NiTi shape memory alloy. Transactions of Nonferrous Metals Society of China, 2006, 16, 1295-1300.	1.7	3
1685	Experimental and numerical evaluations of adhesion strength and stress in TiN films deposited on ti-implanted aluminum. Journal of Vacuum Science and Technology A: Vacuum, Surfaces and Films, 2006, 24, 212-217.	0.9	3
1686	Energy anisotropy of bimetal core–shell nanorods and its effects on morphology. Nanotechnology, 2007, 18, 445101.	1.3	3
1687	Mechanism of enhanced adhesion between hydrogenated amorphous carbon films and tungsten preimplanted steel substrates. Journal of Applied Physics, 2007, 101, 053520.	1.1	3
1688	Quantum-confined and tunable optical emission from sub-10-nm silicon oxide nanowires in aqueous suspension. Applied Physics Letters, 2007, 91, 193111.	1.5	3
1689	Synthesis of indium oxide nanorods on indium phosphide substrate using plasma immersion ion implantation. Surface and Coatings Technology, 2007, 201, 6816-6818.	2.2	3
1690	Implantation-assisted synthesis of gallium oxide nanoribbons on gallium arsenide using carbon and nitrogen. Surface and Coatings Technology, 2007, 201, 6804-6807.	2.2	3
1691	Broad beam gas ion source with hollow cathode discharge and four-grid accelerator system. Nuclear Instruments & Methods in Physics Research B, 2007, 257, 801-804.	0.6	3
1692	Effective passivation on Si nanocrystal surface by peroxide. Journal of Crystal Growth, 2007, 304, 86-89.	0.7	3

#	Article	IF	CITATIONS
1693	Synthesis and field-emission properties of roselike ZnO nanostructures. Applied Physics A: Materials Science and Processing, 2008, 91, 247-250.	1.1	3
1694	Origin of the 745 nm photoluminescence from small diameter silicon nanowires. Solid State Communications, 2008, 148, 182-185.	0.9	3
1695	lon trajectories in plasma ion implantation of slender cylindrical bores using a small inner end source. Applied Physics Letters, 2008, 93, 191501.	1.5	3
1696	Asymmetrical reorientation of bimetallic core–shell nanowires. Nanotechnology, 2009, 20, 045601.	1.3	3
1697	Three-Dimensional Quasi-Direct-Current Plasma Immersion Ion Implantation Into Biomedical Nickel–Titanium Shape Memory Alloy Rod. IEEE Transactions on Plasma Science, 2009, 37, 2245-2249.	0.6	3
1698	Optical properties of plastic scintillators coated with copper, aluminum and silver by magnetron sputtering. Thin Solid Films, 2009, 517, 4443-4447.	0.8	3
1699	Effects of nitrogen incorporation into lanthana film by plasma immersion ion implantation. Solid-State Electronics, 2009, 53, 355-358.	0.8	3
1700	Surface Properties of AZ31B Magnesium Alloy by Oxygen Plasma Immersion Ion Implantation. Plasma Science and Technology, 2009, 11, 33-37.	0.7	3
1701	Uniformity of TiN Films Fabricated by Hollow Cathode Discharge. Plasma Science and Technology, 2010, 12, 212-217.	0.7	3
1702	Enhanced retained dose uniformity in NiTi spinal correction rod treated by three-dimensional mesh-assisted nitrogen plasma immersion ion implantation. Journal of Vacuum Science and Technology A: Vacuum, Surfaces and Films, 2010, 28, 407-410.	0.9	3
1703	Evidence of recombination enhanced diffusion of impurities at low temperature into high-k dielectric with tantalum oxide as an example. Applied Physics Letters, 2010, 96, .	1.5	3
1704	Plasma Immersion Ion Implantation Into Inner Surface of Cylindrical Bore Using Moving Auxiliary Electrode. IEEE Transactions on Plasma Science, 2011, 39, 3120-3124.	0.6	3
1705	Cytocompatibility and haemocompatibility of Zr, ZrC and ZrCN films. Surface Engineering, 2012, 28, 448-452.	1.1	3
1706	Anisotropic etching of microscale β-FeSi2 particles: Formation, mechanism, and quantum confinement of β-FeSi2 nanowhiskers. RSC Advances, 2012, 2, 3254.	1.7	3
1707	Novel functional materials with active adsorption and antimicrobial properties. Materials Letters, 2012, 89, 19-21.	1.3	3
1708	Facile preparation of cationic P (Stâ€BAâ€METAC) copolymer nanoparticles and the investigation of their interaction with bovine serum albumin. Journal of Applied Polymer Science, 2012, 125, 864-869.	1.3	3
1709	Photocatalytic behaviors of porous ZnO hierarchical structures fabricated via a precursor-pyrolyzing route. Journal of Materials Science: Materials in Electronics, 2013, 24, 89-95.	1.1	3
1710	Effects of surface properties of red mud on interactions with Escherichia coli. Journal of Materials Research, 2013, 28, 2332-2338.	1.2	3

#	Article	IF	CITATIONS
1711	CdS:Mn–Polysulfido Complex Nanoclusters with H <sub>2</sub> O <sub>2</sub> -Dependent and Site-Specific Color Changes. Journal of Physical Chemistry C, 2014, 118, 11085-11092.	1.5	3
1712	Surface changes in Fe–Cr–Ni alloy bombarded by relativistic pulsed electron beam and associated mechanism. Vacuum, 2014, 101, 136-141.	1.6	3
1713	An experimental study of magnetorheological fluids on electrical conductivity property. Journal of Materials Science: Materials in Electronics, 2017, 28, 8130-8135.	1.1	3
1714	Morphological and electrical properties of SrTiO 3 /TiO 2 /SrTiO 3 sandwich structures prepared by plasma sputtering. Chinese Physics B, 2017, 26, 010702.	0.7	3
1715	Investigation of Corrosion Behavior of Ti/TiN Multilayers on Al7075 Deposited by High-Vacuum Magnetron Sputtering in 3.5% NaCl Solution. Journal of Materials Engineering and Performance, 2018, 27, 2216-2225.	1.2	3
1716	Asymmetrical photonic crystal fiber based on the surface plasmon resonance sensor and analysis by the lower-birefringence peak method. Optik, 2019, 189, 121-129.	1.4	3
1717	Optical diode composed of subwavelength slit-groove arrays with ultrahigh transmission contrast based on surface plasmon polariton. Optik, 2019, 186, 266-274.	1.4	3
1718	Self-supported electrodes composed of silicon nanocrystals in 3D hierarchical carbon network for reversible sodium storage. Journal of Materials Science: Materials in Electronics, 2019, 30, 2732-2742.	1.1	3
1719	Nitrogen-doped carbon coated TiC nanofiber arrays deposited on Ti-6Al-4V for selective and sensitive electrochemical detection of dopamine. Surface and Coatings Technology, 2020, 402, 126266.	2.2	3
1720	Forward and Backward Unidirectional Scattering by the Core-Shell Nanocube Dimer with Balanced Gain and Loss. Nanomaterials, 2020, 10, 1440.	1.9	3
1721	Nano-second temporal particle behavior in high-power impulse magnetron sputtering discharge in a cylindrical cathode. Journal of Applied Physics, 2020, 127, 023301.	1.1	3
1722	Multi-functional gallium arsenide photonic crystal polarization splitter with a gold core. Modern Physics Letters B, 2021, 35, 2150229.	1.0	3
1723	Characteristics of continuous high power magnetron sputtering (C-HPMS) in reactive O2/Ar atmospheres. Journal of Applied Physics, 2021, 129, .	1.1	3
1724	Engineering CsPbBr3 quantum dots with efficient luminescence and stability by damage-free encapsulation with a-SiCx:H. Journal of Luminescence, 2021, 236, 118086.	1.5	3
1725	Photonic spin Hall effect: a new window in D-shaped fiber by weak measurements. Optics Express, 2019, 27, 14064.	1.7	3
1726	Dual-band directional scattering with all-dielectric trimer in the near-infrared region. Applied Optics, 2019, 58, 5082.	0.9	3
1727	Degradation of gemfibrozil in aqueous solutions by gas–liquid dielectric barrier discharge plasma combined with CNTs/Ĵ³Fe <sub>2</sub> O <sub>3</sub> . Plasma Processes and Polymers, 2022, 19, .	1.6	3
1728	Detection of kerosene adulteration in automobile fuel by a low-loss surface plasmon resonance (SPR) chemical sensor. Analytical Methods, 2022, 14, 2153-2160.	1.3	3

#	Article	IF	CITATIONS
1729	Numerical Analysis of Multifunctional Biosensor with Dual-Channel Photonic Crystal Fibers Based on Localized Surface Plasmon Resonance. Coatings, 2022, 12, 742.	1.2	3
1730	Simulation of dose uniformity for different pulse durations during inner surface plasma immersion ion implantation. Journal of Vacuum Science & Technology an Official Journal of the American Vacuum Society B, Microelectronics Processing and Phenomena, 1999, 17, 875.	1.6	2
1731	Assistant Anode in a Cathodic Arc Plasma Source. Chinese Physics Letters, 2001, 18, 1103-1104.	1.3	2
1732	Ion enhanced deposition by dual titanium and acetylene plasma immersion ion implantation. Journal of Vacuum Science and Technology A: Vacuum, Surfaces and Films, 2003, 21, 175-179.	0.9	2
1733	Formation of silicon on plasma synthesized aluminum nitride structure by ion cutting. Journal of Vacuum Science & Technology an Official Journal of the American Vacuum Society B, Microelectronics Processing and Phenomena, 2004, 22, 2748.	1.6	2
1734	Formation of silicon-on-aluminum nitride using ion-cut and theoretical investigation of self-heating effects. Materials Letters, 2005, 59, 510-513.	1.3	2
1735	Nitrogen Plasma Source Ion Implantation (PSII) for Improvement of Blood-Compatibility of Silicon. Key Engineering Materials, 2005, 288-289, 335-338.	0.4	2
1736	Effects of pulsing parameters on production and distribution of macroparticles in cathodic vacuum arc deposition. Journal of Vacuum Science and Technology A: Vacuum, Surfaces and Films, 2006, 24, 957-961.	0.9	2
1737	Optical emission from C60-coupled Î <sup>2</sup> -FeSi2 nanocomposites. Applied Physics Letters, 2006, 89, 233114.	1.5	2
1738	Photoluminescence from C60-coupled porous structures formed on Fe+-implanted silicon. Journal of Chemical Physics, 2006, 125, 014706.	1.2	2
1739	Experimental and theoretical investigation of the effects of sample size on copper plasma immersion ion implantation into polyethylene. Journal of Applied Physics, 2007, 101, 113302.	1.1	2
1740	Effects of bias on surface properties of TiN films fabricated by hollow cathode discharge. Journal of Vacuum Science and Technology A: Vacuum, Surfaces and Films, 2007, 25, 837-842.	0.9	2
1741	Behaviors of Platelets Adherent on Si-N(H) Surface Prepared from Ammonia Plasma-Implanted Silicon. Key Engineering Materials, 2007, 330-332, 889-892.	0.4	2
1742	Microwave enhanced ion-cut silicon layer transfer. Journal of Applied Physics, 2007, 101, 114915.	1.1	2
1743	A flexible curvilinear electromagnetic filter for direct current cathodic arc source. Review of Scientific Instruments, 2007, 78, 095103.	0.6	2
1744	Electrical Stability Improvement for Lanthanum Oxide Films by Nitrogen Incorporation using Plasma Immersion Ion Implantation. , 2007, , .		2
1745	Investigation of cytocompatibility of surface-treated cellulose nitrate films by using plasma immersion ion implantation. Surface and Coatings Technology, 2007, 201, 6897-6900.	2.2	2
1746	Effects of pulsing frequencies on macro-particle contamination during pulsed vacuum arc deposition. Surface and Coatings Technology, 2007, 201, 6545-6549.	2.2	2

#	Article	IF	CITATIONS
1747	Improved detection resolution in single particle microbeam system. Nuclear Instruments and Methods in Physics Research, Section A: Accelerators, Spectrometers, Detectors and Associated Equipment, 2008, 595, 312-316.	0.7	2
1748	Direct coupling of pulsed radio frequency and pulsed high power in novel pulsed power system for plasma immersion ion implantation. Review of Scientific Instruments, 2008, 79, 043501.	0.6	2
1749	Role of fluorine in plasma nitridated ZrO2 thin films under irradiation. Applied Physics Letters, 2008, 93, 122907.	1.5	2
1750	Mechanical properties of amorphous hydrogenated carbon films fabricated on polyethylene terephthalate foils by plasma immersion ion implantation and deposition. Journal of Vacuum Science and Technology A: Vacuum, Surfaces and Films, 2008, 26, 438-443.	0.9	2
1751	Stress influence on band-edge luminescence properties of 4H-AlN. Applied Physics Letters, 2009, 95, 121902.	1.5	2
1752	One-step, non-contact pattern transfer by direct-current plasma immersion ion implantation. Journal Physics D: Applied Physics, 2009, 42, 195201.	1.3	2
1753	High-voltage glow discharge plasma immersion ion implantation assisted by magnetic field. Surface and Coatings Technology, 2009, 203, 2751-2754.	2.2	2
1754	Synthesis and Characteristics of Cubic Silicon Carbide Nanospheres with Smooth Surfaces. Journal of Nanoscience and Nanotechnology, 2009, 9, 6643-6647.	0.9	2
1755	Growth of Well-Aligned ZnO Nanorod Arrays on Si Substrates by Thermal Evaporation of Cu–Zn Alloy Powders. Journal of Nanoscience and Nanotechnology, 2010, 10, 4786-4791.	0.9	2
1756	Surface Nanomechanical Behavior of ZrN and ZrCN Films Deposited on NiTi Shape Memory Alloy by Magnetron Sputtering. Journal of Nanoscience and Nanotechnology, 2011, 11, 11176-11180.	0.9	2
1757	Influence of annular magnet on discharge characteristics in enhanced glow discharge plasma immersion ion implantation. Applied Physics Letters, 2011, 98, 021502.	1.5	2
1758	Electronic structure and optical properties of β-FeSi2(100)/Si(001) interface at high pressure. Applied Physics Letters, 2012, 101, 111909.	1.5	2
1759	Transformation of Enhanced Glow Discharge Dynamics in Nitrogen Plasma Immersion Ion Implantation. IEEE Transactions on Plasma Science, 2013, 41, 553-558.	0.6	2
1760	Resonant energy transfer from nanocrystal Si to β-FeSi <sub>2</sub> in hybrid Si/β-FeSi <sub>2</sub> film. Chinese Physics B, 2013, 22, 106804.	0.7	2
1761	Improved ion implant fluence uniformity in hydrogen enhanced glow discharge plasma immersion ion implantation into silicon. Review of Scientific Instruments, 2014, 85, 063506.	0.6	2
1762	SiC Nanostructured Films. Engineering Materials and Processes, 2014, , 295-315.	0.2	2
1763	Resonance-enhanced electroresistance-magnetoresistance effects in multiferroic tunnel junctions. Materials Research Express, 2015, 2, 046303.	0.8	2
1764	Energy dissipation in mechanical loading of nano-grained graphene sheets. RSC Advances, 2016, 6, 60856-60861.	1.7	2

#	Article	IF	CITATIONS
1765	Modification of Biomaterials and Biomedical Devices by Plasma Immersion Ion Implantation & Deposition and Related Techniques. , 2016, , .		2
1766	Tribological and Corrosion Properties of Nickel/TiC Bilayered Coatings Produced by Electroless Deposition and PACVD. Journal of Materials Engineering and Performance, 2016, 25, 4796-4804.	1.2	2
1767	Reutilization of industrial ultrafine carbon ash ( <scp>PM</scp> 2.5) as rubber reinforcement filler. Environmental Progress and Sustainable Energy, 2016, 35, 1132-1138.	1.3	2
1768	Synthesis and cathodoluminescent properties of Lu3(Al,Ga)5O12:Tb3+ with and without niobium-doped TiO2 coating. Journal of Sol-Gel Science and Technology, 2016, 77, 355-360.	1.1	2
1769	Recent Applications of Scanning Microscopy in Surface Engineering. Scanning, 2018, 2018, 1-2.	0.7	2
1770	Modulation of resistive switching in Pt/LiCoO2/SiO2/Si stacks. Journal of Materials Science: Materials in Electronics, 2019, 30, 4753-4759.	1.1	2
1771	Microwave synthesis and enhancement of power factors of HfxTi1â^'xNiSn. Materials Letters, 2019, 251, 13-17.	1.3	2
1772	Bioactive inorganic-ion-doped titania nanotube coatings on bone implants with enhanced osteogenic activity and antibacterial properties. , 2019, , 401-427.		2
1773	Numerical analysis of a high-birefringent photonic quasi-crystal fiber with circular air holes. Optik, 2020, 207, 163850.	1.4	2
1774	Controllable deposition of MoS2 nanosheets on titanium by the vapor-phase hydrothermal technique and comparison with the conventional liquid-phase hydrothermal method. Surface and Coatings Technology, 2020, 404, 126497.	2.2	2
1775	Photoluminescence Properties of GaN Nanowires Grown in a Gradient-Plasma Environment. Journal of Physical Chemistry C, 2020, 124, 16002-16008.	1.5	2
1776	Natural Nanominerals Show Enzyme-Like Activities. Journal of Nanomaterials, 2021, 2021, 1-12.	1.5	2
1777	N-doped TiO <sub>2</sub> Immobilized on Nickel Foam and Its Photocatalytic Performance for Formaldehyde Degradation under Visible Light. Wuji Cailiao Xuebao/Journal of Inorganic Materials, 2010, 25, 753-757.	0.6	2
1778	Efficient photonic crystal fiber polarization splitters composed of gallium arsenide and nematic liquid crystals. Modern Physics Letters B, 2021, 35, 2150077.	1.0	2
1779	Exosomes derived from magnesium ion—stimulated macrophages inhibit angiogenesis. Biomedical Materials (Bristol), 2022, 17, 045008.	1.7	2
1780	Synthesis of Nitrogen-Doped Diamond-Like Carbon Films Produced by Plasma-Enhanced Chemical Vapor Deposition and their Tribocorrosion Behavior in Hanks' Solution. Journal of Materials Engineering and Performance, 2022, 31, 8334-8345.	1.2	2
1781	Competitive Oxidation During Buried Oxide Formation Using Separation by Plasma Implantation of Oxygen (Spimox). Materials Research Society Symposia Proceedings, 1995, 388, 385.	0.1	1
1782	Interpretation of in-plane and out-of-plane anisotropic surface–interface reflectance and transmittance difference spectroscopy. Journal of the Optical Society of America B: Optical Physics, 1998, 15, 1198.	0.9	1

#	Article	IF	CITATIONS
1783	A simplified surface photoreflectance measurement system. Measurement Science and Technology, 2000, 11, 1348-1351.	1.4	1
1784	Enhancement of tribological properties of 9Cr18 stainless steel by dual Mo and S Co implantation. Journal of Vacuum Science and Technology A: Vacuum, Surfaces and Films, 2001, 19, 295-298.	0.9	1
1785	Oxygen segregation and Ge diffusion in annealed oxygen ion-implanted relaxed SiGe/Si heterostructures. Journal of Electronic Materials, 2004, 33, 207-212.	1.0	1
1786	Effects of buried oxide layer on indium diffusion in separation by implantation of oxygen. Journal of Applied Physics, 2004, 96, 3217-3220.	1.1	1
1787	<title>Relaxation mechanism of SiGe thin film on SOI substrate</title> . , 2004, , .		1
1788	Controlled Growth of ZnO films on Si Substrate and N-doping Behavior. Materials Research Society Symposia Proceedings, 2005, 864, 7111.	0.1	1
1789	Electrical and interfacial characteristics of nanolaminate (Al2O3/ZrO2/Al2O3) gate stack on fully depleted SiGe-on-insulator. Materials Science in Semiconductor Processing, 2006, 9, 959-963.	1.9	1
1790	Si nanowires sheathed with thin diamondlike carbon films. Journal of Vacuum Science & Technology B, 2006, 24, 1702.	1.3	1
1791	Energy band mixing in core-shell-structured Siâ^•FeSi2 nanocomposites. Applied Physics Letters, 2006, 89, 053114.	1.5	1
1792	Influence of acetylene to argon flow rate ratios on structure and properties of hydrogenated amorphous carbon films produced on steel substrates by plasma immersion ion implantation and deposition. Journal of Materials Research, 2007, 22, 982-988.	1.2	1
1793	Effects of layer patterns on magnetic and other properties of single and multilayered Fe–C films. Journal of Applied Physics, 2007, 101, 034902.	1.1	1
1794	Experimental tests and numerical simulation studies on nano-indentation of TiN film deposited on N+-implanted aluminum. Surface and Coatings Technology, 2007, 201, 6707-6711.	2.2	1
1795	Fabrication and characteristics of novel microelectronic structures fabricated by plasma-based techniques. Surface and Coatings Technology, 2007, 201, 6745-6751.	2.2	1
1796	Fabrication of silicon-on-insulator (SOI) and high-k materials using plasma technology. , 2008, , .		1
1797	Fabrication for multilayered composite thin films by dual-channel vacuum arc deposition. Review of Scientific Instruments, 2008, 79, 065104.	0.6	1
1798	Hybrid radio-frequency/direct-current plasma-enhanced chemical vapor deposition system for deposition on inner surfaces of polyethylene terephthalate bottles. Review of Scientific Instruments, 2009, 80, 123504.	0.6	1
1799	Microstructural characteristics and biocompatibility of a Type-B carbonated hydroxyapatite coating deposited on NiTi shape memory alloy. Bio-Medical Materials and Engineering, 2009, 19, 401-408.	0.4	1
1800	Fabrication and Surface Modification of Porous Nano-Structured NiTi Orthopedic Scaffolds for Bone Implants. Materials Research Society Symposia Proceedings, 2009, 1181, 7.	0.1	1

#	Article	IF	CITATIONS
1801	Direct Growth of Hexagonal Cd(OH) <sub>2</sub> Nanoplates from and on Cadmium Substrate. Journal of Nanoscience and Nanotechnology, 2009, 9, 3747-3751.	0.9	1
1802	Hot spots in silver nano-dendrites fabricated by self-selective electroless plating. , 2010, , .		1
1803	Crystalline Core/Shell Si/SiO <sub>2</sub> Nanotubes Formed via Interfacial Stress Imbalance. Journal of Nanoscience and Nanotechnology, 2010, 10, 5583-5586.	0.9	1
1804	Controllable growth of hierarchical AlN nanostructures based on dynamic equilibrium. CrystEngComm, 2011, 13, 6337.	1.3	1
1805	Surface Treatments of Nearly Equiatomic NiTi Alloy (Nitinol) for Surgical Implants. , 2011, , .		1
1806	Enhanced Wet Etching of Patterned GaN with Ion Implantation. Journal of Nanoscience and Nanotechnology, 2011, 11, 10949-10953.	0.9	1
1807	Fabrication and Characterization of Silicon Microchannel Plates as Temperature-Sensing Materials. Journal of Electronic Materials, 2011, 40, 2363-2367.	1.0	1
1808	Structure of ceramics treated with hot-pressing. Solid State Communications, 2011, 151, 5-8.	0.9	1
1809	Interaction Between Fluorinated Amphiphilic Copolymer P(HFMA)-g-P(SPEG) and BSA. Journal of Dispersion Science and Technology, 2011, 32, 1185-1190.	1.3	1
1810	Ion trajectories and shadow effects in mesh-assisted plasma immersion ion implantation of insulator. Applied Surface Science, 2012, 258, 2910-2913.	3.1	1
1811	Fabrication of Si–Ag "wire-cap―nanostructures for metal-enhanced fluorescence. Journal of Luminescence, 2012, 132, 2586-2589.	1.5	1
1812	Enhanced Photoelectrochemical Oxygen Evolution Reaction based on Surface Autocatalytic Effect of Ultrathin 3C-SiC Nanocrystals. Journal of the Electrochemical Society, 2013, 160, H620-H623.	1.3	1
1813	Concentrated ion beam emitted from an enlarged cylindrical-anode-layer Hall plasma accelerator and mechanism. Journal of Applied Physics, 2013, 113, 043302.	1.1	1
1814	Self-sealing SiO2 pores on silicon formed by oxidation of microporous silicon. Microporous and Mesoporous Materials, 2013, 174, 10-13.	2.2	1
1815	Titania Nanotube Coatings on Dental Implants with Enhanced Osteogenic Activity and Anti-Infection Properties. , 2013, , 337-357.		1
1816	Response to "Comment on â€~Three-dimensional numerical investigation of electron transport with rotating spoke in a cylindrical anode layer Hall plasma accelerator'―[Phys. Plasmas 20, 014701 (2013)]. Physics of Plasmas, 2013, 20, .	0.7	1
1817	SiC Nanotubes. Engineering Materials and Processes, 2014, , 271-294.	0.2	1
1818	Metal oxide coating on first mirror in fusion reactor with carbon wall. Surface and Coatings Technology, 2014, 240, 464-469.	2.2	1

#	Article	IF	CITATIONS
1819	Demagnification and Magnification Effects in One-Step Noncontact Pattern Transfer by Direct-Current Plasma Immersion Ion Implantation. IEEE Transactions on Plasma Science, 2015, 43, 552-556.	0.6	1
1820	Effect of Ag and Ti electrodes on capacitance tunability of oxygen-deficient SrTiO3based MIM varactors prepared by plasma sputtering. Materials Research Express, 2017, 4, 046401.	0.8	1
1821	Effects of Duty Cycle on Texture Orientation and Composition of TiCx Nanostructured coatings. Protection of Metals and Physical Chemistry of Surfaces, 2018, 54, 642-647.	0.3	1
1822	Biaxially strained germanium micro-dot array by hydrogen ion implantation. Surface and Coatings Technology, 2019, 365, 248-252.	2.2	1
1823	Analysis of defect states in optical microcavities based on the photonic quantum well structure. Optics Communications, 2020, 458, 124880.	1.0	1
1824	Toroidal dipole and magnetic multipole excitations from the same nanostructure with different direction of electric dipole emitters. Applied Physics A: Materials Science and Processing, 2020, 126, 1.	1.1	1
1825	Stable Discharge Mechanism in Microarc Oxidation and Processing in Phosphate Electrolytes. IEEE Transactions on Plasma Science, 2021, 49, 3126-3131.	0.6	1
1826	Effects of different interlayers on the microstructure and properties of Mg/Cu dissimilar alloy welded joints. Journal of Laser Applications, 2021, 33, 012055.	0.8	1
1827	Enhancement of unidirectional forward scattering and suppression of backward scattering in hollow silicon nanoblocks. Applied Optics, 2021, 60, 8737.	0.9	1
1828	A water-soluble membrane for SARS-CoV-2 viral nucleic acid sampling and detection. Nanoscale, 2021, 13, 18084-18088.	2.8	1
1829	Tunable Ordered Silver Nano-Arrays Prepared by TiO <sub>2</sub> Templates as Surface-Enhanced Raman Scattering Substrates. Nanoscience and Nanotechnology Letters, 2015, 7, 892-896.	0.4	1
1830	Multiple unidirectional forward scattering of hybrid metal-dielectric nanoantenna in the near-infrared region. Optical Materials Express, 2018, 8, 3410.	1.6	1
1831	Finite phosphorene derived partial reduction of metal organic framework nanofoams for enhanced lithium storage capability. Journal of Power Sources, 2022, 525, 231025.	4.0	1
1832	Influence of photon reabsorption on the optical and catalytic properties of carbon nanodots/titanium oxide composites. Applied Physics Letters, 2022, 120, 213902.	1.5	1
1833	In situ synthesis of 3D metal oxides/Ni3C on the macroporous electrically conductive network for enhanced electron field emission. Materials Letters, 2022, 323, 132524.	1.3	1
1834	A static three-chamber zinc-polyiodide redox battery for decoupling of active anions and cations. Journal of Energy Storage, 2022, 54, 105258.	3.9	1
1835	Low-Dielectric Constant SiO(F,C) Films for ULSI Interconnections Prepared by CF4 Plasma Ion Implantation. Materials Research Society Symposia Proceedings, 1998, 511, 63.	0.1	0
1836	Two Step O2/N2O Plasma Annealing for the Reduction of Leakage Current in Amorphous Ta2O5 Films. Materials Research Society Symposia Proceedings, 1999, 567, 501.	0.1	0

#	Article	IF	CITATIONS
1837	Process and Mechanism of CoSi2/Si Solid Phase Epitaxy by Multilayer Reaction. Materials Research Society Symposia Proceedings, 1999, 580, 117.	0.1	0
1838	Formation of Callium Nitride (GaN) Transition Layer by Plasma Immersion Ion Implantation and Rapid Thermal Annealing. Materials Research Society Symposia Proceedings, 2000, 618, 309.	0.1	0
1839	H DISTRIBUTION AND STRAIN EVOLUTION IN SIGe/SI HETEROSTRUCTURE IMPLANTED BY H DIMERS. International Journal of Modern Physics B, 2002, 16, 4199-4202.	1.0	0
1840	SiGe-on-insulator material fabrication by oxygen implantation into SiGe/Si heterostructure and novel two-step annealing. Materials Science and Engineering B: Solid-State Materials for Advanced Technology, 2004, 114-115, 255-259.	1.7	0
1841	<title>Plasma-implantation-based surface modification of metals with single-implantation&lt;br&gt;mode</title> . , 2004, , .		0
1842	Various Methods to Reduce Defect States in Tantalum Oxide Capacitors for DRAM Applications. Materials Research Society Symposia Proceedings, 2005, 864, 4221.	0.1	0
1843	Stable optical emission from annealed poly (p-phenylene vinylene) derivative films containing oxadiazole. Journal of Electronic Materials, 2006, 35, 1689-1692.	1.0	0
1844	Influence of electron beam and ultraviolet ozone irradiation on blue-emission properties of C60-coupled porous silicon. Materials Chemistry and Physics, 2006, 97, 379-383.	2.0	0
1845	Fabrication of novel silicon-on-insulator substrates using plasma-based technology. , 2006, , .		0
1846	Aluminium Incorporation in Lanthanum Oxide Films by using Plasma Immersion Ion Implantation. , 2007,		0
1847	Nano-film and Coating for Biomedical Application Prepared by Plasma-based Technologies. Materials Research Society Symposia Proceedings, 2007, 1020, 1.	0.1	0
1848	Soft ferromagnetic materials based on iron/carbon multilayers. Physica B: Condensed Matter, 2007, 394, 273-276.	1.3	0
1849	SIA spotlight on Asia. Surface and Interface Analysis, 2007, 39, 715-739.	0.8	0
1850	Plasma ion implantation to thin polymer foils. Physica Status Solidi (A) Applications and Materials Science, 2008, 205, 953-956.	0.8	0
1851	Uniformity of Plasma Density and Film Thickness of Coatings Deposited Inside a Cylindrical Tube by Radio Frequency Sputtering. Plasma Science and Technology, 2008, 10, 560-564.	0.7	0
1852	Characteristics of La <inf>2</inf> O <inf>3</inf> gate dielectric film with Al implantation using plasma immersion ion implantation. , 2008, , .		0
1853	Response to "Comment on `Effects of magnetic field gradient on ion beam current in cylindrical Hall ion source' '' [J. Appl. Phys. 104, 066102 (2008)]. Journal of Applied Physics, 2008, 104, 066103.	1.1	0
1854	Synthesis of Hierarchical Tree-Like and Jellyfish-Like Silicon Oxide Nanostructures. Journal of Nanoscience and Nanotechnology, 2009, 9, 3914-3920.	0.9	0

#	Article	IF	CITATIONS
1855	Effects of capacitively-coupled radio-frequency discharge on operation voltage in magnetron sputtering. Surface and Coatings Technology, 2009, 203, 2767-2770.	2.2	0
1856	Transparency, wettability, and tribological properties of amorphous hydrogenated carbon films deposited on PMMA by RF-PECVD. , 2009, , .		0
1857	Interaction between the fluorinated amphiphilic copolymer poly(2,2,3,4,4,4â€hexafluorobutyl) Tj ETQq1 1 0.7843	814 rgBT / 1.3	Overlock 10
1858	The surface properties modification of polyethylene by enhanced glow discharge plasma immersion ion implantation. , 2010, , .		0
1859	Direct growth of Nb <inf>2</inf> O <inf>5</inf> nanobelts on Nb foil. , 2010, , .		0
1860	Plasma immersion ion implantation into cylindrical bore using internal inductively-coupled radio-frequency discharge. Surface and Coatings Technology, 2010, , .	2.2	0
1861	Selected Peer-Reviewed Articles from the 3rd IEEE International NanoElectronics Conference (INEC) Tj ETQq1 1 0.	784314 r 0.9	gBT /Overloo
1862	Investigation of Inner Surface of Silicon Microchannels Fabricated by Electrochemical Method. Journal of Nanoscience and Nanotechnology, 2011, 11, 11045-11048.	0.9	0
1863	Thermoelectric Properties of Silicon Microchannel Plates Structures. Journal of Physics: Conference Series, 2011, 276, 012043.	0.3	0
1864	Anisotropic dissipative effects on the buoyancy instability with background heat flux. Physics of Plasmas, 2011, 18, 032106.	0.7	0
1865	A novel method for effective sodium ion implantation into silicon. Review of Scientific Instruments, 2012, 83, 075116.	0.6	0
1866	Production of Three-Dimensional Hierarchical Nano Ti-Based Metals Scaffolds for Bone Tissue Grafts. , 2012, , 69-82.		0
1867	Fabrication of porous silicon nanotips by using argon ion-beam irradiation. Journal of the Korean Physical Society, 2013, 63, 206-208.	0.3	0
1868	Breathing oscillations in enlarged cylindrical-anode-layer Hall plasma accelerator. Journal of Applied Physics, 2013, 113, 203302.	1.1	0
1869	Zno Nanorod Synthesis via Controlled ZnO Seed Layer by Filtered Pulse Cathodic Vacuum Arc: Luminescence Enhancement. Advanced Materials Research, 2013, 802, 1-6.	0.3	0
1870	Characterization of SnO <sub>2</sub> /Ni/SiO <sub>2</sub> -MCP anode in three-dimensional lithium-ion battery. Proceedings of SPIE, 2013, , .	0.8	0
1871	Porous SiC. Engineering Materials and Processes, 2014, , 115-130.	0.2	0
1872	Biological Applications. Engineering Materials and Processes, 2014, , 317-330.	0.2	0

#	Article	lF	CITATIONS
1873	Analysis of Localized Surface Plasmon Resonance in Ag/ITO/CdS/SiO2 Multilayered Nanostructured Composite. Nano, 2015, 10, 1550117.	O.5	0
1874	Response to "Comment on â€~Surface electromagnetic wave equations in a warm magnetized quantum plasma'―[Phys. Plasmas 23, 074701 (2016)]. Physics of Plasmas, 2016, 23, 074702.	0.7	0
1875	Study on the strain in a silicon microchannel plate by micro-Raman analysis. Semiconductor Science and Technology, 2016, 31, 055010.	1.0	0
1876	Origin of Initial Current Peak in High Power Impulse Magnetron Sputtering and Verification by Non-Sputtering Discharge. Chinese Physics Letters, 2016, 33, 075201.	1.3	0
1877	Electrochemiluminescent Spinâ€Polarized Modulation by Magnetic Ions and Surface Plasmon Coupling. Angewandte Chemie, 2016, 128, 2057-2061.	1.6	0
1878	Three-dimensional graphene nanosheets supported by NiO/Si-MCP as electrode materials for high-performance supercapacitors. lonics, 2017, 23, 2185-2191.	1.2	0
1879	The effect of copper pretreatment on graphene synthesis by ion implantation into Ni/Cu substrate. Semiconductor Science and Technology, 2018, 33, 074001.	1.0	0
1880	Influence of plasma excitation power on mechanical property and biocompatibility of titania/alumina composite thin films for medical implant prepared by magnetron sputtering. Materials Research Express, 2019, 6, 116418.	0.8	0
1881	Localized Surface Plasmon Resonance Properties of Concentric Dual-Ring Nanodisk. Nano, 2019, 14, 1950071.	0.5	0
1882	Influence of Acetylene on Ti Target Poisoning During Pulse-Enhanced Vacuum Arc Evaporation. IEEE Transactions on Plasma Science, 2020, 48, 2799-2809.	0.6	0
1883	Nanometer-Scale Surface Modification Using Scanning Force Microscopy in Chemically Active Environments. , 2004, , .		0
1884	Biomaterials Using Plasma Immersion Ion Implantation and Deposition Surface Modification of. , 2008, , 573-631.		0
1885	Synthesis of ZnO Nanorods Arrays on ITO and Their Photoelectrochemical Performance. Journal of Scientific Conference Proceedings, 2009, 1, 286-289.	0.1	0
1886	Surface-enhanced Raman Scattering Substrates Prepared by Magnetron Sputtering Using Anodized Titanium Oxide Nanotube Ends as Template. , 2013, , .		0
1887	SiC Nanowires. Engineering Materials and Processes, 2014, , 195-269.	0.2	0
1888	Boron segregation in As-implanted Si due to electric field and transient enhanced diffusion. , 1997, , .		0
1889	Plasma Surface Modification of Magnesium-Based and Related Materials. , 2016, , 329-330.		0
1890	Fano resonances in symmetric plasmonic split-ring/ring dimer nanostructures. Applied Optics, 2019, 58, 8069.	0.9	0